Development of a new polymeric DNA delivery system

Mater Thesis Report

Miquel Santos Llinàs

Aalborg University
Materials and production

Materials and production
Aalborg University
http://www.aau.dk

AALBORG UNIVERSITY
STUDENT REPORT

Title:
Development of a new polymeric DNA delivery system

Theme:
DNA delivery

Project Period:
September 2020-June 2021

Project Group:
5.319

Participant(s):
Miquel Santos Llinàs

Supervisor(s):
Dr. Leonid Gurevich

Page Numbers: 101

Date of Completion:
June 2, 2021

Abstract:

Gene therapy is a promising strategy for curing diseases that have a genetic origin, but so far it has been limited due to the difficulties of delivering DNA to human cells. In this thesis, a new non-viral DNA delivery system has been created using the amphiphilic polymer PVP-OD and a short cationic peptide. Some properties of the new nanocarrier such as the size, the shape or the safety have bee studied, as well as its efficiency inducing foreign gene expression in human cells. Although the nanocarrier seems optimal for gene delivery, high levels of transfection has not yet been observed, suggesting that more work is necessary to optimize this new system. Considering the promise that the PVP-OD nanocarrier may have, and given the technical limitations that the 2D transfection experiments have, a COMSOL model has been created to aid in the future development of a microfluidic chip that could be used for testing this DNA delivery system in conditions that more closely resemble real humans.

agreement with the author.

Preface

This master thesis is composed of 4 main chapters. In the first one, a review of the literature regarding gene delivery will be provided as a means to motivate the need for this project. A short explanation of the main methods that have been used will also be included to help the reader understand the meaning of the experiments that have been performed. In the second chapter, the specific protocols that have been used will be presented together with the materials. The third and fourth chapters will respectively cover the results and the discussion of the results, and in the end a summary of the project conclusions and some proposals for future work will be added.

I would like to thank both Dr Leonid Gurevich and Dr Pablo Pennisi for their support throughout the entire thesis in their respective areas of expertise. Without their help, this project could not have advanced so far. I would also like to show my gratitude to Dr Shtilman from Mendeleev University of Chemical Technology of Russia, Moscow, Russia for preparing the PVP-OD that has been used throughout the entire project. Finally, I would also like to thank Dr Eva Maria Petersen and Dr Peter Fojan for their contribution in some experiments such as peptide synthesis and DNA extraction as well as Daniel Ameljan and Tushar Kumar sharing all their expertise with EDC/NHS coupling.

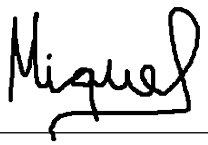

Miquel Santos Llinas
<msanto19@student.aau.dk>

List of Abbreviations

PVP-OD Poly-N-vinyl-2-pyrrolidonethiooctadecyl
KKKA_5 KKKAAAAA
GFP Green Fluorescent Protein
AFM Atomic Force Microscopy
FTIR Fourier Transform Infrared

Contents

Chapter 1

Introduction

1.1 Challenges in DNA delivery

Nucleotide delivery has long been considered a promising approach to efficiently introduce genetic modifications to cells. DNA can cause expression of a foreign gene inside a cell, while other smaller nucleotides such as siRNA can change the expression of the cells native genome [1]. It is expected that these ideas will lead to therapies that can be use against certain diseases that have a genetic origin (cancer, Alzheimer's disease, etc). Despite how promising it is, nucleotide delivery suffers from several drawbacks that make it challenging for an intact peace of DNA or RNA to reach the interior of a cell. To understand the magnitude of this problem, it is interesting to look at the therapeutic agents that were based on delivering nucleotides and have been tested in clinical trials. Only 3 of all clinical trials have reached phase IV (proved efficacy) in the last 20 years. This represents a success rate of approximately 0.1 % [2]. This comes to show the difficulty of making a nucleotide delivery system that combines safety and high efficiency, and it motivates the need for constant research trying to improve them. In this section, the challenges of DNA delivery will be summarised to better understand the goal of this project.

The first problem for DNA application to healthcare is the frail nature of DNA itself. Several enzymes called DNases exist in *in vivo* and *in vitro* systems and they are specialised in degrading DNA. This means that, without protection, genetic material will not reach the interior of cells and be able to carry out its function. This has forced researchers to create different delivery vehicles for DNA that can protect the genetic information from degradation. In some cases, DNA is encapsulated in a virus [3, 4], which is naturally capable of injecting genetic material into cells while protecting it from environmental threats. Although this can be an efficient system, these viral delivery systems are questioned in terms of safety

due to adverse immune system response and production of toxins. Moreover, not all viral vectors have shown high efficacy (retrovirus) or are able to incorporate DNA in the cell's genome permanently (adenovirus) [4]. Because of this, non-viral delivery systems have been developed to overcome the shortcomings of viral systems, although none of them have yet proved high efficiency in clinical trials. These systems consist of particles made by encapsulating DNA inside polymer or lipids, which usually carries positive charges to condense the negatively charged DNA to a size of a few tens to a few hundred nanometers. [2]

The delivery systems above need to overcome several barriers to successfully deliver their DNA cargo inside cells and induce expression. First, the particles need to be able to protect the cargo from degradation completely, but they must also be able to enter the cell. Crossing the cell membrane is naturally done by viruses, so viral systems are usually effective, while polymeric systems need to be internalized by energy-dependent processes such as macropinocytosis. These internalization pathways have size limitations, and the fate of the particle and the cargo once it is inside the cell can vary depending on the method of entry (see Section 1.2.1). When dealing with *in vivo* systems, delivery to specific parts of the body can be even more challenging, as there is no way of easily controlling the destination of the delivery particles. In some cases, when cancer treatment is the main goal of DNA delivery, the enhanced permeability and retention effect (EPR effect) can be used. This effect is caused by the fact that tumors tend to be more leaky because of the inflammation of the vasculature around it, causing more particles containing DNA to accumulate in the tumor rather than other parts of the body [5]. This is a method of passive targeting that has been widely used, although there is some debate whether the EPR effect is a phenomenon that occurs in every solid tumor. For instance, in [6], they found differences in the retention of a fluorophore between sarcoma and carcinoma, two types of cancer. When the target of the delivery is not a tumor, specific targeting can be accomplished by coupling the delivery vehicle with some other molecule that can be recognized by receptors in cell membranes. For example, if the brain is being targeted, a particle can be coupled with glucose, which is one of the few molecules that can cross the blood-brain barrier [7].

Reaching and entering the cell is not the end of the delivery process. Once the particles carrying DNA enter the cell, they need to avoid lysosomal degradation and then they must be able to either fall apart, leaving DNA free, or target the cell nucleus and then disassemble. Disassembly is a necessary step to accomplish expression, because DNA cannot be condensed or encapsulated during transcription [8]. Interestingly, high efficiency in the protection given by the carrier can be detrimental to the chances of DNA being expressed inside the cell. While

viral delivery systems are naturally optimized to induce expression, in polymeric systems there can be a tradeoff between protection and expression. For instance, Kataoka et al. found that a polymeric system made of PEtOx-b-PnPrOx-b-PLys triblock copolymer was improving overall delivery expression thanks to increased protection of the transfected genetic material, but the actual rate of expression in a cell-free transcription/translation system was lower than for free pDNA [8]. This paper shows that designing a system which is efficient at every step in the delivery process is incredibly challenging. In one of the following section (section 1.3), the state of the art in this field will be reviewed to understand what is currently being done and how it could be improved.

1.2 Internalization pathways in cells and intracellular trafficking

1.2.1 Internalization pathways

Gene delivery vehicles need to be able to bypass the cell membrane so the cargo can be released in the cytoplasm, so it is necessary to understand the mechanisms that cells use to internalize foreign particles. Moreover, several transportation pathways exist inside the cell, some of which that lead to the destruction of the foreign particle. Understanding both of these processes is of the utmost importance for designing and evaluating any new nanocarrier, so this section will provide a short review of the literature that exists in the field, paying special attention to the most common internalization pathways. Phagocytosis, which is the process in which a cell engulfs a foreign particle, will not be reviewed because it is a process that is specific to some specialized cells called phagocytes that are not relevant for this work.

Cell internalization can be divided into two general types of processes: passive and active processes. The former not require energy consumption and they are usually associated with very small molecules that can diffuse through the membrane naturally; while the latter do require energy from the cell and they meidate entry o molecules and particles that are either too large or have some charge that makes passive diffusion impossible [9]. Since any particle bigger than a small molecule is not able to diffuse freely, DNA delivery systems have to be internalized actively. In practice, the division between passive and active is very generalist and there are several processes that are different from one another despite the fact that they all require energy (1.1). The most well-known of these processes is clathrin-mediated endocytosis. When a particle reaches a ligand on the membrane outer surface, clathrin attaches to the inner membrane and causes the formation of a pit. Once the pit has the shape of a vesicle, several proteins

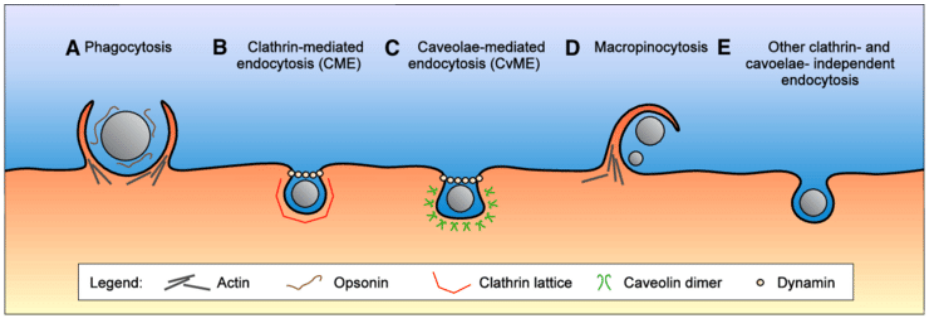

Figure 1.1: Active internalization in cells, including the discussed clathrin-mediated endocytosis, caveolae-mediated endocytoosis and macropinocytosis. Figure reprinted from [12] with permission, copyright Springer Nature 2009

(the most important one being dynamin) cleave it from the membrane, leaving it in the cytoplasm with the cargo inside. This type of endocytosis forms vesicles with a diameter between 80 and 200 nm, so no particle larger than that will be internalized through this pathway [10, 11].

Another active internalization process is caveolae-dependent endocytosis. Caveolins are a group of proteins that have a tendency to oligomerize in the cell membrane. The accumulation of caveolins, together with other molecules such as cholesterol, create a lipid raft. Lipid rafts are small sections of the lipid bilayer where there is an accumulation of cholesterol and sphingolipids, making the lipids be more tightly packed. These rafts have been found to mediate internalization of molecules such as growth factors , but not much is known about them, including the exact molecular composition of the rafts [13]. In the specific case of lipid rafts formed due to caveolin, it has been found that, similar to clathrin mediated endocytosis, vesicles are created by forming a pit in the membrane once a foreign molecule reaches it. Then, the mature vesicle is separated from the membrane by proteins such as dynamin. The diameters of these vesicles has been found to be between 50 and 80 nm [10, 11].

The last internalization pathway that will be discussed is macropinoctyosis. In the cell membrane there are certain regions that have a high concentration of actin filaments, projecting the membrane outwards and forming a lamellipodium. This type of region is called a membrane ruffle and it can stretch and then fold back creating a cavity completely surrounded by membrane. Then, that piece of membrane is detached, leaving a vesicle in the cytoplasm with a cargo inside [10]. Macropinocytosis is considered to be an non-specific pathway, which means that internalization does not depend on membrane receptors and any particle that is floating around the cell can be taken provided it is small enough. The cavities

formed by the membrane ruffles can be more than 500 nm in diameter [10, 11] so it is can be used to get larger particles inside the cell. Just like with lipid rafts, research on macropinocytosis is still necessary to uncover many unknowns, one of them being what is the best size and shape of particles to make internalization as efficient as possible [14].

1.2.2 Effect of particle properties on cell internalization

When any given foreign particle is delivered to cells, it will be internalized through one or more of the pathways described above depending on its properties such as size, shape or charge, among others. These properties will also define the efficiency of internalization and the rate at which the particles are absorbed by cells. Before starting reviewing this topic however, it is worth mentioning that there is still a huge debate around how these parameters affect internalization, and there are different groups that have published contradictory results. These discrepancies are probably caused by the difficulty to design an experiment where only one property of the tested particles is evaluated. In this section, several examples of papers in this field will be briefly reviewed , but a more extensive review of this topic with different points of view can be found in [15].

Size might seem to be the most straight-forward property to study, considering that the range of diameters for the vesicles formed in the different pathways is known. For instance, particles below 200 nm can be internalized through clathrin-dependent endocytosis and also macropinocytosis while much bigger particles can only enter the cell through the latter. This causes that smaller particles are internalized with higher efficiencies. However, smaller is not always better, as it was found that silica nanoparticles between 30 and 50 nm internalized better than particles below 30 nm [16]. Another interesting result regarding size can be seen in [17], where particles below 200 nm were internalized by clathrin-mediated endocytosis but bigger particles used caveolae-mediated endocytosis, despite the latter forming smaller vesicles than the former [10, 11]. This comes to show how results can be influenced by so many factors that it is difficult to come to a definite conclusion as to what size is best. It is even possible for some cells to change their shape to fit very large particles where one dimension is larger than the cell was originally [18]. One consistent result however, is that particles below 500 nm seem to be internalized by different types of cells [15], and even particles up to 3000 nm can be internalized in some cell types [14].

Shape of the particle also affects internalization, but once again there is disagreement over what shape is best. For instance, one group found that spherical

gold nanoparticles were internalized better than rods [19]. In contrast, in [14], it was found that rod-shaped hydrogel particles internalized better than spherical ones. Similarly, Banerjee et al. found that polystyrene particles that had shapes of a rod or a disk were better than spherical particles [20]. Again, the discrepancies are probably caused by the different interactions that different particles have with the cell membrane and its receptors. Moreover, certain situations that cannot be controlled during an experiment can also play a role in the results. For example, even the angle formed between particle and the line tangential to the cell membrane can play a role [21]. In summary, although shapes with higher aspect ratio seem to be favoured for internalization, there is also research supporting the advantages of spherical, more compact particles, so it is impossible to make an accurate prediction as to what shape is more desirable for a new particle, and it is necessary to test on a case by case basis.

The last property that will be reviewed is a particle's surface charge. There seems to be a general agreement that cationic particles are internalized more efficiently than negative or neutral ones [22, 23, 24]. It has also been found that positively charged particles tend to be absorbed through macropinoctytosis, in contrast to negatively charged particles that prefer clathrin and caveolin-dependent endocytosis [25]. It is worth pointing out that cationic particles have been linked to membrane disruption and cell death when the concentration of charges is high [26], so a moderately cationic particle would be a good tradeoff between internalization efficiency and cell survival. There are other properties of particles that influence internalization, such as hydrophobicity or mechanical properties like stiffness [15], but they are not so widely studied and they are less relevant for this project, so they will not be discussed further.

1.2.3 Intracellular fate of non-viral delivery systems

While crossing the cell membrane can pose a challenge, it is usually intracellular processes that limit the efficiency of delivery systems. So much so that they have been regarded as the 'bottleneck' of cell delivery [27, 28]. During internalization through the main pathways discussed above, foreign particles are found inside a vesicle called endosome. Endosomes mature to become late endosomes and then they fuse with a lysosome, which is a cell organelle that contains several enzymes for degrading foreign agents and avoid damage to the cell. These enzymes are capable of destroying the delivery system together with the DNA cargo, so it is of the utmost importance to bypass lysosomal degradation for efficient gene delivery.

Most polymeric delivery systems rely on the proton sponge effect to escape degradation by the lysosomes. This effect has been theorized to take place when there are groups with buffering capacity in the nanocarrier. Since the enzymes in

lysosomes need an acidic pH to work properly, protons are pumped inside the lysosome together with chloride ions by the membrane pump V-ATPase but, if the polymer inside can bind these protons, pH will not turn acidic. As a consequence, more and more hydrogen and chloride ions will be pumped inside, creating a concentration gradient across the membrane. This will lead to water entering the lysosome by osmosis and eventually pressure inside will grow so much that the membrane will burst [28, 27, 29]. This has been and still is the most widely-spread theory for lysosomal escape, and many nanocarrier designs rely on it. However, there are several unknowns about the exact process, while others even doubt the existence of such a mechanism [27]. Polyethylenimine (PEI) was the first polymer to be reported to induce the proton sponge effect thanks to all the amines it carries [29], but research by Benjamisen et al. showed that PEI did not cause a change in the normal pH of lysosomes by attaching two fluorescent dyes to the PEI that have different working pH ranges, allowing them to measure pH as a function of the signal of both dyes. Their results indicate that pH is acidic even when PEI is present, casting doubts on the escape mechanism proposed by the proton sponge effect [28]. Moreover, it has been reported that polymers with improved buffering capacities do not lead to better gene expression [30]. Still, there are groups that maintain that the swelling of the lysosome is still possible and it would be caused by the V-ATPase pump trying to maintain pH by pumping more ions.

More recently, a new theory explaining lysosomal escape has been formulated. This theory suggests that cationic polymer is able to intercalate with the lipid bilayer of the endosome and disrupt it momentarily, creating pores that can be used for nanocarriers to release into the cytosol. This would not lead to a complete destruction of the vesicle, but it would open the possibility of avoiding degradation before it starts. The cationic polymer can intercalate before, during or after the vesicle is fully formed, but the evidence seems to suggest that the pores are formed in the endosomal or late endosomal stage and not in the cell membrane proper [31, 32]. Moreover, it has been found that free cationic polymer increases delivery efficiency thanks to its ability to disrupt the membrane more easily. This phenomenon has been observed in studies where membrane-disruptive polymer has been added to cells together with a nanocarrier [30] and also when the polymer that is used to form the nanocarrier is added in excess [33].

The two theories above try to explain how a nanocarrier may escape degradation, but in order to get expression, DNA needs to reach the nucleus. One common strategy is to incorporate a nuclear localisation motif extracted from the SV40 T antigen [34] in the plasmid, but it is also common to simply wait for the cell to reproduce. During cell division, the nuclear membrane breaks, and foreign DNA can be incorporated into the cells genome [35]. However, the biggest

problem is that some delivery systems are so good at protecting the cargo that they do not disassemble in the cytosol, blocking DNA integration in the genome and expression. Osawa et al [8] found that a delivery system composed of tri-block copolymer exhibited great protection capabilities but, when the system was placed in a cell-free transcription-translation system, expression was lower than that of free DNA or a less protective system. Despite this, enough DNA was let free to allow expression and making the delivery systems better than other systems in real cells. Relying on spontaneous release of DNA in the cytosol is also common in this field.

1.3 Non-viral gene delivery: Polyplexes

Non-viral delivery systems hold great promise for introducing foreign DNA pieces in cells to genetically modify them. However, due to the poor efficiencies displayed by these systems so far, more research is till necessary to make them adequate for widespread use *in vivo*. In this section, a small review of non-viral delivery systems will be included in order to understand where the field stands now and what challenges still remain. The two main types of non-viral delivery systems are lipoplexes and polyplexes. The former are prepared by using cationic lipids that can interact with DNA and protect it, while the latter are made of cationic polymer that can condense DNA and form small aggregates in the nanometer range. Of these two, more emphasis will be made on reviewing polyplexes, as they are closer to the topic of this thesis, but some examples of lipoplexes and the advantages they provide will also be included.

As mentioned above, polyplexes are made of polymers that have some cationic side. The positive charges in the polymer are able to electrostatically bind to the negative charges in the DNA backbone and it has been found that, when the ratio of positive to negative charges is equal or bigger than three, the DNA is condensed [33]. This process reduces the size occupied by a piece of DNA, making it more likely that it will be internalized by cells. As has been described in section 1.2.3, positive charges in a nanocarrier can also mediate endosomal escape, which increases transfection efficiency, and the protection provided by the polymer prevents degradation of DNA by enzymes like DNases. The two most widely-used cationic polymers for DNA are poly-L-lysine and polyethylenimine (PEI), both of which have been used in different delivery system for a long time [36, 37]. Due to the positive charges they carry, they can condense DNA to form nanocarriers in the nanometer range, improving transfection efficiency in cells. Still, not all forms of these polymers have the same properties. For instance, it has been found that branched PEI is able to create smaller polyplexes compared to linear PEI, a difference that was attributed to the presence of secondary and

tertiary amines in the branched version [38]. In a different study, it was found that DNA condensates prepared with arginine-rich molecules increased stability of polyplexes when compared to lysine-rich compounds, even though both were able to form aggregates [39].

Nowadays, it is not common to use only a cationic polymer for nanocarrier formation. Instead, the properties of different polymer can be combined to incorporate new functionalities to polyplexes. This is usually done by synthesizing block copolymers with two or more blocks, each made with a different compound, one of which must be cationic to induce polyplex formation. The other blocks can improve the nanocarrier's properties such as protection against degradation or improved circulation in blood. For example, it was found that complexes of DNA and PEI cannot be easily dissolved in water, even though the two components alone can [38]. This could lead to poor circulation in blood during *in vivo* delivery, as well as aggregation and precipitation in water-based solution such as cell culture medium in *in vitro* experiments. To compensate for this, PEI can be coupled with a non-charged hydrophilic polymer that will be able to interact with water-based solvents while the PEI block interacts with the negative charges of DNA and condenses it. One example of such a system can be found in [40], where they synthesized a di-block copolymer by combining PEI and poly-ethylenglycol (PEG), which is hydrophilic. The resulting polymer was able to condense DNA into rod-shaped polyplexes, while the PEG block improved solubility in water and increased the protection of the cargo from nucleases.

The tuning of the properties of polyplexes can be taken even further by incorporating more components. Nomoto et al. synthesized a polyplex formed of three layers: an inner layer of cationic poly-L-lysine to condense DNA, an outer layer of PEG for improved protection and a middle layer of poly(N-(N-(2-aminoethyl)-2-aminoethyl)aspartamide) that was used to incorporate photosensitive dendrimer phthalocyanine particles. When pH turns acidic in the late endosome or lysosome and light is irradiated on the cell, the dendrimer phtalocyanine mediate the escape of plasmid DNA to the cytosol, thus increasing transfection efficiency more than a hundred times [41]. In this case, a third block was incorporated in the copolymer to induce endosomal escape while retaining the ability of poly-L-lysine to condense DNA and the increased protection offered by PEG. In another study, stability against degradation was improved by creating a polyplex made of a tri-block copolymer that had cationic and hydrophilic blocks as well as one that could transition from hydrophilic to hydrophobic at 30 ºC and was composed of poly(2-n-propyl-2-oxazoline). This allowed for easy polyplex formation below 30 degrees, but in a physiological environment, at 37 ºC, the thermoswitchable compartment created a hydrophobic barrier between the

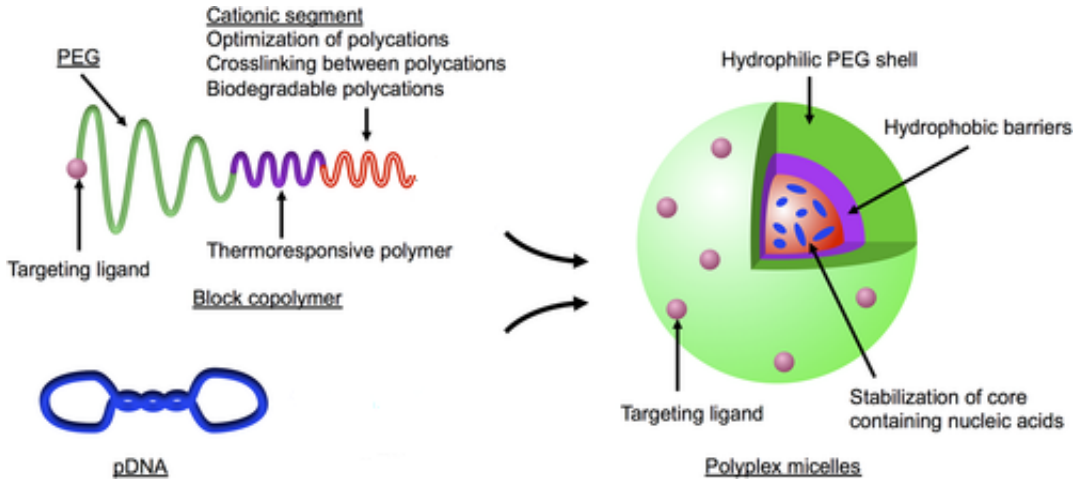

Figure 1.2: Example of polyplex formed by a cationic block, a thermoresponsive block and a PEG block that is attached to a cell membrane ligand. Figure adapted from [42] with permission, copyright John Wiley and Sons 2019

condensed DNA and the hydrophilic outer layer. Since nucleases are found and work in water-based medium, the hydrophobic wall increased protection of the cargo significantly [8]. These are only two examples, but they already show the great flexibility that polyplexes offer, and it opens the possibility of improving delivery systems based on specific needs (Figure 1.2).

Despite their versatility, polyplexes have only accomplished moderate success in gene delivery so far. In contrast to viral delivery systems, polyplexes have not evolved specifically to introduce DNA in cells and, as a consequence, they need to be internalized like any other particle and they end up in lysosomes, where they can be degraded. As explained in section 1.2.3, escape of the polyplexes into the cytosol is the most limiting step in the delivery process, reducing the efficiency of these systems. Another drawback of polymer-based delivery system comes from the fact that enhanced shielding of DNA is usually related to poorer expression in cells because DNA needs to be free to be transcribed. This effect can be seen in the paper by Osawa et al. mentioned above [8], where they tested their polyplex in a cell-free transcription/translation system and found that overall expression was lower than for free plasmid. In summary, polyplexes only improve delivery because they allow a higher amount of DNA to reach cells unharmed, but a smaller percentage of the genetic material that enters the cell is actually expressed. This tradeoff does not exist in viral systems, as they provide protection for the cargo and then they release it free in the cytosol [43]. Finally, another drawback of polyplexes is that polymers carrying many positive charges have been reported to cause cytotoxicity, with the effect being more pronounced in places of the body

where particles tend to accumulate such as the liver or lungs [44, 45].

Lipoplexes are also used as non-viral delivery systems. They consist of lipids that often have a non-charged tail and a cationic head that can interact with DNA. However, DNA is not always condensed to the same degree as with cationic polymers. One typical structure found in lipoplexes is composed of multiple monolayers of lipids that trap DNA in between them. Another structure that has been found in lipoplexes is a honeycomb structure in which DNA is compressed inside seven cylinders formed with the lipid [46]. These structures tend to be bigger than polyplexes so internalization is not as easy, so there have been attempts in which lipids have been coupled with some ligand that binds to a receptor of the cell membrane such as transferrin [47]. On the other hand, lipids provide an effective protective layer that can be superior to polyplexes. Some notable examples of cationic lipids that have been used for transfection include DOTAP, DV-Cholesterol and DOSPA [46].

As a final remark, it is important to point out that there is the possibility of combining polyplexes and lipoplexes to take the best of each system. The result is called lipopolyplex, and it usually consists of a cationic polymer coupled with a neutral lipid. This gives the resulting molecule the ability to condense DNA to very small sizes while retaining the enhanced protection provided by lipids[48, 49]. It has also been found that these structures cause lower cytotoxicity and can be coupled with ligands to target receptors of the cell membrane and increase transfection. These systems are promising tools for gene delivery, but most research in this topic is relatively new, with a majority of papers being published since 2010 (according to Google Scholar statistics), so more research is still necessary to make this kind of delivery systems good enough for clinical purposes.

1.4 Fourier Transform Infrared Spectroscopy

Fourier transform infrared spectroscopy (usually shortened as FTIR spectroscopy) is an analytical technique that is able to detect certain chemical groups found in a sample. As its name suggests, FTIR spectroscopy uses radiation in the infrared part of the spectrum, which has low energy, and therefore samples are not damaged during the analysis. This technique is able to detect different chemical groups because covalent bonds between atoms can move, bend, stretch or perform other movements, and that means that, for every bond, there is a resonance frequency associated with it [50]. When infrared light containing several frequencies hits a molecule, some energy will be absorbed, but the absorbance will be higher for the resonant frequencies of the bonds found in it. This means that by

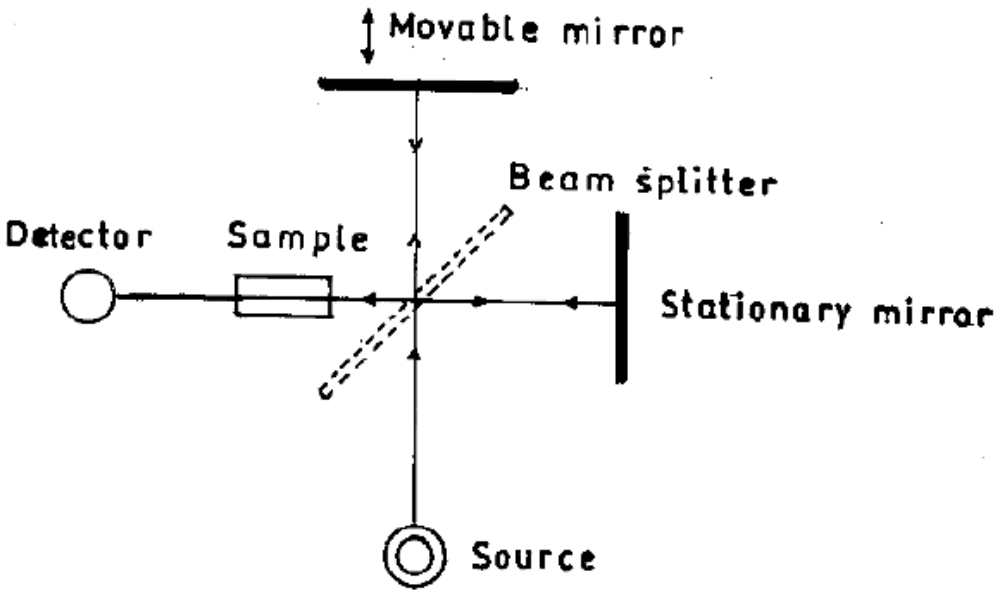

Figure 1.3: Simple diagram of the Michelson interferometer that is used in FTIR spectroscopy. Figure printed from [53] with permission, copyright Springer Nature 2006

recording the amount of absorbed infrared light at every frequency, a fingerprint of the molecule is obtained in the form of a spectrum [51, 52].

The most common tool for performing FTIR spectrosocpy is the Michelson interferometer (Figure 1.3). In this piece of machinery, there is a beam splitting glass that separates the ray of infrared light in two equal beams. One of the beams travels to a fixed mirror and it rebounds, while the second beam travels to a moving mirror and then it also rebounds. The two beams reunite at the glass, but they are no longer equal. Since one of the mirrors is moving back and forth, the beam reflected from it will have to travel a shorter or longer distance than the other beam, so they might be out of phase when they reunite. This causes that, depending on the position of the moving mirror, the total intensity of the reunited signal can vary in intensity, having the original intensity as a maximum and a complete interference as a minimum. After this, the light is shone on the sample and the absorbance is recorded. Then, a plot of absorbance versus mirror position called interferogram can be constructed and, applying Fourier transform, the interferogram is converted into a spectrum, in which absorbance is a function of wavenumber [51, 52]. The results are recorded and processed by a computer, so the Fast Fourier Transform algorithm is commonly used. In the end, a the spectrum will show peaks at the wavenumbers that resonate with some bond found in the ample, so some structural information about it can be obtained. For

example, around 1600 to 1700 cm^{-} there is a region referred to as the amide I band. A peak in this region is usually associated with the stretching of a double bond between carbon and oxygen [52]. In summary, FTIR spectroscopy can be used to learn information about the composition of a sample in a fast, simple and non-destructive way but, contrary to other techniques like NMR, the information provided by it is usually insufficient to obtain a full description of the molecules found in the sample [51].

1.5 Atomic force microscopy

Atomic force microscopy (AFM) has been used extensively during this thesis to evaluate different characteristics of the developed gene delivery system. In this section, a short of review of the theory behind this technique will be provided. AFM is a scanning probe microscopy technique that measures the topography of a surface. The scanning is performed using a small (nanometer range) tip whose atoms interact with the atoms found on the surface, creating either an attractive or repulsive force. The tip is attached at the end of a flexible cantilever that will bend in different ways depending on the forces acting on the tip. By shooting a laser at the cantilever and reading the reflected light in a photodiode one can translate the force acting on the tip to something that can be easily measured such as the position of a laser (Figure 1.4). The AFM system is calibrated at the start of a measurement such that the laser hits exactly in the middle of the diode, making the recorded voltage on the upper side of the photodiode equal to that of the lower side. When the force applied on the tip changes, the laser moves, and the difference between these two voltages changes, indicating the extent of such a force [54, 55].

The force that a tip feels changes depending on the distance between it and the surface. When the two are very close, a repulsive force appears due to the overlap between the orbitals of the atoms, but when the two are further away, an attractive force appears, mostly caused by Van der Waals interactions [54]. Nowadays, most AFM systems work by trying to maintain a constant distance between tip and surface by moving the tip up or down, and the laser is used as feedback to ensure that the force and therefore the distance remain constant. Recording the position of the tip with respect to the surface, a map of the roughness of the surface is obtained and, if there is any larger structure deposited on the surface, it appears as a mound of the same height. AFM can operate in different modes: contact, semi-contact (also called tapping mode) and non-contact. As the name implies, in the first mode, the tip is touching the surface all the time while taking the measurement. This poses a problem, as the tip can easily break if it hits a large structure or, in the cases of soft samples such as biological material,

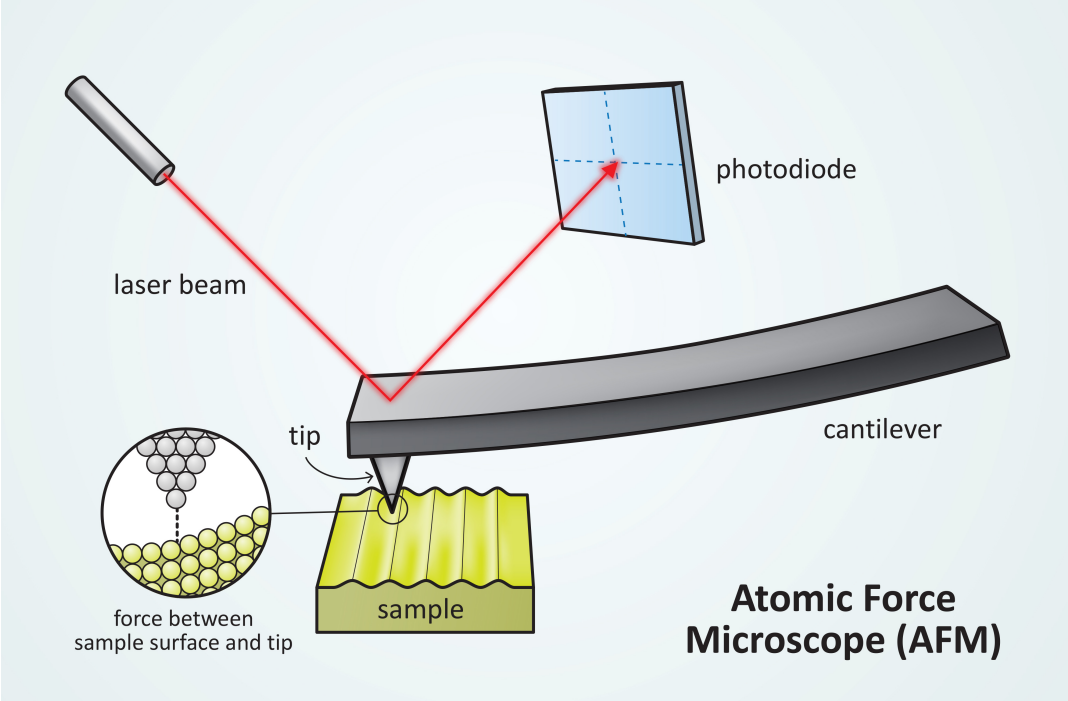

Figure 1.4: Example of the setup of an AFM machine. The tip atoms interact with the surface atoms, causing the cantilever to bend, which is measured by the reflection of laser. Figure reprinted from [56](this image was originally published under Creative Commons license)

the sample itself can be damaged. In non-contact mode, the cantilever is set to oscillate above the surface so that the tip never touches the surface, removing the problem of sample or tip damage but also reducing the ability to reconstruct the topology of the sample due to the forces being weaker. As a middle ground between the contact and non-contact there is tapping mode, in which the cantilever is set to oscillate close to its resonance frequency and the tip makes contact with (or gets very close to) the surface when it is at the lower point of the oscillation. This means that the profile of the surface is measured similarly to contact mode, but the tip is not touching the surface all the time during scanning, reducing the possibility of damage to the tip or to the sample. The laser is used as feedback to control the amplitude of the oscillation and maintain a constant interaction between tip and surface [55, 57]. This mode is the one that has been used for all the AFM experiments that have been performed in this thesis, as it provides a good balance between accurate topological information and preservation of the samples.

1.6 Experimental evaluation of cytotoxicity

One of the most important features when developing any delivery system,if not the most important, is that it must not be toxic to cells. Even if a system is able to deliver its cargo efficiently, it cannot be used if it causes high levels of cell death, especially for *in vivo* applications due to the possible health problems (e.g. tissue damage). In this work, a system consisting of polymer and small cationic peptides will be used to condense DNA and assemble a gene delivery vehicle. Therefore, it is necessary to asses the cytotoxicity of each of these components and of the final particle. There are many different assays for determining toxicity. Some common types include fluorimetric, colorimetric, luminometric and dye exclusion assays. Although they all have advantages and disadvantages, in this work an LDH release assay will be used, which belongs to the fluorimetric category. This kind of cytotoxicity assays are widely-used as they tend to have higher sensitivity [58]

This assay estimates cytotoxicity percentage by indirectly measuring the amount of lactate dehydrogenase (LDH) present in the culture medium. LDH is usually present in trace amounts in the mediums that are used for this test, but it can be found mostly inside cells. Once cells die, their membranes fall apart, releasing the content of the cytoplasm. Because of this, the amount of LDH found in the medium is directly proportional to the number of dead cells. When LDH and NAD+ are present, lactate will be converted to pyruvate and NADH will be formed. The latter will then be used as a proton donor for the reaction that transforms resazurin into resorufin with the aid of the enzyme diaphorase.

Resorufin is fluorescent, so the amount present in a sample can be easily measured by observing the fluorescence intensity at an excitation wavelength of 560 nm and emission wavelength of 590 nm [59].

In order to test the toxicity of a certain molecule, a cell culture must be incubated with the molecule and then the substrate buffer is incorporated to generate resorufin. Then, a stop solution provided in the kit is used to stop the formation of the fluorescent molecule, and the intensity is measured. In order for the assay to give meaningful information, it is of the utmost importance to use controls. A lysis solution that will kill almost all of the cells present in the culture well serves as a positive control that sets an upper bar for the intensity that corresponds to maximum toxicity. Another key control is a background measurement of the fluorescent intensity. LDH might be present even before cell death due to the serum that is used to make the culture medium containing high levels of LDH. That is the case of fetal bovine serum [13], while others such as horse serum have much lower levels. The background intensity must be subtracted from the measured values to obtain the true results that reflect the percentage of cell death. For any given sample, the percentage of cell death can be computed as:

$$\%Celldeath = \frac{Measuredintensity - Backgroundintensity}{Positivecontrolintensity - Backgroundintensity} \tag{1.1}$$

1.7 Electroporation

Transfection of foreign DNA into mammalian cells is significantly more difficult than bacterial transformation. The cell membrane is less permeable, so forming pores is often the only option to achieve a high delivery success. However, contrary to bacteria, the disruption of the membrane can, under certain circumstances, lead to high cell death [60]. There exist several transfection methods such as microinjection or chemical transfection, but electroporation is the most widely-used thanks to its high levels of efficiency in many cell lines [60, 61]. This technique creates pores in the cells by applying a voltage, allowing free pieces of DNA to enter the cytosol (Figure 1.5). Given its versatility and widespread use, electroporation has been selected as the baseline to evaluate the performance of the nanocarrier that has been developed in this project.

As mentioned above, electroporation consists in creating pores in the cell membrane by applying a voltage, allowing certain molecules like DNA to move inside the cell, even if they are not able to cross the membrane under normal circumstances. Because of this, this technique is often referred to as electropermeation. When a voltage is applied, the potential across the cell membrane suddenly

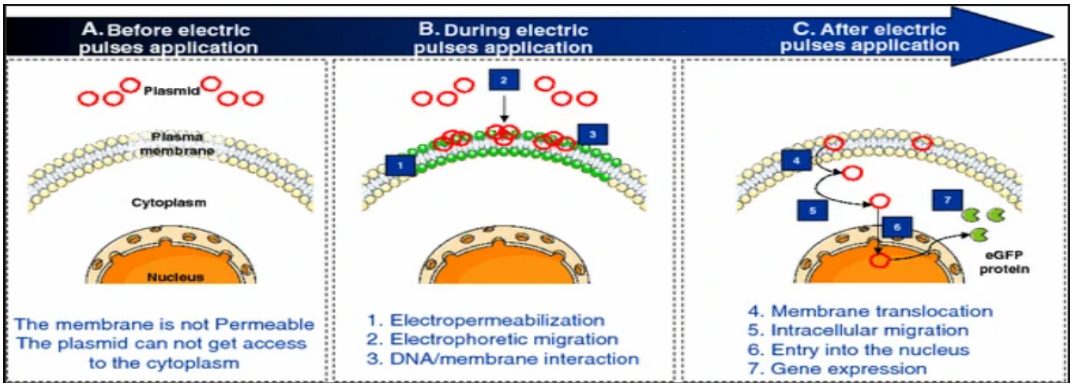

Figure 1.5: Illustration of the electroporation method of gene transfection. Reprinted from [62] with permission, copyright Springer Nature 2008.

changes, disrupting its natural state. In response, the cell membrane opens pores that are quickly filled by the extracellular medium, which helps reduce the voltage drop across the membrane [63, 64]. These pores are usually small in size, but sufficient for molecules like DNA plasmids to go through due to diffusion and convection. As long as the external voltage continues to be applied, the pores tend to grow larger, but when the voltage is removed and the membrane potential is restored, the pores collapse. However, if the holes grow up to a critical size, they may continue to grow after the electroporation process is over, leading to cell death. Cell damage can also be mediated by stable pores being formed in some section of the membrane [65, 64].

Considering that, before reaching a critical size, pores can only grow as long as an external voltage is applied, different methods have been developed to control exposure time. One option consists in regulating voltage as a periodic square function, alternating high potential phases with low potential phases. Another option consists of using a capacitor to store energy, and then use it to deliver the desired voltage. As time goes by, the total applied voltage decreases exponentially as the capacitor discharges the stored energy. This method ensures that a high voltage can be applied to the cells to improve pore formation while reducing the total exposure time [66]. The best way to quantify the discharge time is to calculate the time constant of the voltage drop. This constant is defined as the time it takes for the voltage to decrease to 37 % of its maximum, and it can be estimated as $\tau = C * R$, where C is the capacitance and R is the electrical resistance of the sample. In practice, τ is measured by the electroporation machinery, giving a good indicator about the success of the process [63].

There are different factors that influence the efficiency of electroporation,

the most important ones being the strength of the applied voltage, the medium of the sample, the cell density and the time constant mentioned above. The latter is strongly related to the choice of medium for the cells, as a solvent with high ionic strength such as PBS will lead to a higher voltage drop across the sample, that is, a higher voltage is applied to the cell membrane. This is usually desirable for mammalian cell transfection. The amount of cells that are present can also have an effect on the conductivity of the sample. Typically, a density between $5x10^6$ and $1x10^7$ cells/ml yields good results. Finally, the maximum applied voltage is also a key factor because, if it is too low, not enough pores will be formed, leading to very low transfection efficiency. If instead, it is too high, the membrane disruption might be too strong and cause high cell death. According to the literature, voltages between 0.2 to 0.5 kV are commonly used [61].

It is important to consider that, even if electroporation is a useful transfection method, it still has limitations. First, cell survival can be low, especially if some of the parameters of the experiment are not optimized, leading to low overall efficiency. Secondly, and perhaps more importantly, this transfection method is limited to *in vitro* cell cultures, which limits its use to the laboratory. Moreover, it has been found that large plasmids with 10 kilobases or more have quite lower transfection efficiencies [67], so incorporating large genes such as Cas9 (more than 6000 bases not counting regulatory sequences) via electroporation can become quite challenging.

1.8 Project description and objectives

Delivery systems for DNA could help improve the therapeutic use of gene therapy in several diseases, so creating new designs that can overcome the existing limitations in the field is still necessary. Because of this, this thesis will attempt to create a new DNA nanocarrier that can safely and efficiently transfect human cells with a plasmid. This new delivery system will be build using poly-N-vinyl-2-pyrrolidone thiooctadecyl (courtesy by Prof. Shtilman, Mendeleev University of Chemical Technology of Russia, Moscow, Russia), commonly referred to as PVP-OD, an amphiphilic block copolymer that has been previously used in drug delivery systems [68]. The polymer has a hydrophilic block, poly-N-vinyl-2-pyrrolidone, and a hydrophobic block, thiooctadecyl, so when the polymer is found dissolved in a polar solvent it will tend to form micelles, with the hydrophobic groups shielded of the inside and the hydrophilic groups interacting with the solvent. PVP-OD can be synthesized with different weights, but throughout this project 12 kDa PVP-OD has been used. Previously, PVP-OD has been approved as a safe material to use in humans by the FDA and it is generally accepted that PVP-OD below 20 kDa is not harmful for humans [69]. Moreover, the fact that it

includes a hydrophobic block can enhance protection of the cargo, as nucleases act in hydrophilic environments [8]. Because of this, it is a perfect candidate for developing a new DNA delivery system.

The main reason why PVP-OD has not been used for gene delivery so far is that, as has been mentioned before, DNA needs to be condensed with positive charges to be able to fit inside a carrier and be delivered, but PVP-OD has no such charges. To compensate for this, a short cationic peptide composed of 3 arginines and 5 alanines will be synthesized and then coupled to PVP-OD by means of amide bonds. This is possible because PVP-OD has acrylic acid groups which allow linking of other molecules using EDC/NHS coupling. It is expected that the charges of the peptide will be enough to condense DNA down to a size that can be integrated by a cell. One advantage of using short peptides is that the total number of charges that are introduced in the body is reduced compared to cationic polymers. It has been found that molecules with many charges can cause damage, specially in the liver [44, 45], so reducing the charges also minimizes the risk of adverse effects. Moreover, production of short peptides is relatively easy and inexpensive, so it might be a good alternative to the synthesis of cationic polymers [70]. The plasmid that has been selected for transfection is composed of 10 kilobases and it contains the genes for the nuclease Cas9 and for Green Fluorescent Protein (GFP), optimized for expression in mammalian cells. The latter is included in the plasmid as a reporter gene to check if transfection has been successful. The transfection efficiency has been tested previously in stem cells and expression of GFP was obtained, but it remains to be tested in primary cells such as fibroblasts [71]. The main objectives of this project can be summarised in the following points:
1. Assemble the new DNA nanocarrier using the components stated above.
2. Characterize the nanocarrier in terms of size, shape and other relevant parameters.
3. Test the safety of the nanocarrier components in human fibroblasts and establish a range of concentrations that do not lead to widespread cell death.
4. Test the transfection efficiency of the new DNA nanocarrier in human fibroblasts and compare it to a control transfected by electroporation.

1.8.1 Limitations of 2D culture experiments

Throughout this work, all of the cell experiments took place *in vitro*, in two-dimensional cultures. This is a standard procedure for testing new biological agents (drugs, polyplex, lipoplex, etc.), as it is not legal or ethical to use a completely new, unknown compound in humans or even in animals. However, after reviewing the literature, it becomes apparent that 2D cell cultures have certain limitations that make them significantly different to more complex systems

such as the human body. In this section, said limitations will be summarised in order to understand the real scope of the experiments that have been performed.

The first limitation of traditional cell cultures lies precisely in the fact that it is two-dimensional, in contrast to the complex 3D environments that can be found in the human body. This has a profound effect on how DNA nanocarriers would be distributed among the cells, as some of them are more exposed to the blood flow than others. This unequal distribution does not happen in the 2D culture, where there is a layer of cells submerged in culture medium with the nanocarrier particles evenly distributed inside. This discrepancy between 2D culture and *in vivo* systems makes a difference in key parameters such as transfection efficiency or cytotoxicity. If a specific tissue or organ has to be transfected, one cannot assume that the efficiency will be as high as for 2D culture because not all cells will be equally exposed to the nanocarrier. As for the toxicity, the fact that concentration is not uniform could mean that a high amount of nanocarrier accumulates in one place, leading to higher cell death than what is observed in a culture plate. An example of this can be seen in [44], where a cationic polyplexes were tested *in vivo*, and it was observed that, at certain concentrations, damage could be observed in the liver but not so much in the rest of the body, because the polyplexes were accumulating when they were being removed from the body.

Another difference between traditional 2D culture and complex systems such as the human body relates to the fact that, in cell cultures, there is usually only one type of cells instead of multiple highly specialised cell types that can be found in the body. That means that some of the basic physiology and behavior changes in different parts of the body, making it difficult to translate the results obtained in 2D cultures to *in vivo* systems. Moreover, in a human body, many different tissues and systems and apparatus exist, and this makes the problem of nanocarrier delivery fundamentally different to 2D experiments. In cell cultures, nanocarrier-containing medium is added to cell and allowed to incubate for at least several hours, so the probability of particles reaching the cells is high. However, in a human body, the nanocarrier would have to circulate through blood before it can reach the target cells, increasing the chance for removal or degradation. This drastically reduces the efficiency, especially if a very protected organ such as the brain (it is separated from most components in the blood flow by the blood brain barrier) is targeted.

Because of these reasons, it becomes clear that the results obtained in 2D cell culture experiments cannot be directly extrapolated to real *in vivo* systems, so it is necessary to design better experimental setups to confirm whether the designed nanocarrier is actually efficient and safe. One option that has become

popular in recent years is to use microfluidic chips that are designed to better mimic *in vivo* conditions while still working *in vitro*. For instance, a chip with flow through it is a dynamic system and it is therefore a more accurate representation of how the nanocarrier would reach cells through the blood flow. Moreover, because these chips are miniaturized and work with small volumes it is relatively inexpensive. It is also possible to culture different types of cells and to build membranes that can shield them from the flow in a similar way to the endothelium in animal bodies. Considering how useful such a system could be, this thesis includes a proposal of a microfluidic chip that could be used to further test the developed DNA nanocarrier. To aid in the design of this chip, a model has been created in COMSOL Multiphysics that attempts to replicate its behaviour, allowing the user to test different geometries and conditions easily before spending time and money for building a chip. Because of this, a new objective is defined for the project:
5. Given the limitations that the *in vitro* experiments have, a microfluidic system for more efficient testing will be proposed and a model will be developed in COMSOL Multiphysics 5.5 to aid in the design of such a device.

1.8.2 Fmoc solid phase peptide synthesis

In this work, a short cationic peptide with the sequence KKKAAAAA will be synthesized using fmoc solid phase synthesis to be used in DNA condensation. This method of peptide preparation consists in sequentially adding each amino acid to a growing chain that is attached to a solid resin. The C-terminal of the first amino acid will react with the N terminal of the resin, while all the other amino acids will bind to the N terminal of the last one that has been added to the chain [72, 73]. In order to control the growing of the chain and ensure that the final amino acid sequence is the expected one, all of the N-terminals are protected by an fmoc group. While this group is still present, no incoming amino acid can bind to the N terminal of the growing chain, and instead it is necessary to remove this fmoc group to continue with the synthesis. The step of removing the fmoc group from a growing peptide chain is known as deprotection, and it can be done by adding piperidine, which cleaves fmoc, creating the byproduct dibenzofulvene. By monitoring changes in absorbance caused by this byprodcut, it is possible to evaluate how successful deprotection has been and, if efficiency has been low, more time or deprotection steps can be performed [70].

The entire process of synthesis starts with the deprotection of the N terminal of either the growing chain or the resin (in the first step). Then, the next amino acid to be added in dissolved, activated and added to the vial containing the resin so that it can form an amide bond with the deprotected N terminal of the growing chain. The newly incorporated amino acid still has the fmoc protective group, so

it will not be possible for more than one amino acid to bind to the peptide chain at each step. This process has to be repeated until the peptide has reached the desired sequence. At this point, the peptide can be cleaved from the resin using TFA [72].

Fmoc peptide synthesis is one of the most widely used methods for preparing custom short peptides. It provides great versatility regarding the sequence and properties of the peptide, and most of the components needed for the synthesis are relatively inexpensive [70]. Thanks to the fmoc groups, the yield and purity of the final product is significantly increased but, if necessary, the resulting peptide can be purified using chromatography.

1.8.3 Cross-linking PVP-OD to $KKKA_5$: EDC/NHS coupling

In order to assemble the DNA nanocarrier, it will be necessary to cross-link the polymer PVP-OD to the short cationic peptide that will be synthesized so that it carries positive charges that can condense DNA. Some stock of the 12 kDa PVP-OD has been modified to have acrylic acid groups. The degree of substitution ranges from 10% to 95%, meaning that the amount of peptides bound to every PVP-OD molecule can be tuned. Since acrylic acid contains a carboxylic group and the peptide has a primary amine in its N-terminus, EDC/NHS coupling is the best option for cross-linking.

EDC/NHS coupling is a chemical process that forms an amide bond between a carboxyl group and a primary amine. EDC is a zero length cross-linker, as it allows the reaction to take place but it is completely removed upon completion of the coupling [74, 75]. EDC must be mixed with the molecule that has the carboxyl group, and it will form an intermediate, O-acylisourea ester. If a primary amine is then added to the mixture, an amide bond will form, while the EDC will be released as an isourea byproduct [75]. The main problem with this is that the intermediate ester is highly unstable in water environments because it undergoes hydrolysis and the original carboxyl group is recovered. This can severely hinder the efficiency of coupling. As a solution to this problem, N-hydroxysuccinimide (NHS) is also added to the reaction. NHS reacts with the o-acylisourea ester, forming a stable, amine reactive, NHS ester. When the amine is added, the amide bond forms as it did when only EDC was used, leaving no part of NHS behind [tHERMO]. Sometimes, sulfo-NHS is used instead of NHS, as the former is more soluble in water.

The buffer for the reaction can vary depending on the solubility of the molecules that are being coupled, but regulating the pH can improve efficiency. In the beginning, when EDC and NHS are added, the pH will most likely be acidic, as

EDC is usually bought as a hydrochloride. This will favour the formation of the intermediate esters, but the formation of the amide bond itself is more efficient in slightly basic pH between 7,5 and 8 [74]. Because of this, it can be beneficial to adjust the pH when the amine is added, for instance by mixing DIPEA. DIPEA is a proton scavenger, so it will increase the pH, but it is also a very poor nucleophile, so it will not compete with the primary amine to form an amide bond [76].

Chapter 2

Materials and methods

2.1 Solid Phase Peptide Synthesis

In order to condense DNA, the cationic peptide KKKAAAAA was synthesized using Activo-P11 automatic peptide synthesizer (Activotec). For each lysine in the sequence, 351 mg of Fmoc-Lys(Boc)-OH (Activotec) powder was weighted, while 233 mg of Fmoc-Ala-OH (Activotec) were measured for the alanine residues. Dimethylformamide (DMF, Iris Biotech GMBH) was used for the cleaning steps and also as a solvent for other solutions used in the synthesis. A solution of 0.5 M Hexafluorophosphate Benzotriazole Tetramethyl Uronium (HBTU, Iris Biotech GMBH) and 0.5 M Oxymapure (Iris Biotech GMBH) in DMF was used as a coupling agent for the amino acids and a 1 M N,N-Diisopropylethylamine (DIPEA, Tokyo Chemical Industry) in DMF solution was used as proton scavenger. 25 % (v/v) piperidine (Iris Biotech GMBH) in DMF was used as decoupling reagent and dichloromethane (DCM, Iris Biotech GMBH) for. Rink MBHA amide resin with loading capacity of 0.56 mmol/g (Sigma Aldrich) was used as the substrate for growing the peptide so 273 mg of resin were weighted in the the reaction vial.

For each amino acid that was added to the growing peptide, the cycle performed by the machine was as follows: 1) Use piperidine solution to deprotect (remove Fmoc group) the last amino acid in the chain, 2) Dissolve the amino acid powder with HBTU/Oxymapure solution, 3) Add DIPEA solution to the already dissolved amino acid, 4) Introduce the amino acid solution to the reaction vial and 5) Shake reaction vial to allow for coupling of the amino acid to the growing peptide chain. Every time the reaction vial was emptied, it was rinsed with DMF before moving to the next steps. Every deprotection step cycle consisted of at least two deprotection steps (one step consists on introducing piperidine solution to reaction vial, shaking for 10 min and emptying), after which the UV absorbance value of the solution after emptying the vial was below a threshold (set to 120

in this case). If absorbance was above, up to three more deprotection steps were carried out until the absorbance was below the threshold.

After synthesis, the peptide was cleaved from the resin using the Activo-P12 cleaving machine (Activotec). First, 5 ml of a solution containing 95% trifluoroacetic acid (TFA, Iris Biotech GMBH), 5% triisopropylsilane (TIS,) and 5% dH_2O were prepared and added to the reaction vial. Then the vial was placed in the Activo-P12 and it was shaken for 40 min before emptying the solution into a 50 ml Falcon tube. Then, 5 ml of pure TFA were added to the vial and shaken for 5 min before emptying again in the tube. 10 ml of ice cold diethylether (Iris Biotech GMBH) were added to the Falcon tube before centrifuging at 4 ºC for 10 min. After centrifuging, the supernatant was discarded and the pellet was re-suspended in 10 ml of diethylether, followed by 10 more min of centrifuging. The process was repeated one more time to ensure that the synthesis product was in the pellet. Finally, some holes were made in the tube's lid before placing it in the Christ Alpha 1-4 LD plus (Martin Christ Gefriertrocknungsanlagen GmbH) for freeze drying overnight. The final product powder was kept at -4 ºC for long-term storage.

2.2 DNA Amplification and Extraction

The plasmid pCas9-GFP was amplified and extracted starting from a glycerol stock of transformed Escherichia coli cells.

2.2.1 LB-agar plates and LB medium preparation

LB-agar solution was prepared by mixing 10 g/l tryptone (Sigma Aldrich), 5 g/l yeast extract(VWR), 5 g/l sodium chloride (VWR) and 15 g/l agar (Sigma Aldrich) in water. Another solution was prepared using the same components except for agar, to be used as liquid culture medium. The solutions were autoclaved at a temperature of 121 ºC and a pressure of 1 bar for 30 minutes to ensure sterility and, then, they were allowed to cool down below 60 ºC before adding 100 μg/ml of ampicillin, which worked as a selection marker to grow bacteria that had internalized the plasmid only. Finally, the LB-agar solution was poured into Petri dishes and allowed to solidify before storing the plates at 4 ºC together with the liquid LB medium.

2.2.2 Plasmid extraction

In order to recover the transformed bacteria from the glycerol stock, a pipette tip was dipped into it and introduced in a tube containing 5 ml of LB liquid culture medium. The tube was left at 37 ºC overnight with constant shaking (300 rpm) to

allow bacteria to grow. After checking that bacteria had indeed grown, some of the liquid was spread on a Petri dish containing LB-agar and ampicillin using a sterile cell spreader. The plates were incubated overnight at 37 ºC to allow the growth of bacterial colonies. The morning after, one colony was picked up from the plate with a pipette tip to do another liquid overnight culture. Finally, the plasmid of interest was extracted from the liquid culture using the protocol of the GeneJET Plasmid Miniprep Kit (Thermo Scientific). First, the liquid culture was centrifuged to spin down the bacteria and the liquid medium was discarded. Next, the bacteria in the pellet were resuspended in 250 μl of the Resuspension solution provided in the kit and 250 μl of Lysis solution were also added to induce cell breaking. After less than 5 minutes, 350 μl of Neutralization buffer were added to avoid damage to the plasmid. Then, the solution was centrifuged, causing all cell debris to form a pellet while the supernatant containing the plasmid was transferred to an spin column and centrifuged once more. The plasmid was trapped in the column's filter, while the rest of the liquid passed through and was discarded. The spin column was then washed twice using 500 μl of Wash solution and the empty column was centrifuged without any solution to remove any impurities from the plasmid in the filter. Finally, 50 μl of elution buffer were added to the column, which was incubated for 2 min and the centrifuged one last time to allow for the plasmid to go through the column. The solution containing the plasmid was stored at -20 ºC.

2.2.3 Plasmid analysis

In order to confirm that the extracted plasmid was pCas9-GFP, 5 μl of DNA solution were mixed with 1 μl of Purple Dye (New England Biolabs) and loaded in a 1% agarose (VWR) gel. 6 μl of 1 kB ladder (New England Biolabs) were also loaded for reference. The gel was submerged in 1X TAE buffer inside an electrophoresis chamber and a voltage of 80 mV was applied for one hour. Then, the gel was visualized under UV light to observe the DNA bands that were present.

The final concentration of purified DNA was determined using a Picodrop™ Microliter Spectrophotometer (VWR), which calculates DNA concentration in solution. First, the absorbance of 2 μl of only solvent was measured to be used as baseline. Then, 10 measurements were taken with 2 μl of DNA solution. The average of these 10 measurements was henceforth considered to be the true concentration of the purified DNA.

2.3 AFM imaging of DNA aggregates

2.3.1 Substrate preparation and functionalization

Mica substrates were coated with APTMS to help the deposition of DNA onto them. First, 750 μl of toluene (Sigma Aldrich) were mixed with 250 μl of APTMS (Sigma Aldrich) inside an eppendorf tube. Then, the mica wafers were cleaved using tape and placed inside a vacuum chamber together with the eppendorf containing APTMS, which had the lid off. Once everything was in the chamber, the air inside was pumped out for 5 minutes before filling it again with argon, waiting 10 minutes, and pumping the gas out again. The wafers were left in the chamber for 1 hour to ensure complete functionalization by APTMS.

2.3.2 Determination of condensing properties of synthesized peptide

Once the wafers were removed from the chambers, different procedures for deposition were followed depending on the experimental setup. For free DNA visualization, 30 μl of DNA solution (2.5 μg/ml) were added on top of the substrates, which were then incubated for 10 minutes at room temperature. Then, deionized water was used to rinse the wafers before drying them with N_2. The same was repeated to prepare a sample with 30 μl of only peptide solution (1 mg/ml). In the first condensation experiment, 15 μl of DNA solution were mixed with 15 μl of peptide solution before depositing on the wafers. Then, the wafer was incubated at room temperature for 15 minutes before cleaning it with deionized water and drying it with nitrogen gas. In later experiments, the same mixture of DNA and peptide was used but incubation time was increased to 2 hours. Finally, some samples were prepared in the same way but using a DNA solution with twice the concentration. Every time that a new sample was prepared, a free DNA control was prepared as detailed above to ensure that the plasmid was indeed present in the solution. The samples were imaged using AFM in tapping mode with a cantilever with resonance frequency equal to 250 kHz.

2.3.3 Condensation of DNA by PVP-OD coupled with $KKKA_5$

The condensing properties of 12 kDa PVP-OD coupled with the cationic peptide were tested by mixing the dialysed product of the EDC/NHS coupling with free plasmid in solution and then depositing the mixture onto a mica wafer that had been coated with APTMS. After the dialysis, the concentration of polymer in solution was not known so, as a starting point, 15μl of DNA (concentration of 2,5μg/ml) and 15μl of polymer solutions were mixed. Then, another sample was prepared by adding 15μl of DNA solution to 30μl of polymer solution. In both cases, an incubation time of 2 hours was allowed after

depositing the mixtures on the wafers and then the substrates were rinsed with deionized water. The samples were scanned in AFM in tapping mode using a cantilever with resonance frequency of 250 kHz. The images were analyzed using ImageJ to binarize them and then apply the build-in particle analyzer macro.

The effect of other parameters was also tested. First, the propensity of the formed aggregates to precipitate was tested by preparing a mixture of 15μl of DNA solution and 30μl of polymer solution, but the resulting mixture was not directly transferred to the mica substrate. Instead, the solution stayed in an eppendorf tube for two hours before deposition. After the two hours had passed, part of the solution was gently pipetted from the top of the tube and deposited on a substrate while the rest of the solution was mixed by doing up and down with a micropipette. After mixing, another part of the solution was deposited on a different wafer. In another experiment, DNA solution and polymer solution were mixed at a 1 to 1 ratio and allowed to incubate at 41 ºC. Then, the solution was deposited on a wafer to test the effect of higher temperature on aggregate formation. These samples were also scanned with AFM in tapping mode, but due to the unavailability of 250 kHz cantilevers, it was necessary to change to a cantilever with resonance frequency of 70 kHz. Ideally, this last sample should have been prepared with a 1 to 2 DNA/polymer ratio but, due to the low levels of stock, it was necessary to save as much dialysed polymer solution as possible for the transfection experiments below.

2.4 Coupling of 12 kDa-PVP and $KKKA_5$

The polymer PVP-OD was cross-linked to the syntheiszed cationic peptide $KKKA_5$ by means of EDC/NHS chemistry (see Section 1.8.3). The 12 kDa PVP-OD that was used had been modified to have acrylic acid groups, which allows coupling to primary amines. First, PVP-OD had to be dissolved, but due to its hydrophobic part, it is extremely complicated to dissolve it directly in water. Therefore, the polymer was instead dissolved by slow addition of powder to 96% ethanol under heavy stirring, for a duration of approximately 2 hours.

Once PVP-OD had been dissolved, 115 mg of 1-ethyl-3-(3-dimethylaminopropyl) carbodiimide hydrochloride (EDC, Merck Millipore) were weighted, as well as 23 mg of N-Hydroxysuccinimide (NHS, Merck Millipore). These weights corresponded to the moles necessary to match the amount of acrylic acid groups in PVP-OD. These two compounds were dissolved in ethanol separately, and the resulting solutions were dropwise added to the PVP-OD solution. Then, the activation of the carboxyl groups was allowed to proceed by leaving it at room temperature for 30 minutes, still under heavy stirring. During this incubation

time, 15 mg of cationic peptide were dissolved in 15 ml of deionized water and then 10 ml of DIPEA were mixed with the peptide solution to ensure that the coupling itself would take place in basic pH. After the half hour was over, the polymer and EDC/NHS solution was added to the peptide and DIPEA, and the mixture was placed under stirring for 48 hours to help maximize the efficiency of the coupling reaction.

Once the reaction was complete, it was necessary to remove unreacted cationic peptides and the by-products of the reaction. In order to do this, the solution was introduced in a dialysis bag with pore size of 3.5 kDa that had been previously rinsed in deionized water. The bag was clapped at both ends to ensure that the liquid would not flow out of the bag and then it was placed in a beaker with 500 ml of clean deionized water. For 2 hours, the bag was left in the beaker while the water was being stirred with a magnet and then the liquid in the beaker was changed to 500 ml of fresh deionized water. After two more hours, the water was once again changed before leaving it for approximately two days to ensure complete removal of undesired products. The resulting dialysed solution was stored at 4 degrees for further experiments.

2.5 Analysis of EDC/NHS coupling product

2.5.1 AFM

At first, AFM was used to try to determine whether the EDC/NHS coupling was successful. This was done as an alternative to FTIR spectroscopy when the university had access restrictions and it was easier to use the machinery in Skjernvej rather than going to another department. 15μl of DNA were deposited on mica substrates coated with APTMS as it had been done in the experiments to visualize free plasmid. After allowing one hour of incubation, the substrate was rinsed with deionized water and the 15μl of the dialysed product from EDC/NHS coupling was added on the wafer and allowed to stay for 2 hours. After rinsing with deionized water again, the sample was scanned using AFM in tapping mode.

2.5.2 FTIR spectroscopy

FTIR spectroscopy was used to confirm whether the coupling between 12 kDa PVP-OD and the cationic peptide KKKA_5 was successful. The spectrum of the dialysed product was obtained using the Nicolet™ iS20 FTIR Spectrometer (Thermo Scientific) by placing 50μl of product on top of the machine's diamond sensor. Then, a spectrum of a control sample consisting of 100 mg of PVP-OD dissolved in 100 ml of ethanol was recorded in the same way to serve as a background control.

2.6 Fibroblast culture

2.6.1 Cell culture conditions

In this work, fibroblasts were used as a model for *in vitro* testing of the new delivery system. Specifically, CRL-2429 cells were first thawed in a water bath at 37 ºC before adding culture medium that had also been pre-heated at 37 ºC. The medium consisted of 89% in volume of Dulbecco's Modified Eagle's Medium (Thermofisher scientific), commonly referred to as DMEM, 10% of Fetal Bovine Serum (FBS), and 1% of penicillin. After addition of 15 ml of this medium to the cells, the tube containing the them was centrifuged at 125 rpm for 5 min. Then, the supernatant was discarded before re-suspending the cells in the pellet in 15 ml of fresh medium. This cell suspension was transferred to a 75 cm^2 culture flask to allow for the cells to attach to the wall and grow. Every 3 days, the medium was replaced with 15 ml of fresh medium. Before the change, the cells were observed under a light microscope to check the confluence.

2.6.2 Trypsinization

Once cells reach 80% confluence, they need to be transferred into new flasks or plates, where they can grow more before doing other experiments. Since fibroblasts attach to the wall of the flask, it was necessary to first detach them by trypsinization. First, a solution containing trypsin and EDTA was warmed to 37 ºC, together with fresh culture medium and PBS. Then, the old culture medium is discarded and the flask was gently rinsed with 3 ml of PBS twice. Then, 0.5 ml of trypsin/EDTA solution per every 10 cm^2 of flask wall surface were added. The flask was gently swirled before incubating at 37 ºC for 3 minutes. After checking that most of the cells were detached using a light microscope, 10 ml of fresh culture medium were added to stop the trypsin reaction. Then, the solution containing the cells was transferred to a new 15 ml tube and it was centrifuged at 125 rpm for 5 minutes. The supernatant was discarded and the pellet containing cells was re-suspended in fresh medium. A small sample of this solution was taken for cell counting in a haemocytometer (see Section 2.6.3). Then, more medium was added based on the cell count to achieve the desired cell concentration for transferring. Finally, the volume of solution was divided among new flasks or plates.

2.6.3 Cell counting

In order to control the amount of cells present in a culture at a given point, x μl of cells in suspension were added into a haemocytometer chamber. In the haemocytometer, there are two regions with four quadrants (see Figure 2.1). The number of viable cells in each quadrant were counted and the average was obtained. When

counting in each quadrant, the cells that lay on two of the four boundaries were taken into account, while the cells on the other two sides were not (Figure 2.1, bottom right). Finally, the total concentration of cells is calculated as:

$$cells/ml = Average * 10^4 * Df \tag{2.1}$$

where Df is the dilution factor of the sample that is being counted.

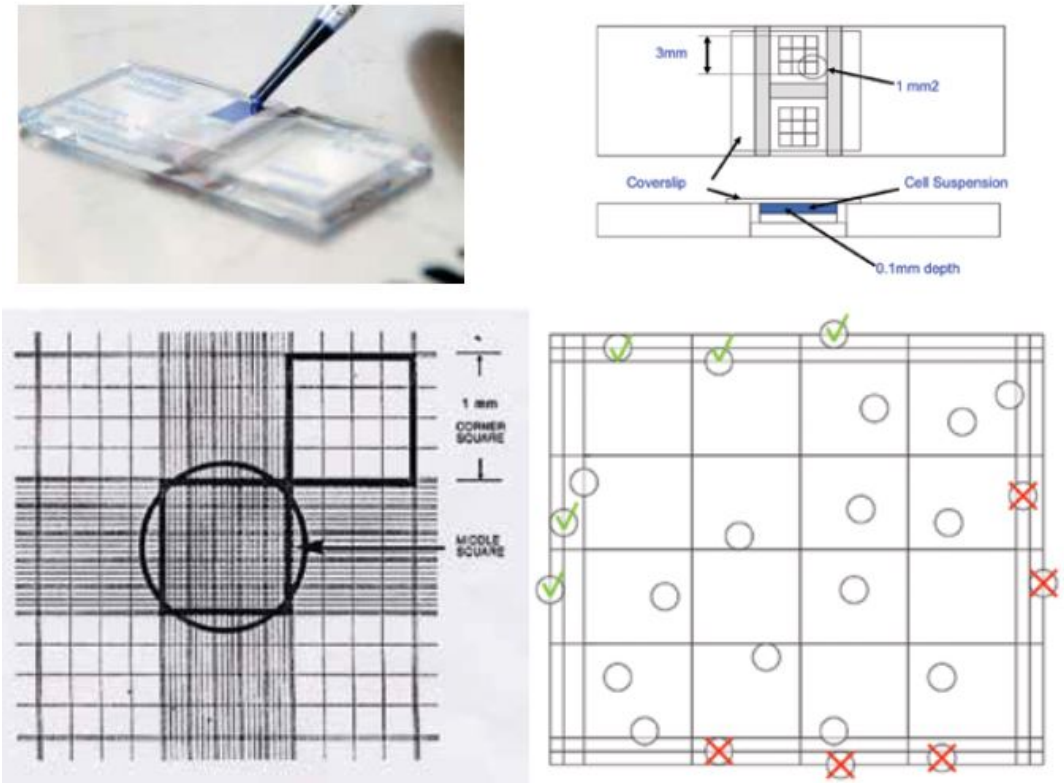

Figure 2.1: Loading of haemocytometer (upper left image), diagram of haemocytometer (upper right image), diagram of the four quadrants (bottom left image) and example of cell counting in one quadrant (bottom right image)[77].

2.7 CytoxONE test

The toxicity of the different components used to form the DNA delivery system (12 kDa PVP-OD and the cationic peptide KKKA5) was assessed *in vitro* using the CytoxONE Homogeneous Membrane Integrity Assay kit (Promega), which measures cell death as a function of LDH release (section 1.6). First, CRL2429 fibroblast cells were trypsinized from a culture flask and transferred to a 24-well plate. When the cell cultures were confluent in the new plates, different amounts of the compound that was being tested were added to different wells and the

plate was incubated at 37 ºC for 24 hours. As negative control, a sample with no compound was used, while a positive control was made by adding 2 μl of lysis buffer provided by the kit, which kills almost all or all of the cells. Every sample was set up in triplicate. The concentrations of 12 kDa PVP-OD that were tested were 4 mg/ml, 1 mg/ml, 0,66 mg/ml, 0,5 mg/ml, 0.33 mg/ml, 0.1 mg/ml and 0.01 mg/ml. For the cationic peptide KKKA_5, the tested concentrations were the same as for PVP-OD except that no sample of 4 mg/ml was prepared. The final volume in each sample was always 400 ul.

After the incubation period, the assay buffer, stop solution and assay substrate were thawed and allowed equilibrate to room temperature. Then, 11 ml assay buffer were added to one substrate vial and mixed by shaking. 100 μl of cell culture medium of each well were transferred to a 96-well plate and 100 μl of the assay buffer mixed with the substrate were added to each of them. Three extra wells were filled only with the assay mix to measure background fluorescence. The plate was gently shaken to allow the two liquids to mix and then it was left for 10 min at room temperature. After that, 50 μl of stop solution were added to each well and the plate was again shaken gently to ensure proper mixture of the newly-added solution over the entire well's volume. Finally, the fluorescence of the filled wells was measured in a plate reader (EnSpire Multimode Plate Reader, PerkinElmer) checking for absorption at 560 nm and emission at 590 nm.

2.8 DNA transfection by electroporation

Electroporation was used to transfect fibroblasts with the plasmid pCas9-GFP with the intent of creating a control for gene expression. This control was created to serve as a confirmation that the plasmid is indeed able to induce GFP expression in mammalian cells and also as a reference measurement to test the efficiency of the new designed nanocarrier. First, fibroblasts were detached from the culture flask wall using trypsinization, similar to the process described in 2.6.2. The main difference was that, after centrifuging, cells were dissolved in PBS to obtain a concentration of approximately 1 x 10^7 cells/ml. Then, 500 μl of this solution were mixed with 4μg of plasmid DNA dissolved in nuclease-free water and placed inside a cuvette, which was then loaded in the electroporation machine (Gene Pulser II, Bio-Rad,etc), making sure that the cuvette made proper contact with the electrodes. The electroporator was programmed with different parameters for every electroporation that was performed. First, a voltage of 0.35 V and a capacitance of 5000 μF was set. The second time, voltage and capacitance were increased to 500 mV and 10000 μF respectively, while for the third experiment voltage was again 500 mV but capacitance increased to 50000 μF. Another difference between the last attempt and the previous two was that, before and after the electrical current was

applied, the cuvette was placed in ice for 5 min. After the discharge had finished, the time constant was recorded and the cells were quickly transferred to a new flask that contained pre-warmed medium. The fluorescent signal was observed under a fluorescent microscope 48, 72 and 96 hours after transfection and cell proliferation was compared under a light microscope to a control of cells that had not been electroporated.

2.9 *in vitro* testing of DNA nanocarriers

The ability of the synthesized DNA delivery vehicles was tested on human fibroblasts in 2D *in vitro* culture. The fibroblasts belonged to the CRL2429 cell line. The aggregates were prepared by mixing 0.15 μg of plasmid DNA in deionized water with 50 μl of dialysed solution containing PVP-OD coupled with cationic peptide. The mixture was let to rest at room temperature for 2 hours before adding it to 3 wells with confluent cell cultures together with fresh culture medium, while 3 other plates were left as a negative control. Then, the cells were incubated at 37 ºC and 5 % CO_2 for 48 hours before observing them under a fluorescent microscope (Axiovert 200M, Zeiss). The experiment was repeated changing the amount of DNA per well to 1.33μg. The amount of polymer solution necessary for fully condensing this amount of DNA was calculated to be 150μlper well, according to an estimation of the concentration of charges in the dialysed polymer solution, and the mixture was allowed to incubate for 2 hours. Nanocarriers were added to three samples while three others were left as a negative control. In a different experiment, 0.5μg of DNA per well were mixed with 150μl of polymer solution and, after 2 hours of incubation, 150μl of free cationic peptide solution (8 mg/ml) were mixed with the nanocarriers and everything was incorporated to 3 cell cultures. The resulting cultures were analysed using a fluorescent microscope (Axiovert 200M, Zeiss) 72 hours after the experiment start, and also 24 hours after that. A control with free DNA and only cationic peptide was also prepared using the same amount as in the last experiment.

2.10 Simulation of a microfluidic system for *in vitro* testing

In order to propose a better *in vitro* system to test nanocarrier transfection efficiency, COMSOL Multiphysics 5.5 has been used to model a microchannel where cells could grow and medium would flow to provide nourishment and to carry any particle that is being tested. The cross-section of the channel can be separated in two main parts: a rectangular region that connects the inlet to the outlet and a rhomboidal part that is placed beneath the rectangle, with an interior wall separating the two. The rectangular section has height and width of 60 and 1000 μm respectively. The membrane section is 740 μm long, and the lower

rhomboidal section has a base of 500 μm and a maximum height of 40 μm. The depth of the whole channel is 100 μm. Images of this geometry can be seen in the results.

Two physics modules have been used to simulate the behaviour of this microfluidic system, the laminar flow module and the particle tracing module. The former has been used to represent the flow inside the channel, while the particle tracing has been used to generate particles of the desired size and see the effect that the flow exerts on said particles. At the inlet, the velocity was set to a specific magnitude value and it was decided how often new particles would be generated at a random position at the inlet boundary. All of the walls in the system except for the one that separates the two sections of the model were set so that the no-slip boundary condition was applied when simulating the flow. This condition states that, at the wall, the velocity of the flow must be equal to the velocity at which the wall is moving. In this system, this was equivalent to setting the velocity at the walls equal to zero. In the particle tracing module, it was decided that particles would be able to rebound when they reached one of this walls. Finally, at the outlet, the pressure was set to be equal to zero in order to suppress any form of backflow.

Other than geometry and the basic physics settings, another key component of this model is the inner wall that separates the rectangular and rhomboidal sections. This wall was modelled so that it could be used as realistic simulation of the barriers that can be found in the body and that separate most cells form the blood flow. Two different approaches to build this wall have been tested and compared. This first approach consisted in building a wall with randomly generated holes with sizes that belong to a distribution that can be set by the user. This creates a sieve with pores that can range in diameter and that can be distributed randomly throughout the wall. The user can also choose what percentage of the wall will be covered by holes. The geometry was generated by writing a COMSOL method, which is a small program written in JavaScript that allows more flexibility when building certain shapes.

The second model of the inner wall is based on probability rather than geometry. The wall is considered to be continuous, with no holes or openings, but the condition that was set in COMSOL is that any particle that reaches that wall will have a certain probability of passing through it and, if it does not make it through, the particle will rebound as if it were a normal wall. The probability is determined as a function of the size of the particle, the pore size and the pore coverage. This probability is modelled in real time using Matlab Livelink, allowing all the calculations to be performed in Matlab before returning the probability to

COMSOL. First, a pseudo-random number generator is used to extract a random particle size from a distribution of sizes that can be set by the user. Once the size of the particle has been decided, the probability of the particle going through the wall depends on the probability of finding a pore that is bigger or equal to the particle. Considering that the pore size distribution was defined as a gaussian distribution, the probability of the pore being bigger than the particle can be calculated as the area under the gaussian curve between the size of the particle and the maximum size that a pore can have. Mathematically, this is expressed as:

$$\gamma = C \int_{Particlesize}^{Maxporesize} \frac{1}{\sigma\sqrt{2\pi}} \exp\left(-\frac{(x-\mu)^2}{2\sigma^2}\right) dx \tag{2.2}$$

where C is the pore coverage, μ is the mean pore size and σ is the standard deviation of the pore size. In practice, this integral is calculated using numerical integration, which is already efficiently implemented in Matlab. Every time that a particle reaches the inner wall, COMSOL calls the Matlab function and calculates the probability of the particle going through the wall.

Chapter 3

Results

3.1 Condensing properties of synthesized peptide

The AFM images of the sample with free DNA clearly show that DNA has indeed been deposited. The chains of the plasmids are distinguishable as very slim lines that are higher than the substrate. The plasmids can be found in different degrees of coiling but, overall, they all span a relatively large surface, in the range of a few hundred nanometers (Figure 3.1). On the other hand, the sample with only peptide seems to be empty, even after scanning different regions of two different samples. In the first attempt of mixing DNA with peptide, 15 μl of both were added to the substrates and left for 15 minutes before rinsing. In the AFM, it could be observed that the DNA had condensed forming a mixture amorphous, spherical and toroid-like conformations (Figure 3.1). Moreover, lying on top of the toroidal structures, it could be seen that there were some aggregates. Elongated segments of condensed DNA seem to come out of some structures and, when the aggregates are looked at closer, it can be seen that some thin chains of DNA are still distinguishable.

After this first result, another attempt was made using the same setting except that the incubation time was extended to 2 hours. This way, it was thought that the condensation would not be interrupted by the rinsing before it was completed. The resulting AFM imaging reveals that DNA was more condensed than before. Toroidal structures are no longer visible, and most aggregates seem to be more spherical, as shown by the fact that the aspect ratio between their surface and their height has been reduced. Moreover, upon a closer look at some of the aggregates, individual DNA chains are not observed (image added to appendix A). The aggregates range in size from approximately 550 nm down to less than a 100 nm (Figure 3.2). Nonetheless, the effect of different DNA to peptide ratio was also studied. This time, the 15 μl of DNA

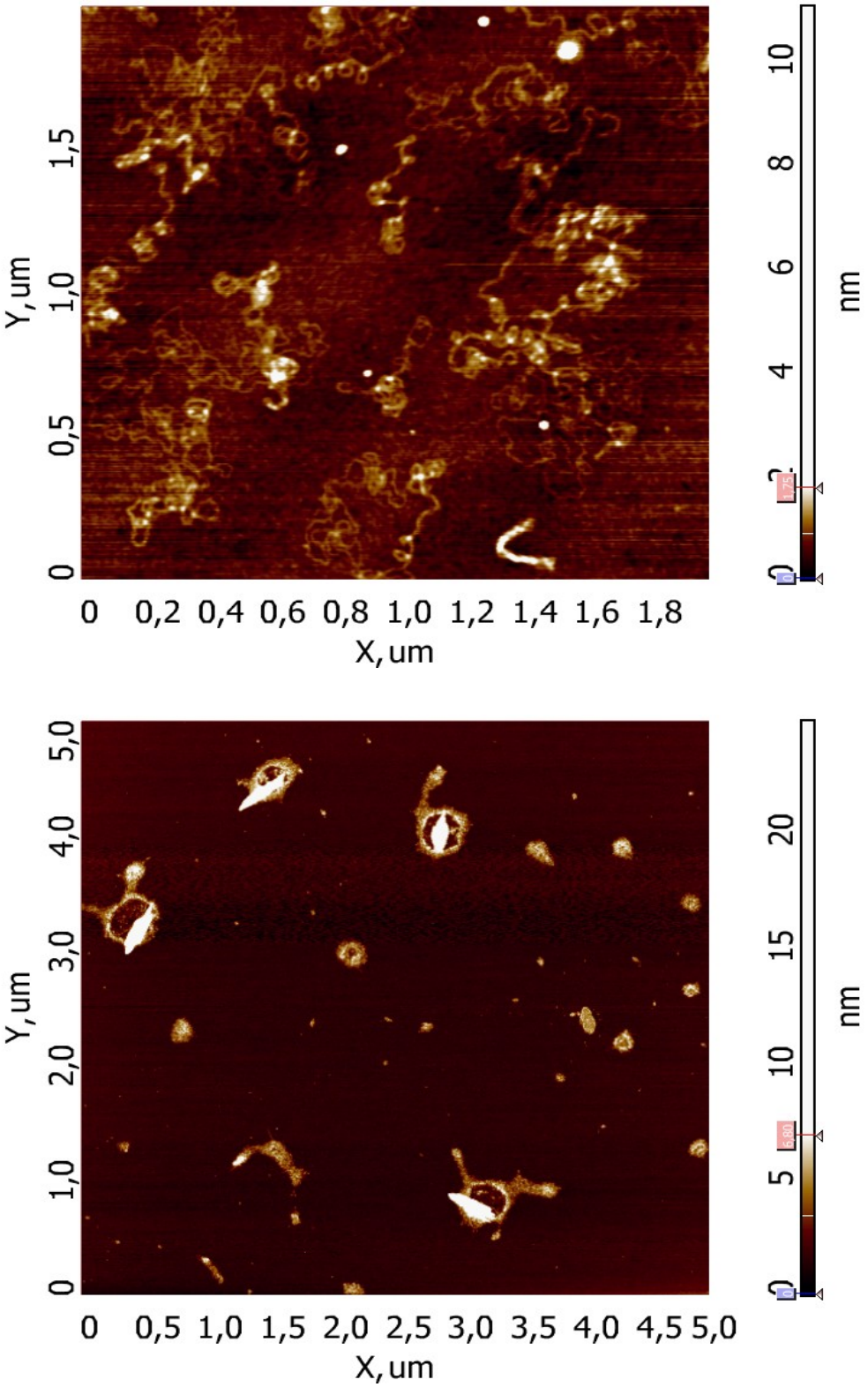

Figure 3.1: AFM images of free DNA (above) and aggregates of DNA and peptide synthesis product after 15 minutes incubation (below). Note that the height scale has been modified to improve visualization of the deposited structures. Both images represent an area of 2μm x 2μm

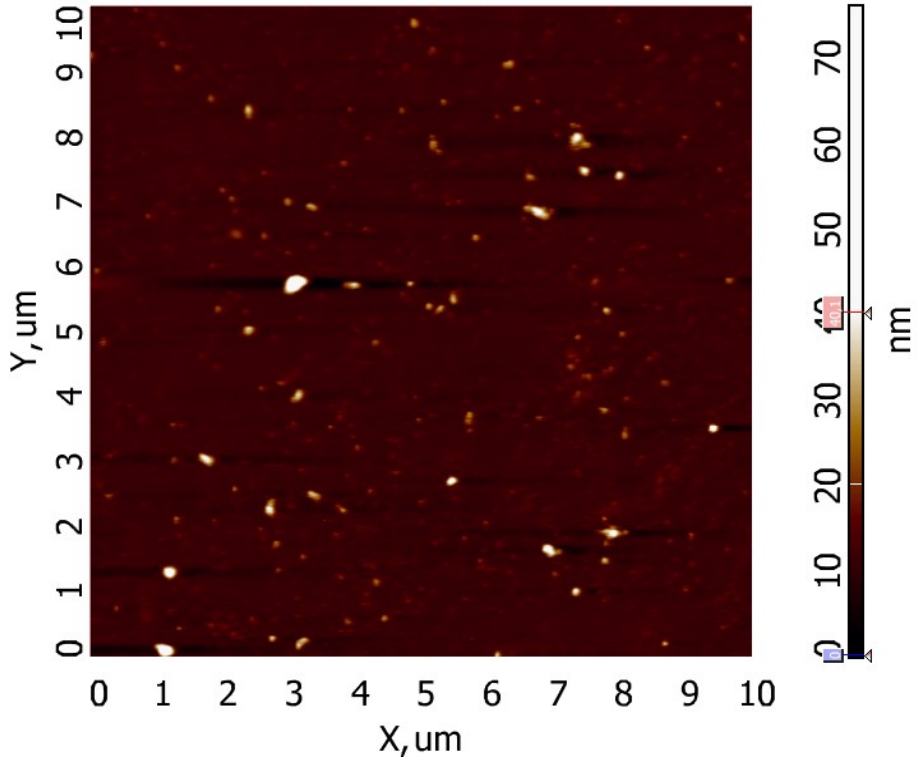

Figure 3.2: AFM image of DNA at concentration of 2,5 μg/ml mixed with 1 mg/ml peptide in solution and incubation time of 120 minutes. An area of 10x10μm is scanned. Note that the contrast of the image has been modified to allow for better visualization of the structures.

solution that were added had a concentration of 5 μg/ml. The resulting images show that aggregation could still occur, similar to the previous experiment, but when looking close to the aggregates, free DNA was clearly visible, suggesting that there was an excess of DNA for the given amount of peptide (image added to appendix A). This, however, did not have an effect on the sizes of the aggregates.

3.2 Characterisation of EDC/NHS coupling product

3.2.1 AFM

AFM was used to scan a sample where DNA had been deposited and the dialysed product of the coupling was added after. The resulting images show that the chains of DNA are still visible but they tend to stick together (Figure 3.3). Compared with a control of free DNA, it seems as though the addition of polymer solution has collapsed several chains of DNA together, but not enough to cause condensation

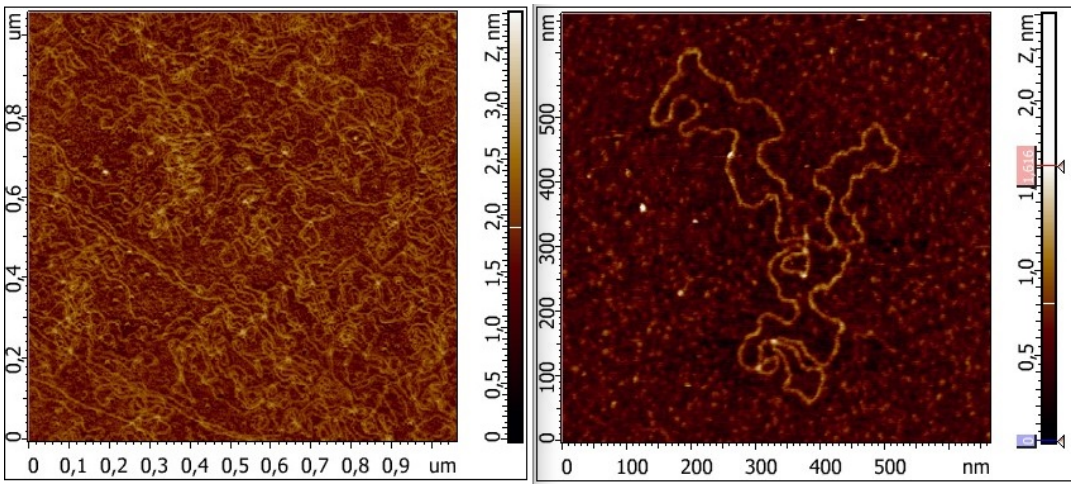

Figure 3.3: AFM images a sample with deposited plasmid DNA with dialysed product of EDC/NHS coupling (left) and free plasmid DNA control (right)

into aggregates. The individual chains maintain a similar range of widths (10 to 20 nm), but the recorded height is higher for the samples with polymer. For free DNA, the height is between 1 and 1,5 nm and for the polymer sample it is between 2,5 and 3 nm.

3.2.2 FTIR Spectroscopy

Fourier transform infrared spectroscopy has been used to determine if the EDC/NHS coupling was successful. In Figure, there are two spectra. The blue one corresponds to a solution that only contained the polymer PVP-OD, while the red spectrum corresponds to the product of EDC/NHS coupling after dialysis. Most of the two spectra's peaks match very closely, with the most notable difference being that the peaks around 3500 cm^{-1} and 1600 cm^{-1}. These two peaks are considerably larger for the synthesis product compared to normal 12 kDa PVP-OD.

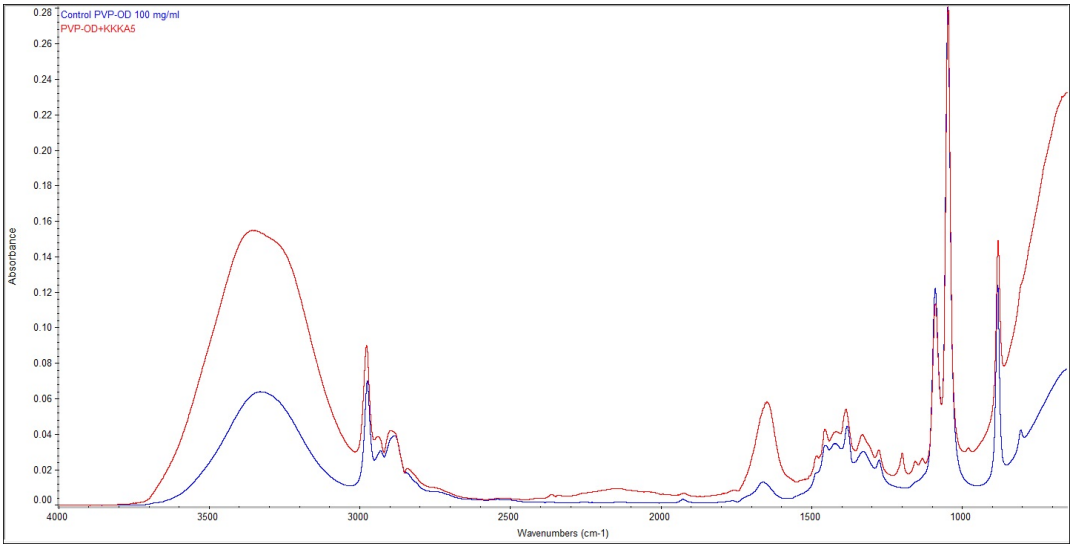

Figure 3.4: FTIR spectroscopy spectra for a 12 kDa PVP-OD solution in ethanol (blue) and the dialysed product of EDC/NHS coupling between 12 kDa PVP-OD and the cationic peptide KKKA_5

3.3 AFM study of nanocarrier formation

The ability of PVP-OD coupled with cationic peptide was tested to investigate its ability to condense DNA and form aggregates. At first, taking into account that the exact concentration of the polymer solution was unknown, a sample was prepared using the same conditions that yielded full condensation for the cationic peptide. The resulting images show that some aggregates have been formed, but free DNA is still visible (an example of these results can be seen in Figure 3.5). Because of this, in the next experiment, 15μl of DNA solution (2,5μg/ml) was mixed with 30μl of polymer solution and deposited on a substrate. The AFM images reveal several aggregates and no observable free DNA(an example of these results can be seen in Figure 3.5). A control sample made by depositing only PVP-OD was also scanned using AFM, but nothing could be observed on the substrate.

In terms of height, the biggest aggregate is approximately 50 nm high, but most other structures are between 10 and 25 nm. The areas of each aggregate correlate positively with height, with the bigger heights corresponding to bigger areas. In Figure 3.6 below, one can see a histogram of the areas of all the aggregates in the most clear images. The majority of the counts appear at or below 2500 nm^2, which correspond to a radius of 28 nm if one assumes that the structures are perfect circles. In that regard, the circularity of the areas has also been studied using ImageJ, and the results can be seen in Figure 3.6. A circularity of one

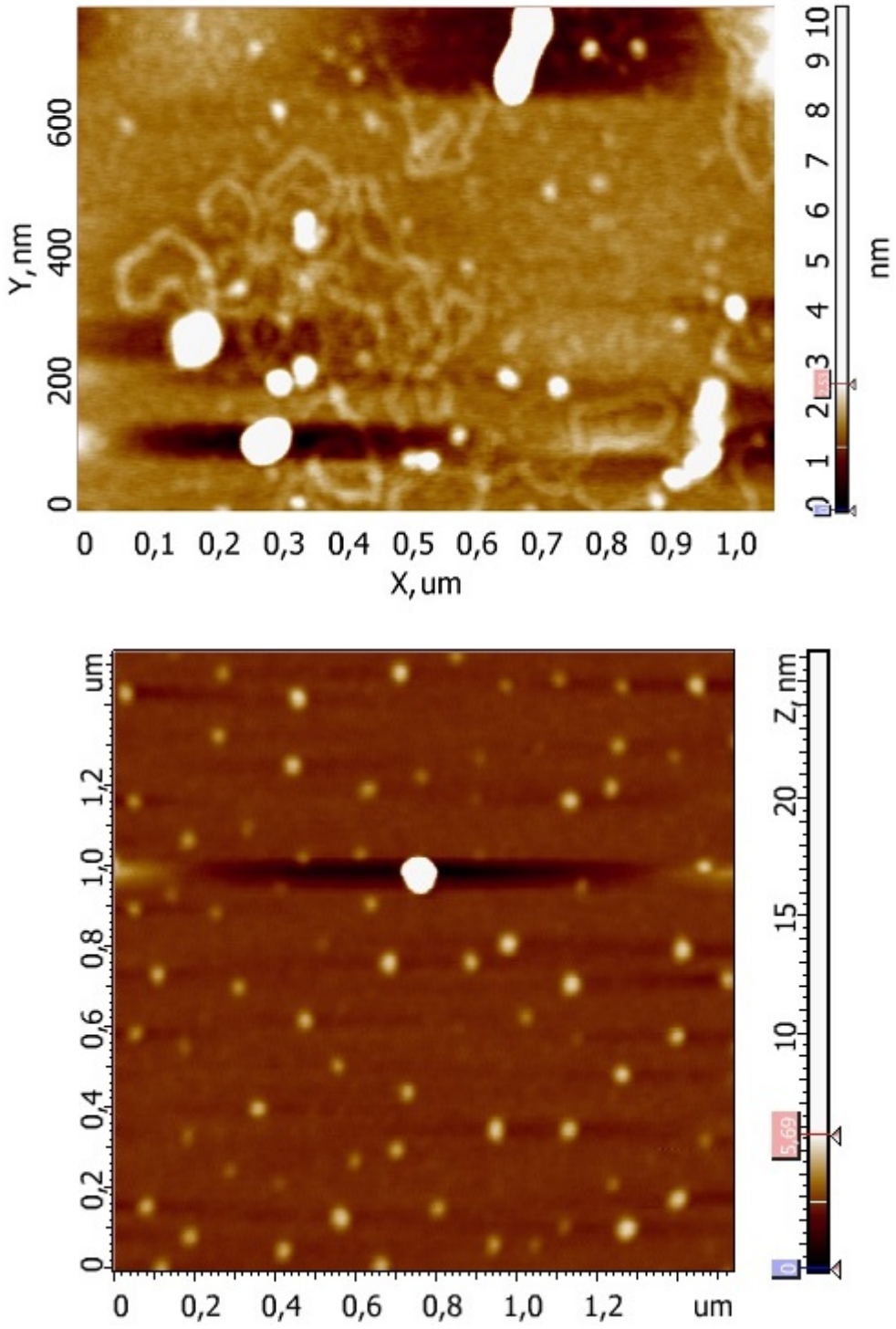

Figure 3.5: AFM images of aggregates formed by mixing 15μl of DNA solution (2.5μg/ml) with 15μl (above) or 30μl (below) of polymer solution.

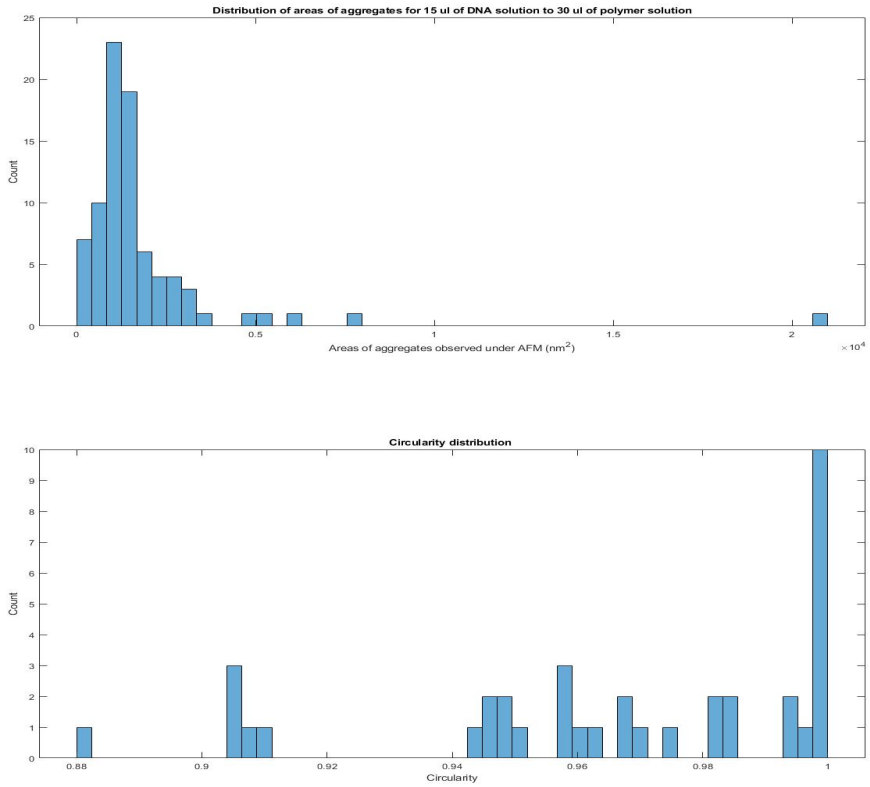

Figure 3.6: Histograms displaying the distribution of areas in nm^2 (above and circularity (below) for the samples prepared by mixing 15μl of DNA solution (2.5μg/ml) and 30μl of polymer solution.

represents a perfect or almost perfect circle, and it can be seen in the plot that most aggregates have high degrees of circularity. In a few images, some larger structures with different shape can be found, although they are usually limited to 500 nm in size and they look as if different normal nanocarriers have aggregated further and they are now attached to one another.

3.3.1 Effect of incubation condition and temperature

DNA and polymer solution were mixed and allowed to incubate in an eppendorf to test if any precipitation occurred. In the samples where the deposited solution was taken from the top of the tube, the images show structures similar to those observed in the previous experiments, with the notable difference that some of the larger aggregates seem to be close together (see Figure 3.7). The smaller aggregates still look as they used to, but the heights recorded by the AFM are very short compared to the previous measurements (all small aggregates are below 5 nm). In the

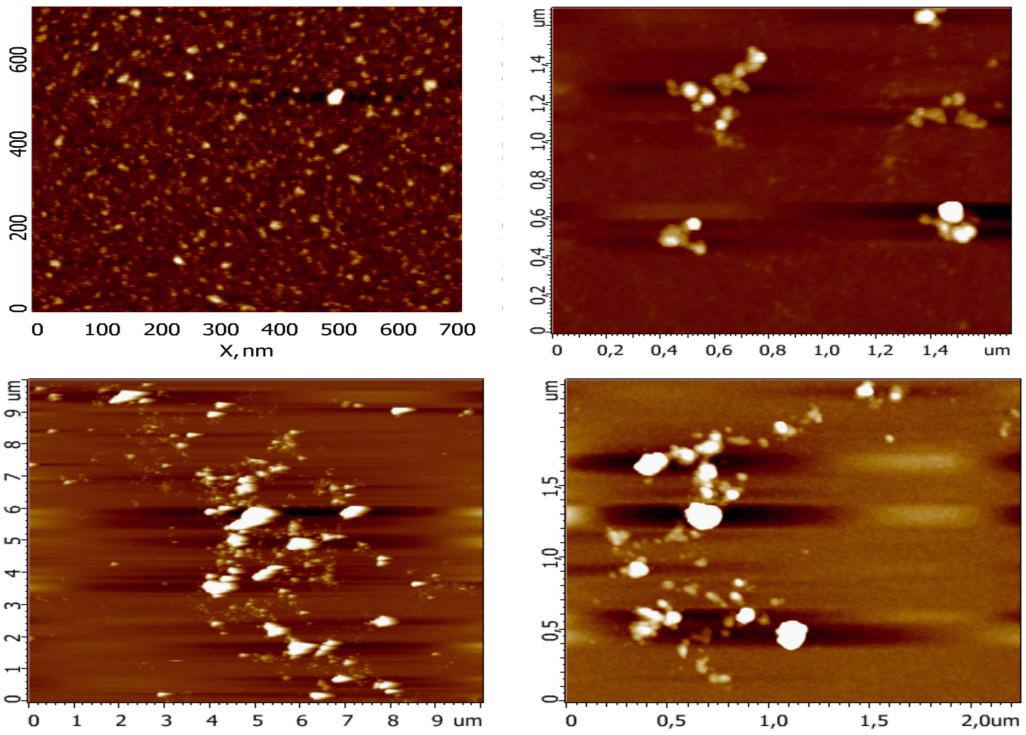

Figure 3.7: Examples of AFM images of aggregates after incubation and with no mixing (above) and after vigorous mixing (below). The height color scale for each image is different: Upper left from to 6μm, maximum intensity from 1.6μm, upper right from 0 to 30μm, maximum intensity from 16μm, bottom left from 0 to 160μm, maximum intensity from 80μm and bottom right from 0 to 65μm, maximum intensity from 22μm.

samples that were prepared after vigorously mixing the solution, some very large aggregates could be seen. Some were so large that they appear heavily smeared in the image (Figure 3.7), while some smaller ones have similar structures to those observed before. Still, it is common to see certain regions where more aggregates are found together, something that was not so common in previous experiments. Another important experiment that was performed using AFM consisted in determining whether the aggregates would form and have the same characteristics at physiological temperature. In order to test this, the 2 hours of incubation time took place at 41 ºC before depositing the resulting solution on the substrate. The AFM images reveal that most aggregates maintain similar structures to the ones observed previously, but there are also other objects in the substrate that have a different, more elongated shape. It is important to consider that this experiment was carried out using a proportion of DNA to polymer solution equal to the very first experiment due to the low reserves of dialysed polymer solution. Two representative images of these results can be seen in Figure 3.8.

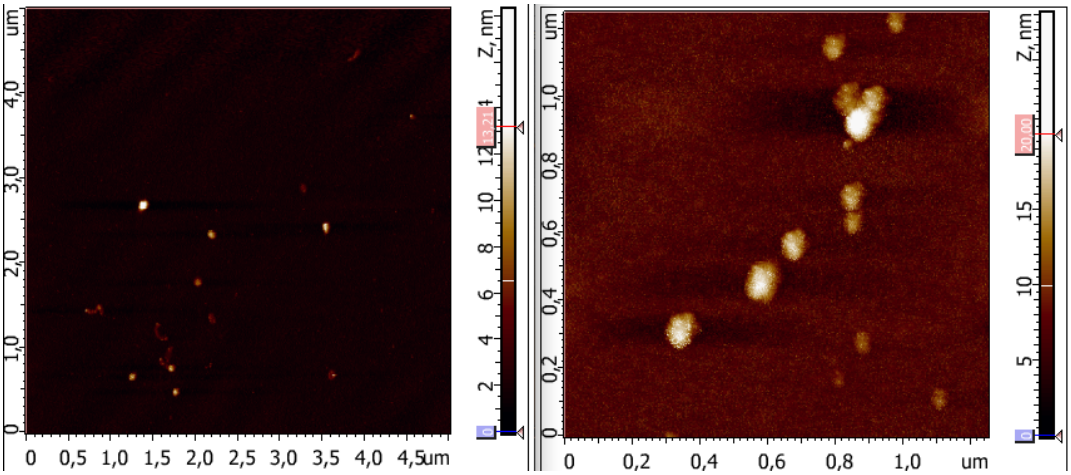

Figure 3.8: AFM images of PVP-OD nanocarriers that have been assembled at 41 ºCTo the left, area of 5μm x 5μm of one sample. To the right, 1.2μm x 1.2μm close-up image of aggregates in a different sample.

3.4 Cytotoxicity studies

3.4.1 12 kDa PVP-OD

The toxicity of 12 kDa PVP-OD was tested at concentrations of 4 mg/ml, 1 mg/ml, 0.1 mg/ml and 0.01 mg/ml. Using the CytoxONE kit, the percentage of cell death was assessed by measuring the fluorescent intensity caused by the release of LDH (see Section 1.6). The results of the measurements can be seen in Table 3.1, expressed as the average of three wells plus/minus the standard deviation.Other than the concentrations above, measurements were also taken for a background, positive and negative controls.

Table 3.1: Summary of the results obtained in the first CytoxONE cytotoxicity test. For each tested concentration, the average fluorescent intensity, corrected average fluorescent intensity and the percentage of cell death are provided.

Sample	Average fluorescent intensity	Corrected average intensity	% Cell death
Background	75808 ±3121	0	0%
4 mg/ml	65018 ±1049	-10790	0%
1 mg/ml	183062 ±5760	107254	69%
0.1 mg/ml	76360 ±2878	552	0.35%
0.01 mg/ml	69175 ±3279	-3354	0%
Positive control	232042 ±9202	155428	100%
Negative control	70665 ±2050	-3274	0%

Before addition of the sample to the cell cultures, light microscopy was used to take pictures of the wells to ensure that the cultures were confluent. After 24 hour incubation and before addition of CytoxONE substrate mix, another image of the same wells was taken as a visual corroboration of the intensity measurements. Figure 3.9 shows the images from before and after incubation for three representative examples. In all three cases, it can be observed that the cultures are confluent before incubation and that they all have a similar number of cells. However, after incubation, almost no cells can be observed in the well where lysis solution was added, while in the sample with 1 mg/ml of PVP-OD there are several cells, but many have been killed too. Not only are there less cells than before incubation, but their shape is no longer the characteristic elongated structure of fibroblasts. In contrast, when incubating with 0.1 mg/ml of PVP-OD, the culture is still confluent. These results are in agreement with those of the CytoxONE test. The same happens for the samples that are not shown in the image below. The highest cell death percentage, taking the positive control as reference, corresponds to a PVP-OD concentration of 1 mg/ml, with cell death of 69 %. However, at a concentration of 4 mg/ml, the recorded intensity is lower than that of the background measurement an therefore cell death becomes zero. Below 1 mg/ml, cell death drops to almost zero and, for the lowest concentration, it is the same as for the negative control.

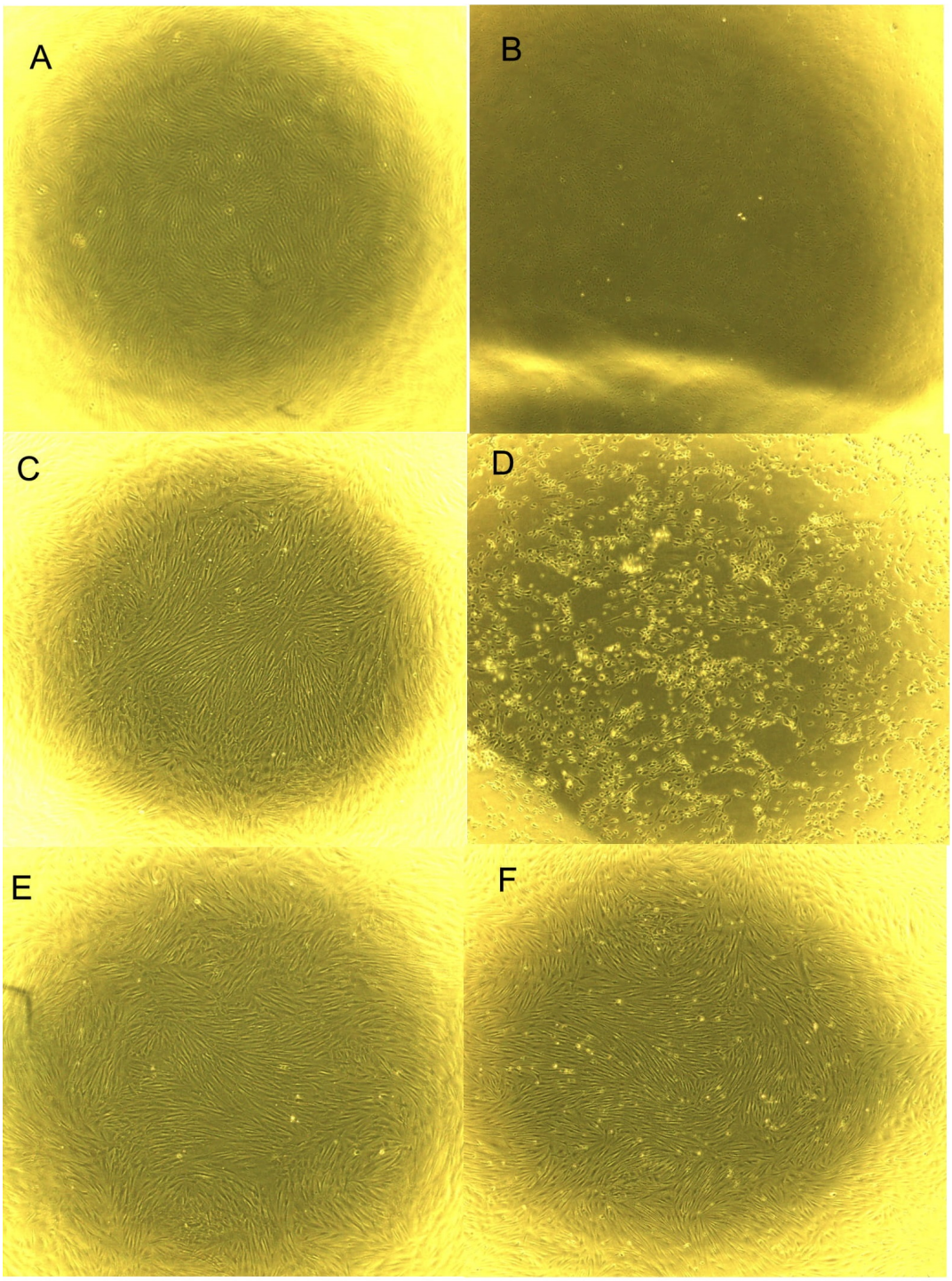

Figure 3.9: Images taken before incubation (A,C and E) and after incubation with lysis solution (B), 1 mg/ml 12 kDa PVP-OD (D) and 0.01 mg/ml 12 kDa PVP-OD (F)

The same experiment was repeated for a different range of concentrations. 4 mg/ml was tested again, together with 1, 0,66, 0.5, 0.33 and 0.1 mg/ml. The goal of the experiment was to have a more accurate estimate of the exact value at which cell death became significant. The results can be seen in Table 3.2 below.

Table 3.2: Summary of the results obtained in the second CytoxONE cytotoxicity test. For each tested concentration, the average fluorescent intensity, corrected average fluorescent intensity and the percentage of cell death are provided.

Sample	Average fluorescent intensity	Corrected average intensity	% Cell death
Background	65318 ±657	0	0%
4 mg/ml	65943 ±3840	-822	0%
1 mg/ml	155635 ±18647	888870	69%
0.66 mg/ml	190298 ±5088	124702	96%
0.5 mg/ml	179969 ±10080	114373	88%
0.33 mg/ml	122437 ±42200	56841	44%
0.1 mg/ml	82667 ±19841	17071	13%
Positive control	195696 ±16533	130101	100%
Negative control	66766 ±3103	1170	0.9%

Once again, no cell death is reported by the CytoxONE test at 4 mg/ml. However, the images taken using a light microscopy contradict this result, as it can be seen that there are no cells that look alive. The result for 1 mg/ml matches very well with the one in the previous experiment, but, cell death is lower than for 0.66 and 0.5 mg/ml. For all the concentrations below 0.66 mg/ml that have been tested there is a positive correlation between cell death and amount of PVP-OD added, but it is important to point out that the result for 0.1 mg/ml is not similar to the one obtained in the first CytoxOne experiment, as cell death goes up to 13 %. To complement these results, light microscopy images from the second Cytox ONE experiment can be found in appendix A. To summarise the results of both experiments, a scatter plot is added in figure 3.10. When a concentration has been measured in both attempts, an average of the two results appear in the plot.

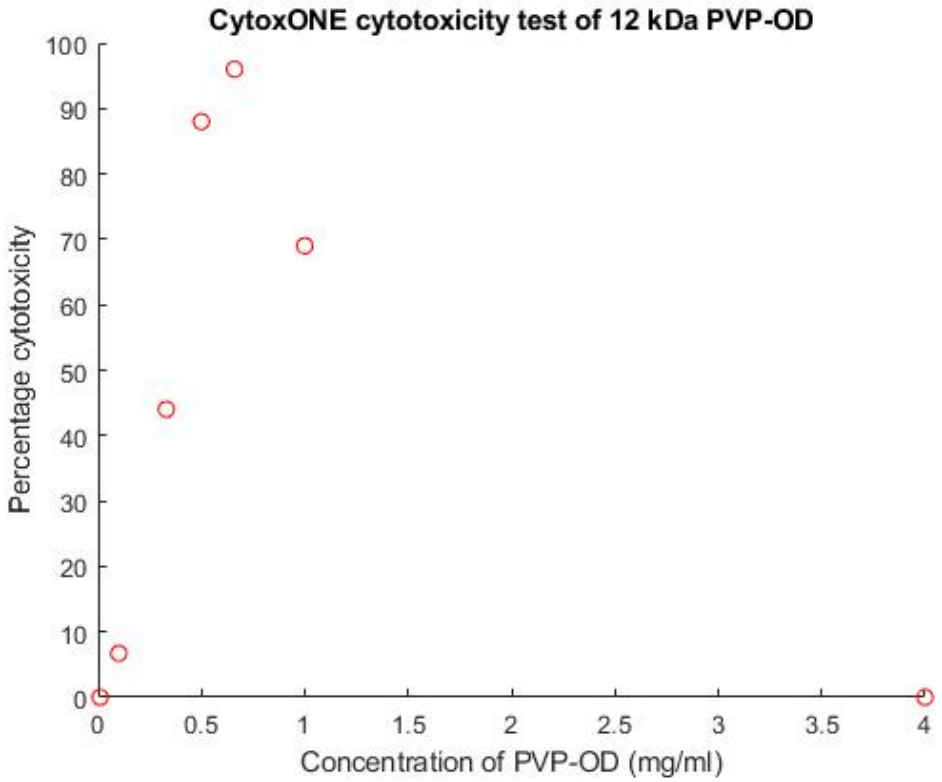

Figure 3.10: Scatter plot representing the results of the two CytoxOne cytotoxicity test. For the concentrations that have been tested twice, the point in the plot corresponds to an average of the two results.

3.4.2 Cationic peptide KKKA_5

The toxicity of the cationic peptide used in this project was tested at different concentrations. The results obtained can be seen in table 3.3. The results show very low cytotoxicity percentages for all tested concentrations. Light microscopy images taken before and after addition of KKKA_5 confirm that cultures were always confluent except for the positive control sample.

Table 3.3: Cytotoxicity of the cationic peptide KKKAAAAA. The average fluorescent intensity is an average of three measurements, while the corrected intensity is calculated by subtracting the average background to the average fluorescent signal. Cell death is calculated by dividing corrected intensity of every sample by the intensity of the positive control.

Sample	Average fluorescent intensity	Corrected average intensity	% Cell death
Background	71613 ±2098	0	0%
1 mg/ml	72569 ±1175	956	0.6%
0.66 mg/ml	72302 ±927	690	0.4%
0.5 mg/ml	73752 ±982	2140	1.3%
0.33 mg/ml	72116 ±3159	504	0.3%
0.1 mg/ml	72865 ±1614	1253	0.8%
0.01 mg/ml	73262 ±1084	1649	1%
Positive control	234425 ±7497	162812	100%
Negative control	74032 ±1857	2419	1.5%

3.5 Transfection by electroporation

Electroporation was used to test the ability of pCAS9-GFP to induce GFP expression in human fibroblasts. First, the electroporation was performed by setting the voltage to 350 V and capacitance to 5000 μF, but the true applied voltage according o to the electroporator was 272 V. The time constant was 0.3 milliseconds. 48 hours after the electroporation, the cells had already formed a fully confluent culture (see Figure), indicating that the level of dead cells was low. However, when the cell culture was observed using fluorescent microscopy, no fluorescent signal corresponding to GFP could be observed. The images are not shown because they consist of background noise only. On a second attempt, both voltage and capacitance were increased to create a stronger current and increase exposition time. The true voltage applied by the electroporator was 414 V (it had been set to 500 V) and the time constant doubled with respect to the former attempt. Again, 2 days after the electroporation had been performed, the cells had formed a confluent culture, but no fluorescent signal could be seen.

A third attempt was made by increasing capacitance to ten times its original value, 50000 μF, hoping to increase exposure time. The voltage was left at 500 V. This time, the true applied voltage reported by the electroporator was 504 V while the time constant increased to 5.4 milliseconds. 48 hours after electroporation, the cells had not reached confluence and there were many cells that did not have the typical elongated shape of fibroblasts. Fluorescent microscopy revealed that the cells that were found on the wall had no signal, but a fluorescent signal could be found in some of the cells that had lost their normal shape (Figure 3.11). 3 days

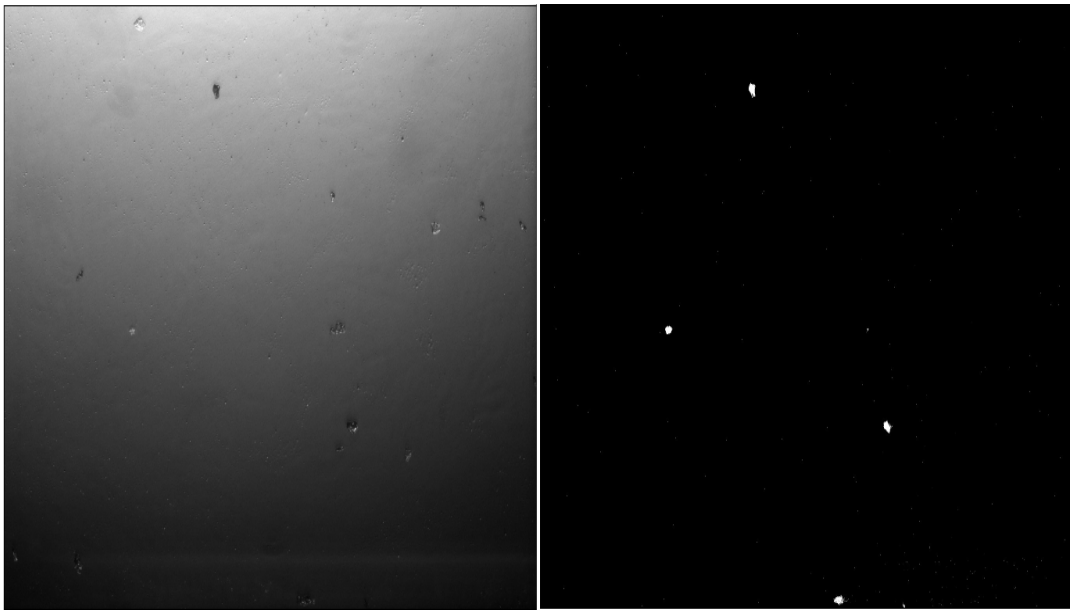

Figure 3.11: Example of the results obtained for the third electroporation (50000μF, 500 mV) . To the left, there is a light microscopy image. To the right, there is the same area when measuring green fluorescence.

after electroporation, the amount of such cells seem to have increased, although counting them all was not possible. No difference in the images taken 72 and 96 hours after electroporation could be noticed.

3.6 Transfection by PVP-OD nanocarriers

In the first transfection experiment, the controls and the samples where PVP-OD nanocarriers were added remain confluent two days after the experiment start. Fluorescent microscopy images do not reveal any signal in any of the cultures either, indicating that GFP has not been produced. In the second experiment, the amount of DNA that was incorporated in the cell culture was increased to 1.33μg hoping to induce GFP expression. Due to the increase in DNA concentration, high levels of polymer had to be used as well, leading to a final concentration above 1 mg/ml. The results show that the cultures where the nanocarriers have been incorporated have high levels of cell death, while the control samples are fully confluent. Fluorescent microscopy shows that some of the apoptotic cells have a signal which is not observed in the control, indicating that GFP is present. An example of these results can be seen in Figure 3.12 (more images can be found in appendix A)

Another experiment was performed to try and obtain high levels of GFP

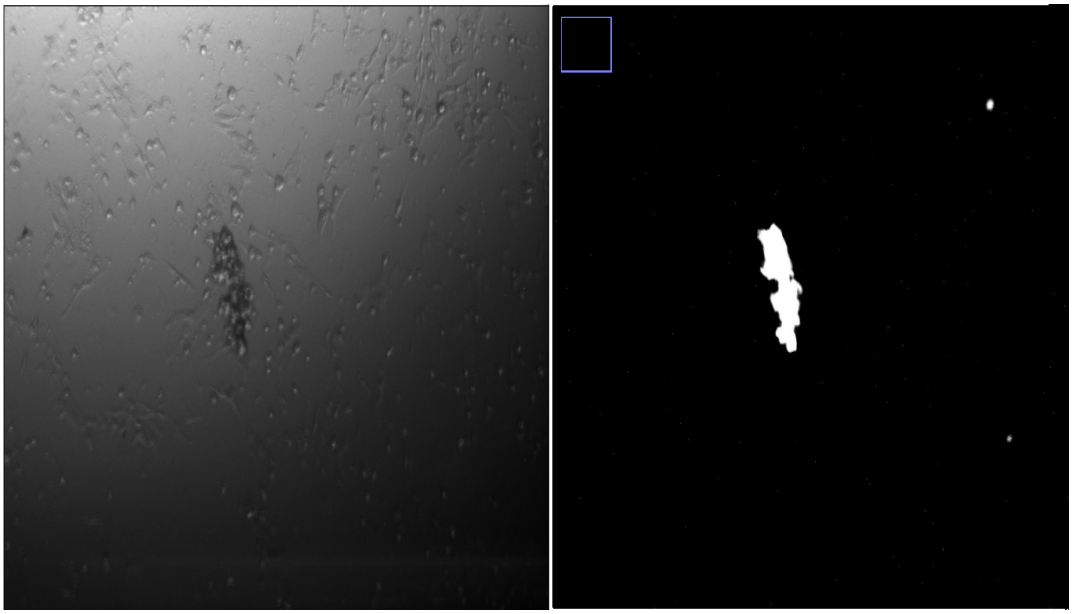

Figure 3.12: Example of the results obtained when testing PVP-OD nanocarriers at high concentration (1.33μg of DNA per sample) . To the left, there is light microscopy image showing apoptotic cells. To the right, there is the same area but measuring green fluorescence.

expression without causing cytotoxicity by forming nanocarriers with 0.45μg of DNA and then mixing them with free cationic peptides. The results are similar to those of the last electroporation experiment, as there is some fluorescent signal that can only be observed in cells that have lost the typical shape of fibroblasts, but not in the majority of cells, which are attached to the bottom of the well. Moreover, the signal is less frequent and less strong than it is for the previous experiment (Figure 3.13). Finally, a sample with the same amount of DNA was prepared by mixing free DNA and free cationic peptide only, but no signal could be observed and there was no obvious cell death.

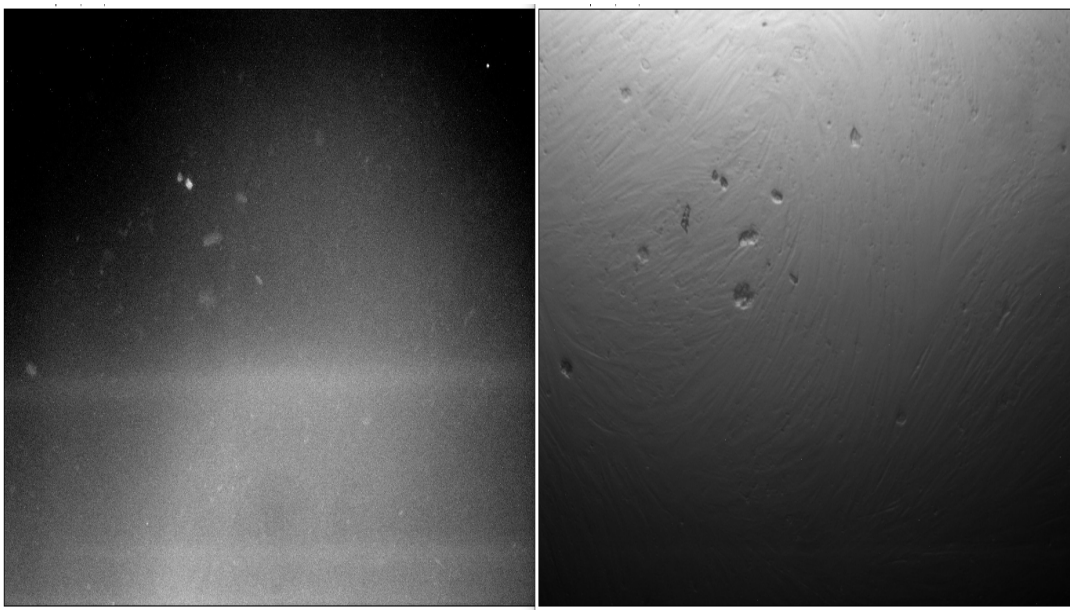

Figure 3.13: Example of the results obtained when testing PVP-OD nanocarriers at lower concentration (0.45μg of DNA per sample). To the left, there is light microscopy image showing apoptotic cells. To the right, there is the same area but measuring green fluorescence.

3.7 Simulation of the microfluidic system for *in vitro* testing

3.7.1 Randomly generated porous solid wall

A COMSOL method that is able to create random holes in a wall was written in JavaScript (code in appendix B) to try to imitate an actual porous membrane. The holes in the wall are randomly spread along the wall and their sizes are also different from one another, always within the specified range given in the code, indicating that the written method can automatically create randomized holes of specific size in a solid wall. However, when a 2D simulation was performed with this wall, the particles were able to freely cross though the holes as regardless of their size, and even particles that had a radius ten times bigger than the maximum pore size could freely cross the membrane. Given the inability of this model to sieve larger particles, a new probabilistic model was created.

3.7.2 Probabilistic model of a membrane

Different test cases have been simulated using COMSOL Multiphyiscs to validate the probabilistic membrane model and confirm that it explains the behaviour that this system would have in real life. First, a comparison between three inner walls has been performed: a normal porous wall, a completely insulating wall and a

wall that allows all particles to cross. Then, different speeds for the flow have been tested to see its effect on the amount of particles crossing the membrane and, finally, particles of different sizes have been simulated.

Velocity profile

The flow in the microfluidic was modelled using the laminar flow module and assuming that steady state had been reached. The distribution of the velocities in the flow are the same for all the tested cases, with the only difference being that the magnitudes of these velocities are directly proportional to the inlet velocity set by the user. In all cases, the flow speed at the walls is zero, an it gets higher and higher towards the center of the channel. It is also interesting to point out that the wall is invisible for the flow, that is the fluid can freely travel across it without any limitations. The system was set like that to ensure that the liquid can reach the bottom of the channel, which would be impossible with a normal solid wall. At the outlet of the channel, the fluid is removed and no backflow is observed.

Comparison between membrane types

In order to validate the performance of the membrane model, two extreme cases (perfectly-insulating wall and completely permeable wall) have been simulated and compared to a more realistic scenario in which the distribution of particle size is roughly the same as the distribution of pore sizes. In the figure below, a side view of the channel can be seen, with the particles represented as spheres, for every one of the three test cases above, at the end of the simulation time (Figure 3.14). As it can be observed, the perfect insulator does not allow any particle to go through the membrane, so they are all in the upper rectangular region. In contrast, both in the normal porous membrane and in the completely permeable membranes, a fraction of the particles can be seen below the membrane, but there are more of them in the latter compared to the former. In these two cases, it is important to note that there is a certain accumulation of particles in the upward slope.

The differences between the three conditions can be quantified by recording the amount of particles found below the membrane at any given point in the simulation. This can be seen in the plot below (Figure 3.15). Just as it could be observed in the geometry above, the amount of particles that are able to cross the membrane increase when the permeability of the membrane is increased. For a perfect insulator wall, zero particles cross the membrane during the simulation. For the other two cases, the amount of particles found below the membrane starts increasing fast at the beginning of the simulation, but the increase slows down after approximately 25 seconds. In both cases, towards the end of the simulation, the number of particles seems to be trending towards a stable value. For the fully permeable

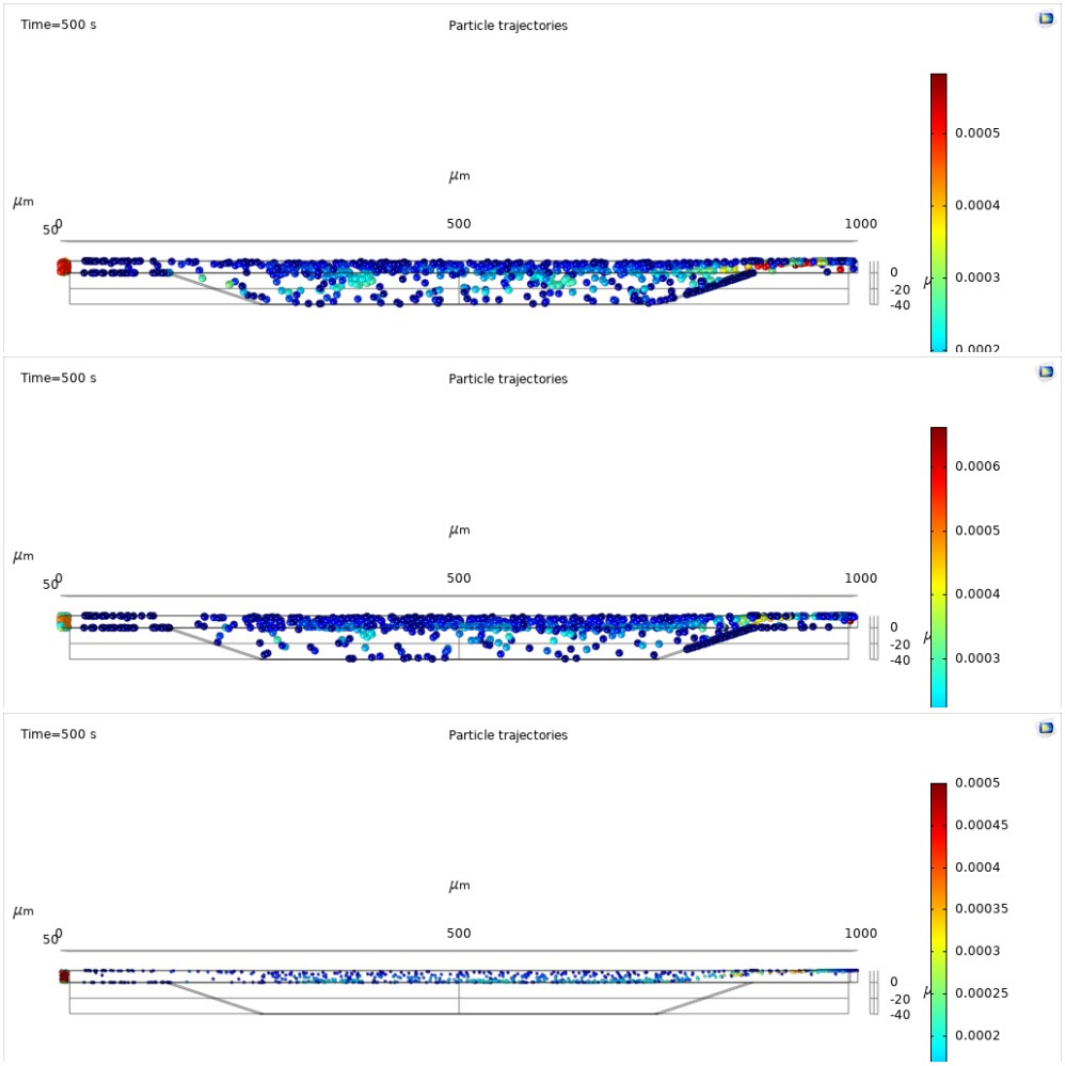

Figure 3.14: Distribution of particles throughout the microchannel at the end of the simulation (500 seconds). From top to bottom, they represent the fully permeable membrane, the porous membrane and the insulating wall cases. Note that every particle is represented with a sphere whose size is not an accurate representation of particles size. The particles are made to be as big as possible without overlapping with each other.

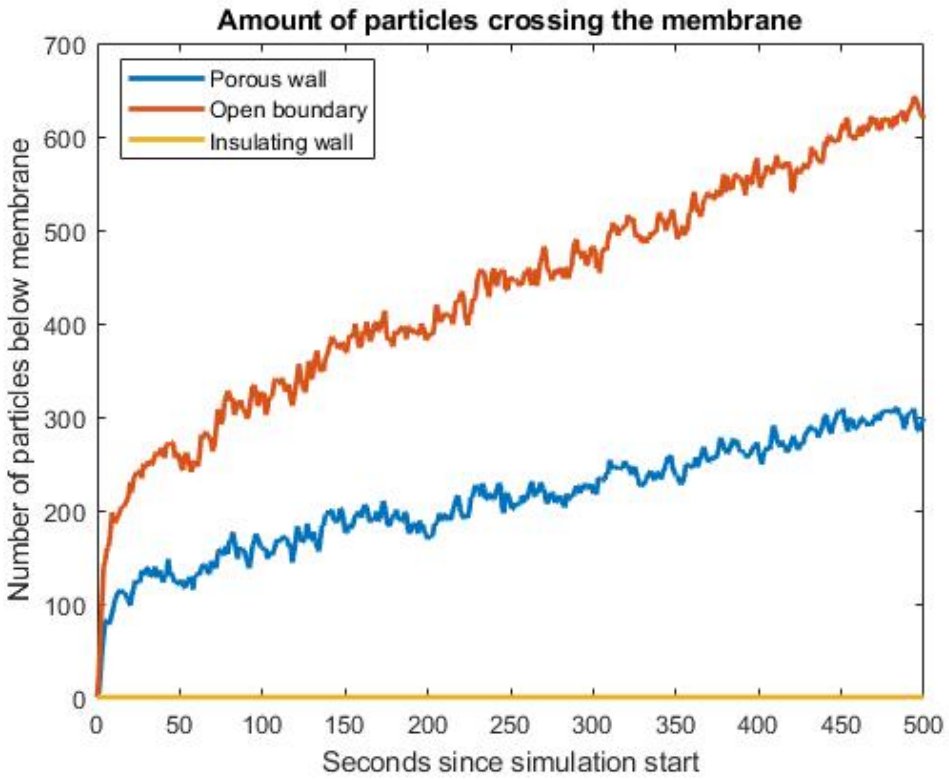

Figure 3.15: Plot showing the amount of particles found below the membrane at every moment during the simulation.

membrane, the final value is above 600, but for the porous wall model this value only reaches slightly below 300.

Effect of flow velocity in membrane crossing

After checking the different types of membrane, the porous membrane was used to test the effect that velocity may have on the amount of particles crossing the membrane. This was done by changing the normal velocity at the inlet of the channel. The values that were tested were 0.005, 0.0005, 0.0001 and 0.00005 m/s. Figure 3.16 shows the distribution of particles in the geometry for the 4 different cases. When the fastest velocity is set, very few particles actually cross the membrane and instead they seem to be moving really fast to the outlet, where they disappear. In the other cases, a higher fraction of particles cross, with more particles crossing the slower the flow is.

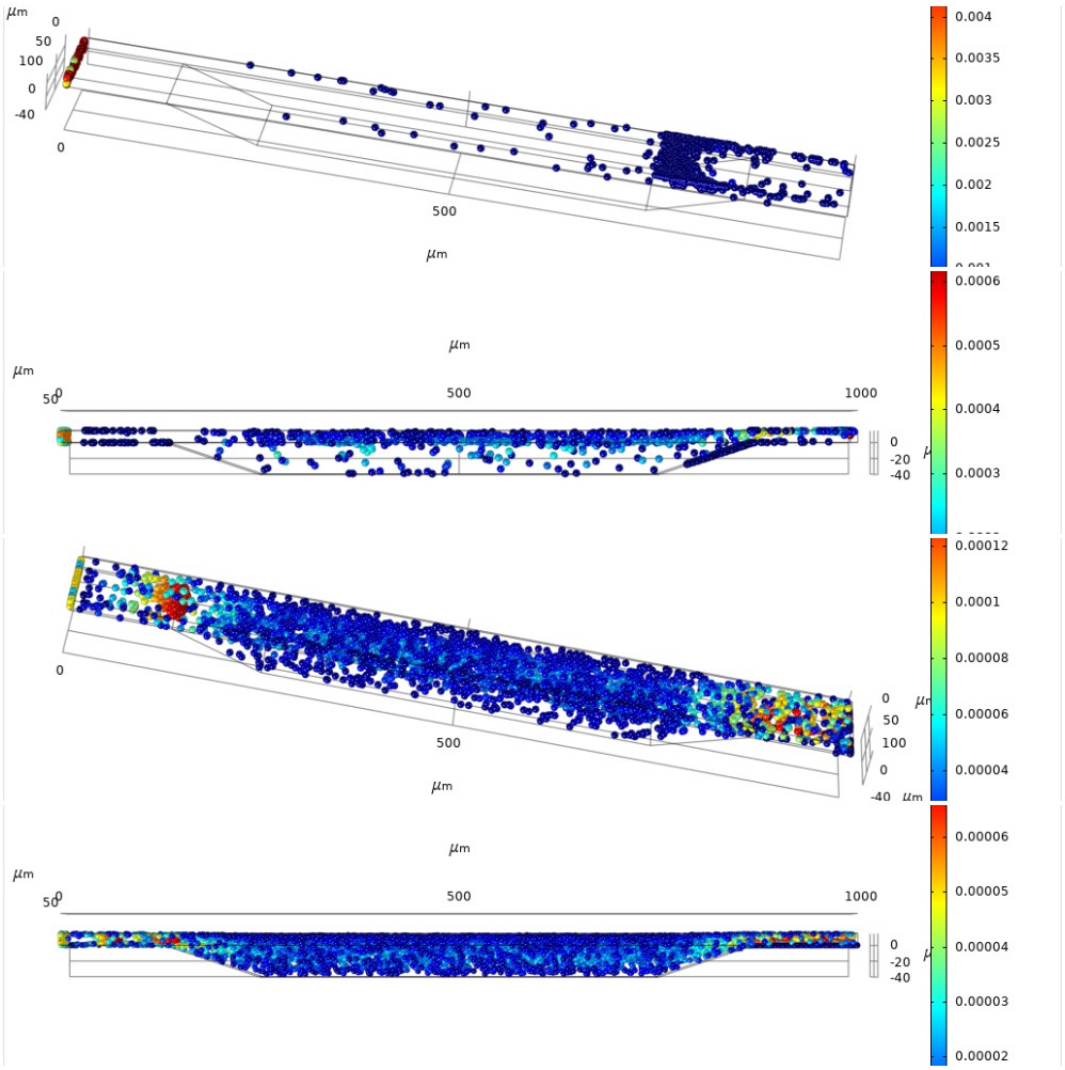

Figure 3.16: Distribution of particles throughout the microchannel at the end of the simulation (500 seconds). From top to bottom, they represent the fully permeable membrane, the porous membrane and the insulating wall cases. Note that every particle is represented with a sphere whose size is not an accurate representation of particles size. The particles are made to be as big as possible without overlapping with each other.

The difference between the different conditions can be studied by recording the amount of particles found below the membrane at any given point in the simulation. This can be seen in the plot below (Figure 3.17). In the plot, one can clearly see that more particles end up crossing the membrane when flow velocity is lower, confirming what can be seen in the geometry. Similar to the test cases simulated before, there is a trend in the plots which indicates that, after a fast increase at the start, the number of particles found below the membrane stabilizes,

albeit at different levels depending on the test condition. One important thing to note is that, for the fastest case (inlet velocity of 0.005 m/s), some particles do cross the membrane, but the amount is so low that it seems to be nothing when plotted with the slower models' results. This makes the faster model different from the situation in which the membrane was perfectly insulating which has been explained above.

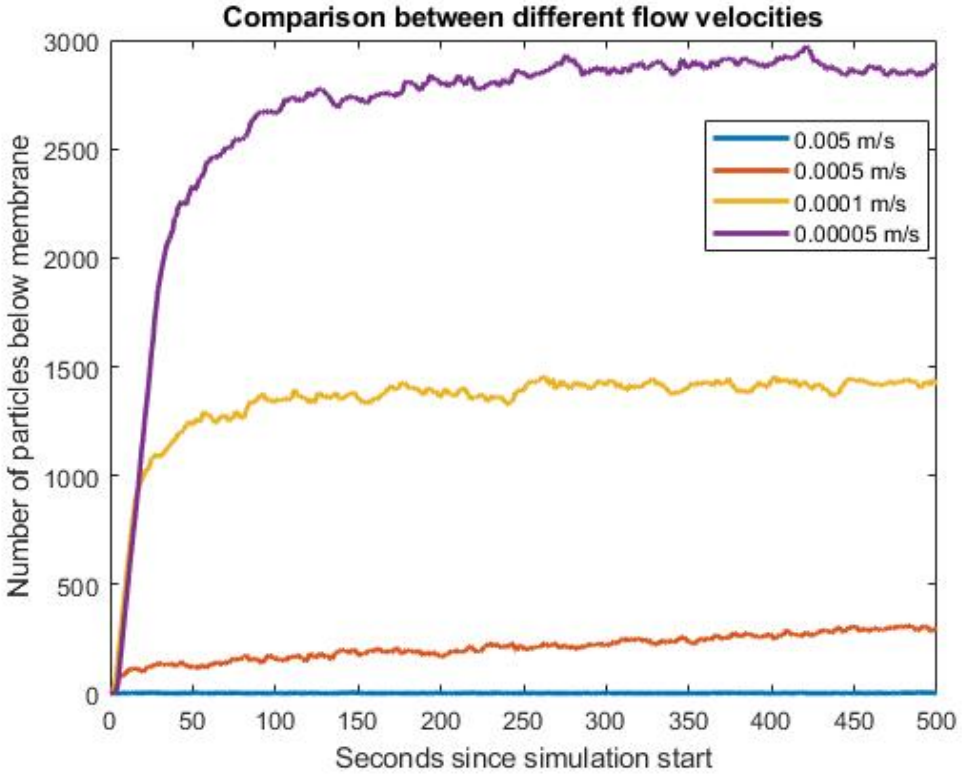

Figure 3.17: Plot showing the amount of particles found below the membrane at every moment during the simulation.

Effect of particle size on membrane crossing

Three simulations were carried out using different particle sizes to see if it had any impact on the amount of particles crossing the membrane. The particles that were used had average diameters of 2, 1 and 0.1 μm, with standard deviation of 0.2 for the first two cases and 0.02 for the latter case. However, the size distribution of the pores remained unchanged throughout the 3 simulations, with mean diameter of 1 and standard deviation of 0.2. The distribution of particles in the

geometry 500 seconds after the simulation start can be seen in Figure 3.18. The picture shows how more particles are found below the membrane as the particle diameter is reduced, although the difference between the case of 1μm and 0.1μm is minimal. In contrast, when the particles have an average diameter of 2μm, a smaller amount of particles have been able to cross the membrane. Nonetheless, the most notorious difference with respect to the other cases is that most particles are found close to the membrane.

The amount of particles below the membrane has been plotted for the three different cases as a function of simulation time (Figure 3.19). As it happened in previous simulations, in the beginning there is a large increase of particles crossing the membrane, but this increase starts slowing down as the simulation goes on, stabilizing at certain value. This value is higher for the smaller particles, 2983 for the 0.1μm particles and 2879 for the 1μm case. In the simulation with particles that are larger that the pores, the number of particle reaches 2120.

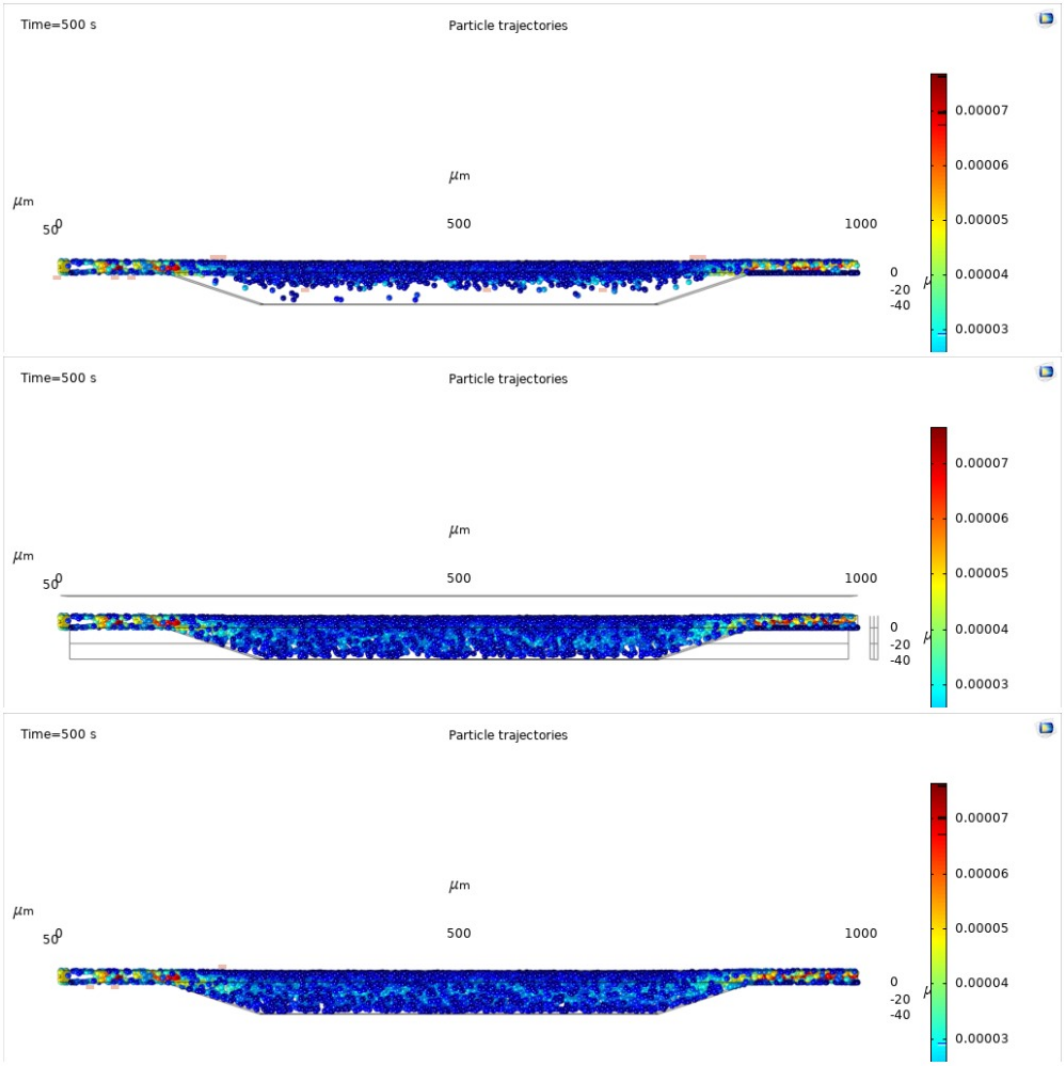

Figure 3.18: Distribution of particles throughout the microchannel at the end of the simulation (500 seconds). From top to bottom, they represent the fully permeable membrane, the porous membrane and the insulating wall cases. Note that every particle is represented with a sphere whose size is not an accurate representation of particles size. The particles are made to be as big as possible without overlapping with each other.

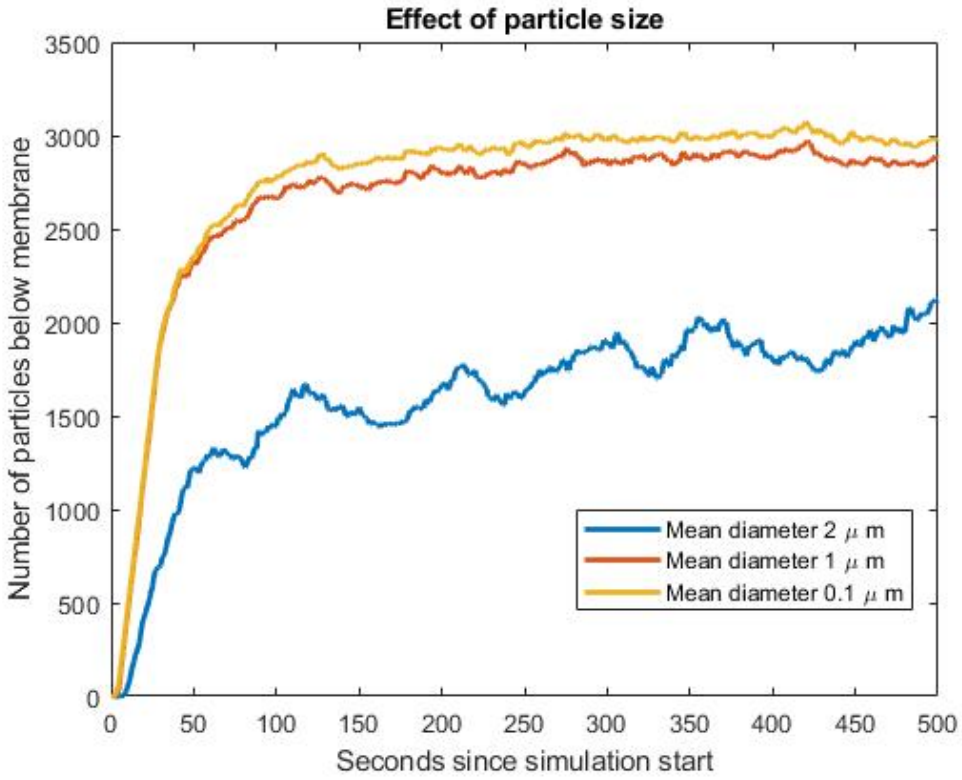

Figure 3.19: Distribution of particles throughout the microchannel at the end of the simulation (500 seconds). From top to bottom, they represent the fully permeable membrane, the porous membrane and the insulating wall cases. Note that every particle is represented with a sphere whose size is not an accurate representation of particles size. The particles are made to be as big as possible without overlapping with each other.

Chapter 4

Discussion

4.1 Condensing properties of synthesized peptide

The results obtained using AFM imaging show that free DNA is made of slim chains that can span a large area, motivating the need for condensation before delivery to cells. At first, when DNA and peptide solution were allowed to incubate for 15 minutes, condensation seems to be partial. Toroidal structures have been observed in condensation experiments before [78] and, in this case, they seem to represent an intermediate stage of the condensation process. The AFM images also show some high structures on top of the toroids that have not been identified, but they could either be more condensed DNA or aggregated peptide bound to the DNA. Although free peptide alone cannot be deposited on the APTMS-coated substrate, the observed aggregates could be partially bound DNA. Whatever the case, looking at the structures, it seems that condensation could still proceed further.

When a longer incubation time of 2 hours is allowed, there are still aggregates, but they seem to be condensed in more compact structures. This confirms that the structures seen in the previous experiment were the product of incomplete condensation and not due to the properties of the synthesized peptide. Moreover, the observed sizes for the aggregates are mostly within the acceptable range of sizes for particles used in DNA delivery, as it is generally accepted that particles up to 300 nm in diameter and below can enter cells [79]), and most observed aggregates are below this figure. When the concentration of DNA is doubled, similar aggregates can still be seen, but some DNA chains are still observable around them. These chains do not seem to be completely free, but rather they look like they are tightly packed. This suggests that, after increasing the amount of plasmid, the peptide was not able to fully condense it as it did in the previous experiment.

Although more experiments would be necessary to fully understand the condensing properties of the synthesized peptide, this would be time-consuming and it would limit the amount of other experiments that could be performed. Since the presented results proof that the synthesized peptide is able to condense DNA down to a size that could be used for gene delivery, it was decided that it was better to move on and try to couple the peptide with the polymer PVP-OD. It is important to mention that this set of experiments does not proof that the synthesized peptide is exactly the expected KKKA_5, however the exact sequence of the peptide is not as important compared as its condensing capabilities. Any synthesized peptide will have an N-terminal that can be used for EDC/NHS coupling, and the fact that condensation was successful confirms that the amount of positive charges per molecule is sufficient.

4.2 EDC/NHS coupling product analysis

4.2.1 AFM

AFM was used to try to determine whether EDC/NHS coupling of PVP-OD to KKKA_5 was successful. The results show that even after being deposited, DNA still has a tendency to collapse onto itself, as if it was being condensed. Full condensation into aggregates is probably not possible due to the electrostatic interaction between DNA and the APTMS coating that already existed before adding the polymer solution. This confirms that some positive charges are present in the solution, but not necessarily that they are coupled with PVP-OD. The reasoning behind the experiment was that the DNA chains would be thicker and/or taller, indicating that something was bound to them. It was thought that perhaps a difference in chain sizes would indicate that polymer was bound to DNA, thus confirming that PVP-OD had been coupled with cationic polymer. The AFM images reveal that there is no notable change in the width of the plasmid chain, although for both samples it is bigger than the theoretical width of a DNA double helix, which has been found to be around 2 nm [80]. This discrepancy between theoretical and experimental width has been observed before [81], and it is probably related to the limit of detection of the AFM tip. The tips used for this experiment have a guaranteed diameter of <10 nm according to manufacturers [82], but it is still too big to allow perfect lateral resolution when the scanned structures are as small as a DNA double-helix.

The measured heights are different, with the ones in the sample with polymer being approximately twice as high. This could be taken as an indicator that some polymer is attached to the DNA chains, but it is difficult to confirm.

Despite the observed differences, there is only 1 to 1,5 nm more in the sample with polymer, and the fact that the width remains unchanged casts some doubts about the presence of PVP-OD. The height difference could be caused by some plasmid chains being buried under the visible ones or it could simply be a difference caused by slightly different scanning conditions. During AFM imaging, the different parameters that control the machine were kept the same when possible, but sometimes it was necessary to make changes to this parameters to obtain clear images. If there is PVP-OD attached, the results could be explained by considering that the positive charges of PVP-OD coupled with cationic peptide create a repulsion with those of APTMS but they can bind the negative charges of the DNA backbone. This would lead to a situation in which the polymer molecules are at an equilibrium, not touching the substrate but bound to the backbone. In any case, these results are ambiguous at best and no information has been found on experiments like this in the literature, so it was considered that it was really necessary to confirm the success of the EDC/NHS coupling using a more direct technique such as FTIR spectroscopy.

4.2.2 FTIR spectroscopy

The spectra that were obtained using Fourier Transform Infrared spectroscopy show several peaks, but the most important ones for the purpose of the experiments are found around 1600 cm^{-1} and around 3300 cm^{-1}. Other than these two peaks, the rest of the two spectra are very similar, with some peaks being indistinguishable. That is to be expected, as the PVP-OD and the solvent are the same in both samples and they should produce the same peaks before and after attempting to use EDC/NHS coupling. Therefore, the differences in the aforementioned peaks must be caused by the compounds that were added during the coupling process. It is important to consider that the tested product was dialysed for two days prior to the analysis with FTIR spectroscopy. This should ensure that no byproducts of the reaction and unreacted short peptides are present in the solution.

Analysis of the two peaks mentioned above can yield confirmation that the coupling between PVP-OD and KKKA_5 was successful, at least to some degree. The peak at 1600 cm^{-1} is associated to the vibrations of the double bond between a carbon and an oxygen atom [52]. This kind of bond is present in the ring of PVP-OD, which could explain the presence of a smaller peak for the control spectrum. However, when the coupling product is tested, the peak becomes significantly higher, which is attributed to the amide bonds that exist within the peptide and between the peptide N-terminal and PVP-OD. As for the peak around 3300 cm^{-1}, the control shows a relatively strong signal, which grows even larger for the coupling product. In principle, there is no apparent reason for that peak to be present for normal PVP-OD so it would seem that, in this spectrum, the

peak corresponds to the ethanol that was used to dissolve the polymer. This is not the only peak that seems to be caused by ethanol, and the similarities between these spectra and the spectrum of liquid ethanol are quite clear [83]. Still, in the coupling product sample, the spectrum shows a bigger peak between 3000 cm^{-1} and 3500 cm^{-1}, which is slightly different in shape. Instead of being a perfect bell, there is a small shoulder at the top. This could suggest that two close peaks are found inside it, one coming from the ethanol and the other from the stretching of single bonds between nitrogen and hydrogen [52]. This second peak would not be present in the control sample due to the lack of bonds between nitrogen and hydrogen in PVP-OD, but this bond exists in the amide bond between PVP-OD and the cationic peptide, as well as in every amino acid. Considering all this, it seems safe to assume that the EDC/NHS coupling was successful and therefore the aggregates formed when mixing this product with DNA are the desired nanocarriers. This experiment is not quantitative, so it is not possible to determine the exact efficiency of the coupling reaction from these data.

4.3 AFM imaging of PVP-OD nanocarriers

Before discussing the results obtained by AFM imaging, it is important to consider that not all experiments were performed using the same cantilever. The precipitation and temperature experiments were imaged using a very soft cantilever with resonant frequency of 70 kHz, while for the previous experiments a harder cantilever with resonance frequency of 250 kHz was used. This made some clear differences in how the images look like, with some aggregates looking as they were granular and some large aggregates being smeared when the softer cantilever was used. As a result of these differences, the particle analysis performed using ImageJ could not be applied to all images, and it was necessary to evaluate them manually and from a more qualitative point of view.

Formation of PVP-OD based DNA nanocarriers is successful according to the AFM experiments. Aggregates can be observed in all samples prepared with the dialysed product of the EDC/NHS coupling reaction, confirming that the polymer has gained the condensing properties from the short cationic peptide KKKA_5. The AFM images cannot detect the composition of the aggregates but, considering the results obtained in FTIR spectroscopy, it seems safe to assume that they are formed by the interaction between the modified PVP-OD and DNA and not by free cationic peptide. Moreover, the fact that the control samples where only polymer solution was deposited do not have any such aggregates suggests that they are formed by both DNA and polymer. The samples prepared with a ratio of 1 to 2 DNA/polymer proportion show fully formed nanocarriers with no visible free DNA, while the sample prepared at a 1 to 1 ratio has some

DNA that has been condensed together with nanocarriers. This second sample is important because it sets a lower limit for the amount of polymer necessary to condense a specific amount of DNA. Knowing this is important because the exact concentration of positive charges in the polymer solution is not known, as it depends on how efficient the EDC/NHS coupling was.

In terms of size, the observed aggregates have areas that correspond to roughly 30 nm of radius or less. This means that the nanocarriers are within a size range that is acceptable for DNA delivery, as all major internalization pathways could fit these particles in their vesicles 1.2.1. Some particles are significantly bigger, but still small enough to be taken up by cells though macropinocytosis. These sizes are smaller than the ones created in [8] and [41], and in both cases they managed to obtain expression in mammalian cells. Moreover sizes between 30 and 200 nm are considered to be optimal for delivery [16, 17], so the range of sizes observed in the AFM images seems adequate for DNA delivery. The circularity of the aggregates is quite high, indicating that aggregates are probably closer to a spherical shape than to other common shapes such as rods [11, 41]. However, due to the discrepancies found in the literature, it is impossible to make a reasonable prediction of whether this shape will be beneficial for internalization or not.

One concern for delivery is whether the nanocarriers will aggregate with each other when they are formed in solution. There have been reports of condensed DNA precipitating as time goes on, which would make it very difficult to deliver the nanocarrier to cells for transfection experiments. To study this effect, the formation of nanocarriers was allowed to proceed for 2 hours in a tube and two sets of samples were prepared. The first set was prepared by taking solution from the top of the tube, and afterwards the tube was vigorously shaken and another set of samples was deposited. The first samples show some very small aggregates and some others that are similar in size to the ones observed before, but no aggregation of different nanocarriers is observed. Only some areas with clusters of nanocarriers are present in some of the samples of this kind, so it would seem that, even after two hours incubation, there is a good number of free PVP-OD and DNA complexes in solution. The samples prepared after shaking show a very different picture. Some very large structures can be seen very close to each other, suggesting that some precipitation did take place during incubation. Even when the observed aggregates are not so large, they are still well above the ones observed before, and they tend to be found in clusters. Despite this obvious aggregation, the fact that there are still nanocarriers in solution after incubation before shaking means that it is possible to let the formation process take place in a tube and add it to cells without fear of not adding any DNA-polymer complexes, but it makes it difficult to accurately estimate how much DNA is actually incorporated in cell cultures.

Another possible factor that could make transfection fail is temperature. Since all experiments had been performed at room temperature, it was necessary to test the stability of the nanocarriers at physiological temperature. To be safe, the solution containing polymer and DNA was incubated at 41 ºC before depositing on a substrate for AFM imaging. Unfortunately, the proportion of DNA to polymer had to be cut to a 1 to 1 proportion due to the lack of polymer solution stock. As explained above, this concentration has been considered as a lower limit at which aggregates can be seen but some free DNA is found as well. The results show aggregates that are similar in size to the ones observed before, but also some structures that have a different shape. Although they are small, these could correspond to partially condensed DNA, but it is difficult to discern whether this partial condensation occurs due to the increase in temperature or because of the DNA to polymer proportion. However, this specific polymer has already been tested in a previous master thesis as a drug delivery mechanism [68], and no adverse effect could be seen at 37 ºC. The fact that normal aggregates can be seen after incubation at 41 ºC suggest that they can be used at physiological temperature for transfection experiments.

In summary, the different experiments that have been performed using AFM show that PVP-OD coupled with cationic peptide is capable of condensing DNA and forming nanocarriers, provided that enough polymer is mixed with the plasmid. The observed aggregates have sizes that are considered adequate for gene delivery applications and they have the shape of imperfect spheres. It has been found that the different aggregates can bind each other when they are left in solution, but many of them are still free, clearing the way for using them in transfection experiments. Finally, it has been found that, at physiological temperatures, most observed DNA-polymer complexes retain their shape and sizes, which is important for using the nanocarriers in mammalian cells.

4.4 Cytotoxicity tests

4.4.1 12 kDa PVP-OD

The results of the first cytotoxicity test of 12 kDa PVP-OD show that, at a concentration of 1 mg/ml, it is toxic enough to kill up to 69 % of the cells. However, at 4 mg/ml, the percentage of dead cells is so low that the recorded fluorescence is lower than it is for the background measurement. This is unexpected because higher concentration of a molecule causes higher toxicity, so it was to be expected that toxicity was higher with 4 mg/ml rather than with 1 mg/ml. These results imply that a mistake was made when preparing one of the samples. For example,

when adding the PVP-OD micelles it is possible that the solution was not sufficiently shaken to ensure a uniform concentration of micelles. This shaking was performed before adding every sample, but when done incorrectly it could lead to the addition of a lower amount than expected. As for the lower concentrations, the percentage of cell death drops to around 0. In the specific case of 0.01 mg/ml, the results are almost identical to those of the negative control, suggesting that at such low concentrations 12 kDa PVP-OD is not toxic to fibroblasts. The images taken under light microscopy before and after incubation with PVP-OD show that the cell cultures had reached confluence before the test, ensuring that comparison between the different concentrations and controls was reliable. Moreover, the images confirm the results obtained from the CytoxONE test. When lysis buffer is added, almost cells die, leaving an empty well, while at 1 mg/ml cells can still be seen, bu there are fewer than before incubation and the ones that can be seen have lost the characteristic elongated shape of fibroblasts, suggesting that the cells are undergoing apoptosis. When no significant cell death was reported by the intensity measurements, the cultures look the same as before incubation.

The second cytotoxicity test was aimed at finding the point between 1 and 0.1 mg/ml at which cell death becomes significant, as well as repeating the measurement at 4 mg/ml. The results show a bizarre trend, as there is maximum cytotoxicity at an intermediate concentration of 0.66 mg/ml and higher concentrations show lower cell death. It was expected that cytotoxicity should increase as a function of concentration, but after 0.66 mg/ml that is not the case. However, it is important to remember that the CytoxOne test measures cell death indirectly, using enzymes to convert amount of LDH released to a fluorescent signal. Looking at the light microscopy images taken before and after PVP-OD addition, it is obvious that there was very high levels of cell death at 1 mg/ml and 4 mg/ml, perhaps even more than in 0.66 and 0.5 mg/ml. To understand the disparity in the results, it is necessary to consider both how enzymes work and the preparation process of the PVP-OD micelles. The micelles were prepared by dissolving the polymer in ethanol and then adding water whose pH had been adjusted to above 10 (according to a pH strip) using sodium hydroxide. Then, the ethanol was fully evaporated to leave the micelles dissolved in the basic water. When performing the cytotoxicity experiments, a stock solution with a concentration of 7 mg/ml was mixed with medium and incorporated in the cell culture so, for instance, when preparing the 4 mg/ml sample there was more volume PVP-OD solution than medium. This must have altered the normal pH of a cell culture, increasing cell death but reducing the efficiency of the enzyme. Enzymes can only function properly in a short range of pH and, for the specific enzyme diaphorase, this range goes from 7 to 9, but the best performance is found at 8.5 [84]. This explains why there were high levels of cell death at high PVP-OD concentrations but the

fluorescent signal was weaker. For intermediate concentrations, the pH did not change enough to disrupt diaphorase, so the fluorescent signal matches what is seen under light microscopy.

The result at 1 mg/ml is almost identical to the one obtained in the first experiment, but that is not the case for 0.1 mg/ml. There is a clear difference between 0.35 % cell death and 13 %, but this difference may actually be caused by only one defective measurement. Out of the three duplicates, two of them show very low cytotoxicity, similar to the first experiment, but the third one has high levels of cell death. This causes an increase in the average fluorescence, but it is possible that there was some mistake when preparing the one sample with high cytotoxicity. Indeed, when only the two lower fluorescent signals are taken into account, cell death drops to 4.5 %, which is still higher than the results obtained in the first experiment but significantly lower than 13 %. In contrast, the remaining well shows cell death of 30 %, which is higher than all other measurements. Looking at one of the wells with lower cell death under light microscopy, one can see that the culture is still confluent, in agreement with the first result (image shown in the annex).

In summary, the cytotoxicity experiments to test PVP-OD show high amounts of cell death for concentrations equal or higher than 0.33 mg/ml, reaching a close to 100 % at 1 mg/ml. The fluorescent readings above 0.66 mg/ml seem to be hindered by the pH change of the cell culture, so it is impossible to determine how much cytotoxicty is caused by the change in culture conditions and how much is caused by the addition of the polymer. Nonetheless, given the high fluorescent values at 0.66 mg/ml, it seems that pH is unaltered at such concentrations, so cell death can be attributed to PVP-OD. 0.1 mg/ml seems to have no effect on the confluence of the cell cultures, despite one sample showing strangely high fluorescence, so it can be considered as a threshold between safe concentrations and cytotoxic concentrations.

4.4.2 **KKK**A_5

There have been reports of cationic molecules exhibiting cytotoxicity due to cell membrane disruption [26, 85], so it was necessary to test the short cationic peptide that has been used throughout this project. The results clearly show that the amount of cell death caused by the different tested concentrations is negligible to the point that all cell cultures remained fully confluent after addition of the peptide. Not only are the levels of cell death are low, but they are lower than the negative control in which no peptide was added. This suggests that the small percentages of cell death are not caused by KKKA_5 and they are probably a results of the normal live cycle of cells in a confluent culture and of external factors in-

duced during the experiment, such as the strength of the pipetting. Considering everything, it seems safe to conclude that the cationic peptide used for building the DNA nanocarrier is not toxic for fibroblasts in this concentration range. The difference between this peptide and other cationic compounds that have shown toxicity could be caused by the difference in size and overall charge. KKKA_5 is a small peptide with only four charges, so it seems plausible that its effects are lower than those of large cationic peptide such as PEI or poly(L-lysine), which are bigger and carry a lot of charges [85].

4.5 Electroporation of fibroblasts

The different electroporation attempts that were tried were not successful, the expectation being that a good percentage of cells found in the culture would be able to produce GFP. The images taken with fluorescence microscopy do not show any fluorescent signal in the cells that are attached to the wall and have regular fibroblast shape. The only observed signal comes from cells that have are not completely attached to the wall and do not have the typical elongated shape. This suggests that the cells are either dead or undergoing apoptosis. To understand these results, it is necessary to consider the size of the plasmid that is being used, which is close to 10 kilobases. Large plasmids such as this one tend to have lower transfection efficiency compared to smaller ones due to the need of creating bigger pores in the cells to fit the plasmid. Moreover, it has been reported that different ends of large plasmids can enter different pores on the same cell membrane, making full internalization impossible and leading to cell death [71]. The size of pores depends directly on the strength of the electric field applied to the cells, which becomes stronger by increasing the voltage, and by increasing exposure time. Exposure time increases with sample resistance and electroporator's capacitance, but only the latter can be changed easily. Therefore, capacitance and total applied voltage were increased for the second and third attempt. An increase in these parameters usually leads to higher levels of cell death but, after the second electroporation, the cells reached confluence within two days.

In the third try, after increasing capacitance to ten times what it was originally, there was some signal, but only in cells that looked apoptotic. This could mean that the electroporation was able to create pores big enough for the plasmid to go into some cells, but the treatment was too harsh and they could not live long after. In contrast, cells that did not have big holes formed in their walls remained healthy and took the shape of normal fibroblasts. Even if this is the case, it is obvious that transfection efficiency is very poor at best. Assuming that the observed signal was indeed GFP, it is possible that more

DNA is necessary to see widespread transfection. Only 4 ug of plasmid were used for each experiment, but some authors use higher amounts [86]. 4 ug was selected as a tradeoff between having enough genetic material and reducing the expenditure of DNA stock, but it may have been insufficient after all, considering that not even all of the apoptotic cells showed strong fluorescent signal, indicating that many cells could not survive electroporation nor internalize pCas9-GFP.

It seems that exposure time was too long for the porated cells to survive during the third attempt, so it could be beneficial to lower capacitance to a middle ground between the first and third experiments while increasing voltage further. This would increase the amount of pores formed and the speed at which they grow and reduce cell death. Other strategies could be used to improve electrophoresis. For example, during the third attempt, for 5 minutes after the electroporation took place, the cells and plasmid solution was put on ice. This is supposed to slow down the recovery of the membrane without the need of maintaining a constant electrical current [61]. This incubation time could be increased up to 10 or even 15 minutes, increasing the chance for a plasmid to enter the fibroblasts. Another option to improve efficiency could be to apply the ideas proposed in [71], where they used small plasmids that do not generate expression in human cells but that can help larger plasmids enter. Although the exact mechanism is not known, it was found that the transfection efficiency of large plasmids containing the Cas9 gene (just like pCas9-GFP)improved when small plasmids between 1 and 5 kilobases were mixed with the larger ones, with the best results corresponding to 3 kb long plasmids.

4.6 Transfection of pCas9-GFP by nanocarriers

The different attempts to use the synthesized nanocarrier to deliver the plasmid pCas9-GFP showed similar results to those obtained in electroporation, as the only green fluorescent signal was found in cells that had lost their typical elongated shape, indicating that they were undergoing apoptosis. At first, a small amount of DNA and polymer solution was used, but no signal was observed in any of the samples, suggesting that a relatively large amount of DNA is necessary for widespread transfection. Because of this, a second experiment was performed increasing the amount of DNA to 1,33 ug per well, hoping to see some GFP signal. However, the amount of polymer solution necessary for condensing this DNA was calculated to be 150 ul, based on the estimation that PVP-OD concentration was approximately 5 mg/ml (the estimation was made by taking the amount of PVP-OD dissolved during EDC/NHS coupling and the final volume of the dialysed sample). This poses a new problem because, upon addition of this quantity of polymer solution, the final concentration of PVP-OD in each sample was above

1 mg/ml, which is considered a toxic concentration for fibroblasts based on the results from CytoxONE experiments. This explains the high levels of cell death in the cultures that were used to do this experiment. Interestingly, this are also the samples that show higher levels of GFP signal. Although quantifying expression numerically is impossible due to the aggregation of apoptotic cells in clumps, the amount of such clumps that showed some signal was higher than for any other tested condition. It seems that some cells internalized the nanocarriers and started producing GFP before apoptosis began. This would mean that more nanocarrier concentration leads to higher transfection, but at the cost of too high cell death.

In order to avoid the adverse effects of high concentrations of PVP-OD, another sample was prepared where the concentrations of DNA and polymer were reduced to a third of what it was in the previous experiment. On top of that, and in order to try and compensate for the lower amount of plasmid, free cationic peptide was added at a concentration of 5 mg/ml. As it has been mentioned earlier in this report (section 1.2.3), the addition of free positively-charged molecules can mediate endosomal escape inside cells, improving the transfection efficiency; but this has been tested in cationic polymers carrying several charges, not short peptides. The results show that, although some cells did internalize the plasmid and produced GFP, the majority did not. That ones that did produce GFP appear to be apoptotic, just as in the previous experiments, but the cultures are confluent. The small amount of cell death could be attributed to the concentration of PVP-OD, which is lower than in the previous experiment but still within the range that can cause some level of cytotoxicity. However, this does not explain why only dead cells show GFP expression. Another explanation for this result could be the effect that culture medium has on cells. It is common to add antibiotics to cell medium to avoid bacterial growth, but it has been found that they can also negatively influence mammalian cells [87, 88]. It is therefore possible that, upon addition of the nanocarriers, several internalization processes started in the cells that later expressed plasmid and penicillin entered in the cell with them, leading to high cell death among the cells that did take up larger amounts of nanocarriers. Penicillin toxicity may have also played a role in the mortality of cells transfected by electroporation.

In summary, the GFP expression induced by the synthesized nanocarriers is far from ideal. Only high amounts of DNA (and therefore polymer) can induce expression, but at the cost of causing high levels of cell death. Despite this, the fact that some levels of GFP could be seen indicate that this delivery vehicle actually has the potential to mediate gene internalization in human cells. Moreover, the ability of PVP-OD to condense DNA is directly dependant on how many peptides are coupled to each polymer molecule. In this work, the PVP-OD that was used

had only 20 % acrylic acid substitutions, but some other versions have up to 95 %. Because of this, EDC/NHS coupling could be used to create PVP-OD that carries more positive charges. This would make it possible to use a lower amount of polymer to condense the same amount of DNA, mitigating the problem of cytotoxicity.

4.7 COMSOL simulation of microchannel

In this section, the results obtained from different simulation will be analysed and discussed, and a conclusion will be made on whether the developed COMSOL system is a good predictor of how a microfluidic *in vitro* testing device might work.

4.7.1 Porous solid wall

The generation of a wall with random pores with determined size range was achieved by creating a COMSOL method. However, particles much bigger than the pores are able to cross the wall during simulations, even if it should not be physically possible. This result does not correlate well with the real behaviour such a system would have, as one would expect to see a sieving effect, with particles smaller than the pores being able to pass through and those bigger than that rebounding or sticking to the wall. The reason for the inability to model this sieving effect is found in the way that the particle tracing module calculates particle trajectories. The particle diameter is used to calculate other parameters such as the drag force that the particles feel inside a flow, but it is not taken into account when determining the position. For this module, particles are points in space that suffer different forces depending on the set diameter [89]. Because of this, the points that represent particles can move freely across pores, despite their diameter. This shortcoming of the particle tracing module makes it incompatible with the desired sieving properties of the membrane, hence the need for the probabilistic model that has been developed.

4.7.2 Probabilistic model

Before discussing the performance of this model, it is important to consider that it is associated with a higher computational cost due to the fact that Matlab Livelink needs to be called every time that a particle hits the membrane, instead of simply using the particle tracing module on its own. Another difference with the previously discussed model is that the flow is different at the membrane and in the space below it. In this probabilistic model, the membrane is invisible for the fluid flow module, allowing liquid to flow across it freely and creating a current that will drive the particles towards the membrane. This was a necessary change because, if the membrane was considered a solid wall, the flow would not be able to go

through and the flow velocity at the membrane would be zero due to the no-slip boundary condition. This would make it impossible for particles to reach and cross the membrane. As a consequence, the liquid does not go through specific small local currents through pores, but there is a larger current across the whole membrane. This behaviour is less realistic compared to the porous solid wall model, but it is necessary to cause many particles to reach the membrane and study the validity of the probabilistic model. The rest of the flow is consistent with the expectations for laminar flow in these conditions, with a higher velocity in the center and zero velocity at the walls due to the no-slip boundary condition.

Comparison of extreme cases: Insulating wall, porous membrane and fully permeable membrane

Comparison of these three cases serves as a basic control on the quality of the model. In principle, one would expect that, when the membrane crossing probability is zero, no particles will be found in the compartment below the membrane. When the particle has pores of a size comparable to the particle sizes, some of them will certainly cross, but not as many as when the wall is fully permeable. In the first case, some particles that reach the membrane will rebound instead of passing through, but that should not happen in the fully permeable case. After running the three simulations, both the distribution of particles across the geometry and the amount of particles found below the membrane show the expected behaviour, with a clear increase in membrane crossing for the fully permeable case compared to a normal porous membrane, while no particles are able to cross when the membrane is changed for an impermeable wall. These results prove that, in broad terms, the probabilistic model of the membrane follows the expected behaviour, as it is a middle case between the extremes of a wall and a fully permeable membrane. Nonetheless, this is only a preliminary study to ensure that the model does not have any fatal conceptual error, and the true performance of the model can only be validated with the other simulations that have been carried out.

Effect of flow velocity on membrane crossing

The velocity of the flow is one of the most important parameters when using a microfluidic device for testing delivery. For once, it is one of the parameters that can be more easily controlled by means of a pump, allowing for a large range of velocities to be tested. Therefore, being able to optimise this parameter can help reduce the amount of times a experiment must be repeated. Because of this, knowing whether this COMSOL model can capture the differences caused by changes in speed is very significant. The results show a clear trend: the

slower the flow, the more particles are found below the membrane. Moreover, the amount of particles that can be found in the geometry at the end of the simulation also grows as velocity decreases. This trend is specially obvious when comparing the slowest velocity tested, 50μm/sec to the fastest, 5 mm/sec. In the former, almost 3000 particles are found under the membrane at the end of the simulation time, while very few particles are found there for the latter. Moreover, at 500 seconds, the distribution of particles across the geometry shows a very small amount of particles for the highest speed. This is explained by the fact that the velocity is too large compared to the length of the channel, and the particles are able to travel in very few time steps from the inlet to the outlet. That also explains why most particles accumulate in two places at 500 seconds. There is a group at the inlet (particles that have been generated in the last time step) and another one close to the outlet. As for the other tested cases, the distribution is more similar to what was seen in the previous simulations.

The changes in particle behaviour and distribution can be explained with two reasons. On one hand, it is to be expected that there will be less particles in the geometry at any given time if the speed is very high because they reach the outlet after a short time. Similarly, particles can never accumulate in the section below the membrane. Most likely, some particles do cross the membrane, but they are quickly returned to the upper channel by the strong flow, before the next released particles can reach the membrane. For the slower flow velocities, there is a certain accumulation below the membrane, as particles are not removed as quickly and, eventually, an equilibrium between the amount of particles crossing from the upper to the lower section and the particles crossing back to the upper section is established. Another possible explanation for the radical differences in particle distribution comes not from the physics, but rather from a simulation parameter: the time step. During these simulations, a time of 500 seconds was simulated with a time step of 1 second. That means that every one second of simulation new particles appear at the inlet and the position of particles is recorded. This time step should be small enough for the simulation to be accurate while maintaining a reasonable computational cost (simulations still take several hours, but a normal home laptop with 16 GB of RAM can handle them). However, a time step of one second might be too large for the highest speed. At a speed of 5 mm/sec, a particle can travel from the inlet to the outlet in one step, ignoring the current that leads some particle to the membrane. This problem is mitigated because COMSOL is able to automatically calculate some intermediate steps when necessary, although that causes the computation time to increase significantly, as simulation time went from around 2 hours for the two slowest flow velocities to about three hours for the second highest and to close to seven hours for the highest speed simulation. Nonetheless, this problem with the time step could still play a role in keeping the

amount of particles below the membrane so low.

Effect of particle size on the model

So far, in all of the simulations, the size of the particles have remained constant, with a average diameter of 1μm and standard deviation of 0.1μm. When a porous membrane was used, the size of the pores followed the same distribution as the particles. However, a porous membrane should be able to sieve smaller particles while making those bigger than the pore diameter rebound. In order to check if this behaviour is represented in the probabilistic membrane model, three simulations with different particle sizes but same pore diameter were performed. Given that the average size of the pores is 1μm, it is expected that, in the simulation with largest particles, little membrane crossing will take place and for the smallest particles there should be a very large amount crossing to the lower section of the geometry. Despite these expectations, the results show that the difference between the cases with particles of 1 and 0.1μm are very small in terms of particle distribution while the simulation with bigger particles showed that the rate of membrane crossing was lower but still significant. For example, the amount of particles below the membrane at the end of the simulation is higher than some of the cases tested before, when the particles were smaller but the flow was faster.

Understanding the results for the bigger particle simulation requires some knowledge of how a normal distribution works. In this case, there is a particle diameter normal distribution with a mean of 2μm and a standard deviation of 0.2μm. In any Gaussian curve, 68.2 % of the area under the curve is found withing the mean plus/minus 1 standard deviation. 95.44 % of the area under the curve is in the range of 2 standard deviations and at that point, the diameter range goes from 1,6μm to 2.4μm. This means that there is a probability for some particles to be small enough to cross the membrane, which is approximately 2.33 %. Moreover, a bigger particle will also move slower in the flow, so it will allow for a higher rate of accumulation below the membrane. It would be interesting to do a simulation with a radius that is way bigger than the pore size and therefore should have zero probability of crossing the membrane. Unfortunately, higher radius increase computational cost to the point where the computer crashed during the simulation. Using a more powerful computer, one could test this more extreme case to assert the sieving properties of the membrane. As a substitute to this simulation, the function that calculates the probability can be used in a 1000 step loop in Matlab for a mean particle radius of 10μm. When this is done, all of the probabilities are calculated to be zero, suggesting that this membrane could prevent very large particles from crossing. Nonetheless, this should be tried with the whole COMSOL model in order to make sure.

Anther interesting piece of these results is how little difference there is between the normal and smallest particles simulation. Both the distribution and the plot showing the amount of particles below the membrane are very similar, despite the fact that smaller particles should have a higher chance of crossing the membrane when they reach it. These results for the smallest particles can be explained as a tradeoff between two different effects. On one hand, and as it has been stated above, it is more likely for particle to cross, but they also move faster in the flow, which causes them to cross back to the upper section and then be removed from the outlet. This last effect seems to be enough to counter-balance the increase in crossing probability due to size. It is important to consider that, because a coverage of 50 % has been used throughout the simulations, the maximum crossing probability has an upper bound, leading to smaller differences between the normal and small cases.

4.7.3 Finals remarks about probabilistic membrane model

The results obtained from the various simulations indicate that the probabilistic model can be used to reproduce the behaviour of particles crossing a porous membrane. All of the observed phenomena could explained and justified. Moreover, thanks to its ability to capture the sieving properties of a porous barrier, it is a superior system to simply creating a wall with holes, as it was originally intended. This, combined with the freedom of design that COMSOL confers, will allow any user to rapidly screen different setups and geometries for microfluidic chips that could be used to test DNA delivery systems in different scenarios that imitate *in vivo*systems better than 2D cultures.

4.8 Future work

This thesis has started the development of a new DNA delivery system, but the results obtained only represent the beginning of something that could be a much longer project. The nanocarrier formed with PVP-OD and KKKA_5 has shown potential to be used in gene delivery, as it has been able to produce moderate amounts of expression and some of its properties such as the size appear to be optimal. The next step in this project could be to try to overcome the high toxicity caused when GFP was expressed. As proposed above, this could fixed by using PVP-OD coupled to more cationic peptides, which would reduce cell death while still condensing a large amount of DNA. This modified version of the polymer should then be tested to ensure that the aggregates it forms are similar to those observed in this work before testing them in fibroblasts again. Parallel to this process, a control for GFP expression should be prepared to be able to evaluate

the performance of the nanocarrier compared to other available gene transfection methods. It could be tried to tune electroporation, or some other commercially available system could be used, such as Lipofectamine 3000 (ThermoFisher).

After high levels of safety and transfection efficiency have been achieved, the developed COMSOL model could be used to test different designs for microfluidic chips where the nanocarrier can be tried. Thanks to the availability of technologies such as 3D printing and different materials, many designs for the chip geometry and nature of the membrane could be created. By screening the different options, one could reach an optimal design with the desired properties. One possible example of this could be to make a membrane that protects cells similarly to the endothelium found in blood vessels with a fluid velocity that resembles that of blood flow.

Chapter 5

Conclusion

In this thesis, a new DNA delivery system has been developed using the amphiphilic polymer PVP-OD, which has been given the ability to condense DNA after coupling it to the cationic peptide KKKAAAAA, forming structures similar to polyplexes. Thanks to the different AFM experiments, it has been confirmed that, when plasmid DNA that includes the gene for GFP is mixed with the modified polymer, nanocarriers with sizes in the range of a few tens to couple hundred nanometers are formed, and their properties appear to be adequate for gene delivery. After testing the cytotoxicity that the different components of this system cause in human fibroblasts, the nanocarriers have been tested *in vitro* as transfection agents, but high levels of expression remain to be seen. Only when high amounts of DNA are delivered can one see widespread GFP production, but this implies that toxic levels of PVP-OD need to be delivered as well. Despite these results, this new delivery system still holds promise as a viable DNA delivery vehicle thanks to the studied properties and the advantages that it may have compared to traditional polyplexes. Finally, the model of a microfluidic chip has been developed in COMSOL Multiphysics with the hope that it will aid in the design of a microfluidic *in vitro* testing system where the nanocarriers can be tried in in conditions that more closely resemble *in vivo*systems. The different simulations performed with this model indicate that it is a good tool that could be used in the future to reduce time and cost of designing a system like this.

Bibliography

[1] Thomas C. Roberts, Robert Langer, and Matthew J.A. Wood. "Advances in oligonucleotide drug delivery". In: *Nature Reviews Drug Discovery* 19.10 (Oct. 2020), pp. 673–694. ISSN: 14741784. DOI: 10.1038/s41573-020-0075-7.

[2] Bingyang Shi, Meng Zheng, Wei Tao, Roger Chung, Dayong Jin, Dariush Ghaffari, and Omid C. Farokhzad. "Challenges in DNA Delivery and Recent Advances in Multifunctional Polymeric DNA Delivery Systems". In: *Biomacromolecules* 18.8 (2017), pp. 2231–2246. ISSN: 15264602. DOI: 10.1021/acs.biomac.7b00803.

[3] Y. K. Sung and S. W. Kim. "Recent advances in the development of gene delivery systems". In: *Biomaterials Research* 23.1 (Mar. 2019), pp. 1–7. ISSN: 20557124. DOI: 10.1186/s40824-019-0156-z.

[4] Nouri Nayerossadat, PalizbanAbas Ali, and Talebi Maedeh. "Viral and non-viral delivery systems for gene delivery". In: *Advanced Biomedical Research* 1.1 (2012), p. 27. ISSN: 2277-9175. DOI: 10.4103/2277-9175.98152.

[5] Arun K. Iyer, Greish Khaled, Jun Fang, and Hiroshi Maeda. "Exploiting the enhanced permeability and retention effect for tumor targeting". In: *Drug Discovery Today* 11.17-18 (Sept. 2006), pp. 812–818. ISSN: 13596446. DOI: 10.1016/j.drudis.2006.07.005.

[6] Hiroshi Maeda, Hideaki Nakamura, and Jun Fang. "The EPR effect for macromolecular drug delivery to solid tumors: Improvement of tumor uptake, lowering of systemic toxicity, and distinct tumor imaging in vivo". In: *Advanced Drug Delivery Reviews* 65.1 (Jan. 2013), pp. 71–79. ISSN: 0169409X. DOI: 10.1016/j.addr.2012.10.002.

[7] William M. Pardridge. "Drug transport across the blood-brain barrier". In: *Journal of Cerebral Blood Flow and Metabolism* 32.11 (Nov. 2012), pp. 1959–1972. ISSN: 0271678X. DOI: 10.1038/jcbfm.2012.126.

[8] Shigehito Osawa, Kensuke Osada, Shigehiro Hiki, Anjaneyulu Dirisala, Takehiko Ishii, and Kazunori Kataoka. "Polyplex Micelles with Double-Protective Compartments of Hydrophilic Shell and Thermoswitchable Pal-

isade of Poly(oxazoline)-Based Block Copolymers for Promoted Gene Transfection". In: *Biomacromolecules* 17.1 (Jan. 2016), pp. 354–361. ISSN: 15264602. DOI: 10.1021/acs.biomac.5b01456.

[9] Nicole J. Yang and Marlon J. Hinner. "Getting across the cell membrane: an overview for small molecules, peptides, and proteins". In: *Methods in molecular biology (Clifton, N.J.)* 1266 (2015), pp. 29–53. ISSN: 19406029. DOI: 10.1007/978-1-4939-2272-7{_}3.

[10] Qiang Gong, Christopher Huntsman, and Dzwokai Ma. "Clathrin-independent internalization and recycling: Membrane Trafficking Review Series". In: *Journal of Cellular and Molecular Medicine* 12.1 (Jan. 2008), pp. 126–144. ISSN: 15821838. DOI: 10.1111/j.1582-4934.2007.00148.x.

[11] Sudha Kumari, Swetha Mg, and Satyajit Mayor. *Endocytosis unplugged: Multiple ways to enter the cell*. Mar. 2010. DOI: 10.1038/cr.2010.19.

[12] Hervé Hillaireau and Patrick Couvreur. "Nanocarriers' entry into the cell: Relevance to drug delivery". In: *Cellular and Molecular Life Sciences* 66.17 (June 2009), pp. 2873–2896. ISSN: 14209071. DOI: 10.1007/s00018-009-0053-z.

[13] Sunil Thomas, Anca Preda-Pais, Sofia Casares, and Teodor D. Brumeanu. "Analysis of lipid rafts in T cells". In: *Molecular Immunology* 41.4 (June 2004), pp. 399–409. ISSN: 01615890. DOI: 10.1016/j.molimm.2004.03.022.

[14] Stephanie E.A. Gratton, Patricia A. Ropp, Patrick D. Pohlhaus, J. Christopher Luft, Victoria J. Madden, Mary E. Napier, and Joseph M. DeSimone. "The effect of particle design on cellular internalization pathways". In: *Proceedings of the National Academy of Sciences of the United States of America* 105.33 (Aug. 2008), pp. 11613–11618. ISSN: 00278424. DOI: 10.1073/pnas.0801763105.

[15] Parisa Foroozandeh and Azlan Abdul Aziz. "Insight into Cellular Uptake and Intracellular Trafficking of Nanoparticles". In: *Nanoscale Research Letters* 13.1 (Oct. 2018), pp. 1–12. ISSN: 1556276X. DOI: 10.1186/s11671-018-2728-6.

[16] Fang Lu, Si Han Wu, Yann Hung, and Chung Yuan Mou. "Size effect on cell uptake in well-suspended, uniform mesoporous silica nanoparticles". In: *Small* 5.12 (June 2009), pp. 1408–1413. ISSN: 16136810. DOI: 10.1002/smll.200900005.

[17] Joanna Rejman, Volker Oberle, Inge S. Zuhorn, and Dick Hoekstra. "Size-dependent internalization of particles via the pathways of clathrin-and caveolae-mediated endocytosis". In: *Biochemical Journal* 377.1 (Jan. 2004), pp. 159–169. ISSN: 02646021. DOI: 10.1042/BJ20031253.

[18] Yuanzu He and Kinam Park. "Effects of the microparticle shape on cellular uptake". In: *Molecular Pharmaceutics* 13.7 (July 2016), pp. 2164–2171. ISSN: 15438392. DOI: 10.1021/acs.molpharmaceut.5b00992.

[19] B. Devika Chithrani, Arezou A. Ghazani, and Warren C.W. Chan. "Determining the size and shape dependence of gold nanoparticle uptake into mammalian cells". In: *Nano Letters* 6.4 (Apr. 2006), pp. 662–668. ISSN: 15306984. DOI: 10.1021/nl052396o.

[20] Amrita Banerjee, Jianping Qi, Rohan Gogoi, Jessica Wong, and Samir Mitragotri. "Role of nanoparticle size, shape and surface chemistry in oral drug delivery". In: *Journal of Controlled Release* 238 (Sept. 2016), pp. 176–185. ISSN: 18734995. DOI: 10.1016/j.jconrel.2016.07.051.

[21] Julie A. Champion and Samir Mitragotri. "Role of target geometry in phagocytosis". In: *Proceedings of the National Academy of Sciences of the United States of America* 103.13 (Mar. 2006), pp. 4930–4934. ISSN: 00278424. DOI: 10.1073/pnas.0600997103.

[22] Francelyne Marano, Salik Hussain, Fernando Rodrigues-Lima, Armelle Baeza-Squiban, and Sonja Boland. "Nanoparticles: Molecular targets and cell signalling". In: *Archives of Toxicology* 85.7 (July 2011), pp. 733–741. ISSN: 03405761. DOI: 10.1007/s00204-010-0546-4.

[23] Tanya S. Hauck, Arezou A. Ghazani, and Warren C.W. Chan. "Assessing the effect of surface chemistry on gold nanorod uptake, toxicity, and gene expression in mammalian cells". In: *Small* 4.1 (Jan. 2008), pp. 153–159. ISSN: 16136810. DOI: 10.1002/smll.200700217.

[24] Dominik Hühn, Karsten Kantner, Christian Geidel, Stefan Brandholt, Ine De Cock, Stefaan J.H. Soenen, Pilar Riveragil, Jose Maria Montenegro, Kevin Braeckmans, Klaus Müllen, G. Ulrich Nienhaus, Markus Klapper, and Wolfgang J. Parak. "Polymer-coated nanoparticles interacting with proteins and cells: Focusing on the sign of the net charge". In: *ACS Nano* 7.4 (Apr. 2013), pp. 3253–3263. ISSN: 19360851. DOI: 10.1021/nn3059295.

[25] Julia Dausend, Anna Musyanovych, Martin Dass, Paul Walther, Hubert Schrezenmeier, Katharina Landfester, and Volker Mailänder. "Uptake mechanism of oppositely charged fluorescent nanoparticles in Hela cells". In: *Macromolecular Bioscience* 8.12 (Dec. 2008), pp. 1135–1143. ISSN: 16165187. DOI: 10.1002/mabi.200800123.

[26] Xiawei Wei, Bin Shao, Zhiyao He, Tinghong Ye, Min Luo, Yaxiong Sang, Xiao Liang, Wei Wang, Shuntao Luo, Shengyong Yang, Shuang Zhang, Changyang Gong, Maling Gou, Hongxing Deng, Yinglan Zhao, Hanshuo Yang, Senyi Deng, Chengjian Zhao, Li Yang, Zhiyong Qian, Jiong Li, Xun Sun, Jiahuai Han, Chengyu Jiang, Min Wu, and Zhirong Zhang. "Cationic nanocarriers induce cell necrosis through impairment of Na+/K+-ATPase and cause subsequent inflammatory response". In: *Cell Research* 25.2 (Feb. 2015), pp. 237–253. ISSN: 17487838. DOI: 10.1038/cr.2015.9.

[27] Tanja Bus, Anja Traeger, and Ulrich S. Schubert. “The great escape: How cationic polyplexes overcome the endosomal barrier”. In: *Journal of Materials Chemistry B* 6.43 (Nov. 2018), pp. 6904–6918. ISSN: 2050750X. DOI: 10.1039/c8tb00967h.

[28] Rikke V. Benjaminsen, Maria A. Mattebjerg, Jonas R. Henriksen, S. Moein Moghimi, and Thomas L. Andresen. “The possible "proton sponge " effect of polyethylenimine (PEI) does not include change in lysosomal pH”. In: *Molecular Therapy* 21.1 (2013), pp. 149–157. ISSN: 15250024. DOI: 10.1038/mt.2012.185.

[29] Jean Paul Behr. “The proton sponge: A trick to enter cells the viruses did not exploit”. In: *Chimia*. Vol. 51. 1-2. Swiss Chemical Society, 1997, pp. 34–36.

[30] Arjen M. Funhoff, Cornelus F. van Nostrum, Gerben A. Koning, Nancy M.E. Schuurmans-Nieuwenbroek, Daan J.A. Crommelin, and Wim E. Hennink. “Endosomal escape of polymeric gene delivery complexes is not always enhanced by polymers buffering at low pH”. In: *Biomacromolecules* 5.1 (2004), pp. 32–39. ISSN: 15257797. DOI: 10.1021/bm034041+.

[31] Sriram Vaidyanathan, Junjie Chen, Bradford G. Orr, and Mark M. Banaszak Holl. “Cationic Polymer Intercalation into the Lipid Membrane Enables Intact Polyplex DNA Escape from Endosomes for Gene Delivery”. In: *Molecular Pharmaceutics* 13.6 (June 2016), pp. 1967–1978. ISSN: 15438392. DOI: 10.1021/acs.molpharmaceut.6b00139.

[32] Sriram Vaidyanathan, Bradford G. Orr, and Mark M. Banaszak Holl. “Role of Cell Membrane-Vector Interactions in Successful Gene Delivery”. In: *Accounts of Chemical Research* 49.8 (Aug. 2016), pp. 1486–1493. ISSN: 15204898. DOI: 10.1021/acs.accounts.6b00200.

[33] Zhuojun Dai, Torben Gjetting, Maria A. Mattebjerg, Chi Wu, and Thomas L. Andresen. “Elucidating the interplay between DNA-condensing and free polycations in gene transfection through a mechanistic study of linear and branched PEI”. In: *Biomaterials* 32.33 (Nov. 2011), pp. 8626–8634. ISSN: 01429612. DOI: 10.1016/j.biomaterials.2011.07.044.

[34] Philippe Collas and Peter Aleström. “Nuclear localization signal of SV40 T antigen directs import of plasmid DNA into sea urchin male pronuclei in vitro”. In: *Molecular Reproduction and Development* 45.4 (1996), pp. 431–438. ISSN: 1040452X. DOI: 10.1002/(SICI)1098-2795(199612)45:4<431::AID-MRD4>3.0.CO;2-S.

[35] S. Brunner, T. Sauer, S. Carotta, M. Cotten, M. Saltik, and E. Wagner. “Cell cycle dependence of gene transfer by lipoplex polyplex and recombinant adenovirus”. In: *Gene Therapy* 7.5 (Feb. 2000), pp. 401–407. ISSN: 09697128. DOI: 10.1038/sj.gt.3301102.

[36] C. H. Wu, J. M. Wilson, and G. Y. Wu. "Targeting genes: Delivery and persistent expression of a foreign gene driven by mammalian regulatory elements in vivo". In: *Journal of Biological Chemistry* 264.29 (Oct. 1989), pp. 16985–16987. ISSN: 00219258. DOI: 10.1016/s0021-9258(18)71447-6.

[37] R. Kircheis, A. Kichler, G. Wallner, M. Kursa, M. Ogris, T. Felzmann, M. Buchberger, and E. Wagner. "Coupling of cell-binding ligands to polyethylenimine for targeted gene delivery". In: *Gene Therapy* 4.5 (1997), pp. 409–418. ISSN: 09697128. DOI: 10.1038/sj.gt.3300418.

[38] Rohan Aggarwal, Monika Targhotra, Bhumika Kumar, P.K Sahoo, and Meenakshi K Chauhan. "Polyplex: A Promising Gene Delivery System". In: *International Journal of Pharmaceutical Sciences and Nanotechnology* 12.6 (2019), pp. 4681–4686. ISSN: 0974-3278. DOI: 10.37285//ijpsn.2019.12.6.1.

[39] S. M.W. van Rossenberg, A. C.I. van Keulen, J. W. Drijfhout, S. Vasto, H. K. Koerten, F. Spies, J. M. van't Noordende, Th J.C. van Berkel, and E. A.L. Biessen. "Stable polyplexes based on arginine-containing oligopeptides for in vivo gene delivery". In: *Gene Therapy* 11.5 (Mar. 2004), pp. 457–464. ISSN: 09697128. DOI: 10.1038/sj.gt.3302183.

[40] Anjaneyulu Dirisala, Kensuke Osada, Qixian Chen, Theofilus A. Tockary, Kaori Machitani, Shigehito Osawa, Xueying Liu, Takehiko Ishii, Kanjiro Miyata, Makoto Oba, Satoshi Uchida, Keiji Itaka, and Kazunori Kataoka. "Optimized rod length of polyplex micelles for maximizing transfection efficiency and their performance in systemic gene therapy against stroma-rich pancreatic tumors". In: *Biomaterials* 35.20 (2014), pp. 5359–5368. ISSN: 18785905. DOI: 10.1016/j.biomaterials.2014.03.037.

[41] Takahiro Nomoto, Shigeto Fukushima, Michiaki Kumagai, Kaori Machitani, Arnida, Yu Matsumoto, Makoto Oba, Kanjiro Miyata, Kensuke Osada, Nobuhiro Nishiyama, and Kazunori Kataoka. "Three-layered polyplex micelle as a multifunctional nanocarrier platform for light-induced systemic gene transfer". In: *Nature Communications* 5.1 (Apr. 2014), pp. 1–10. ISSN: 20411723. DOI: 10.1038/ncomms4545.

[42] Satoshi Uchida and Kazunori Kataoka. "Design concepts of polyplex micelles for in vivo therapeutic delivery of plasmid DNA and messenger RNA". In: *Journal of Biomedical Materials Research - Part A* 107.5 (May 2019), pp. 978–990. ISSN: 15524965. DOI: 10.1002/jbm.a.36614.

[43] Erdal Cevher, Ali Demir, and Emre Sefik. "Gene Delivery Systems: Recent Progress in Viral and Non-Viral Therapy". In: *Recent Advances in Novel Drug Carrier Systems*. InTech, Oct. 2012. DOI: 10.5772/53392.

[44] Yoshiyuki Hattori, Yuki Yoshiike, Takuto Kikuchi, Natsumi Yamamoto, Kei Ichi Ozaki, and Hiraku Onishi. "Evaluation of the injection route of an anionic polymer for small interfering RNA delivery into the liver by sequential injection of anionic polymer and cationic lipoplex of small interfering RNA". In: *Journal of Drug Delivery Science and Technology* 35 (Oct. 2016), pp. 40–49. ISSN: 17732247. DOI: 10.1016/j.jddst.2016.05.005.

[45] Lian Xue, Yunfeng Yan, Petra Kos, Xiaoping Chen, and Daniel J. Siegwart. "PEI fluorination reduces toxicity and promotes liver-targeted siRNA delivery". In: *Drug Delivery and Translational Research* 11.1 (Feb. 2021), pp. 255–260. ISSN: 21903948. DOI: 10.1007/s13346-020-00790-9.

[46] Conchita Tros de Ilarduya, Yan Sun, and Nejat Düzgüneş. "Gene delivery by lipoplexes and polyplexes". In: *European Journal of Pharmaceutical Sciences* 40.3 (June 2010), pp. 159–170. ISSN: 09280987. DOI: 10.1016/j.ejps.2010.03.019.

[47] S. Simões, V. Slepushkin, P. Pires, R. Gaspar, M. C. Pedroso De Lima, and N. Düzgüneş. "Mechanisms of gene transfer mediated by lipoplexes associated with targeting ligands or pH-sensitive peptides". In: *Gene Therapy* 6.11 (Nov. 1999), pp. 1798–1807. ISSN: 09697128. DOI: 10.1038/sj.gt.3301015.

[48] Wei Chen, Hui Li, Zhenguo Liu, and Weien Yuan. "Lipopolyplex for therapeutic gene delivery and its application for the treatment of Parkinson's disease". In: *Frontiers in Aging Neuroscience* 8.APR (Apr. 2016), p. 68. ISSN: 16634365. DOI: 10.3389/fnagi.2016.00068.

[49] Robin Bofinger, May Zaw-Thin, Nicholas J. Mitchell, P. Stephen Patrick, Cassandra Stowe, Ana Gomez-Ramirez, Helen C. Hailes, Tammy L. Kalber, and Alethea B. Tabor. "Development of lipopolyplexes for gene delivery: A comparison of the effects of differing modes of targeting peptide display on the structure and transfection activities of lipopolyplexes". In: *Journal of Peptide Science* 24.12 (Dec. 2018), p. 24. ISSN: 10991387. DOI: 10.1002/psc.3131.

[50] Michael Bradley. *FTIR Spectroscopy Basics | Thermo Fisher Scientific - US*.

[51] Patrick Garidel and Heidrun Schott. "Determination of Secondary Structure in Proteins by FTIR Spectroscopy - JenaLib". In: *BioProcess Technical* (2006), pp. 1–8.

[52] Shahid Ali Khan, Sher Bahadar Khan, Latif Ullah Khan, Aliya Farooq, Kalsoom Akhtar, and Abdullah M. Asiri. "Fourier transform infrared spectroscopy: Fundamentals and application in functional groups and nanomaterials characterization". In: *Handbook of Materials Characterization*. Springer International Publishing, Sept. 2018. Chap. 9, pp. 317–344. ISBN: 9783319929552. DOI: 10.1007/978-3-319-92955-2{_}9.

[53] D. Peak. "Fourier Transform Infrared Spectroscopy". In: *Encyclopedia of Soils in the Environment*. Vol. 4. Boston, MA: Springer US, 2004, pp. 80–85. ISBN: 9780080547954. DOI: 10.1016/B0-12-348530-4/00174-0.

[54] Núria Gavara. "A beginner's guide to atomic force microscopy probing for cell mechanics". In: *Microscopy Research and Technique* 80.1 (Jan. 2017), pp. 75–84. ISSN: 10970029. DOI: 10.1002/jemt.22776.

[55] *AFM: Background information | MyScope*.

[56] *Scientific Image - Atomic Force Microscope Illustration | NISE Network*.

[57] JPK Instruments AG. *NanoWizard ® AFM Handbook JPK Instruments NanoWizard ® Handbook Version 2.2a 1*. Tech. rep. 2012, p. 55.

[58] Senem Kamiloglu, Gulce Sari, Tugba Ozdal, and Esra Capanoglu. "Guidelines for cell viability assays". In: *Food Frontiers* 1.3 (Sept. 2020), pp. 332–349. ISSN: 2643-8429. DOI: 10.1002/fft2.44.

[59] Promega Corporation. "CytoTox-ONE™ Homogeneous Membrane Integrity Assay Instructions for Use of Products G7890, G7891 and G7892". In: *Technical Bulletin* 306 (2009), pp. 608–277.

[60] Lars Kaestner, Anke Scholz, and Peter Lipp. "Conceptual and technical aspects of transfection and gene delivery". In: *Bioorganic and Medicinal Chemistry Letters* 25.6 (Mar. 2015), pp. 1171–1176. ISSN: 14643405. DOI: 10.1016/j.bmcl.2015.01.018.

[61] Huntington Potter and Richard Heller. "Transfection by electroporation". In: *Current Protocols in Molecular Biology* CHAPTER.SUPPL. 92 (Oct. 2010), Unit. ISSN: 19343639. DOI: 10.1002/0471142727.mb0903s62.

[62] Jean Michel Escoffre, Thomas Portet, Luc Wasungu, Justin Teissié, David Dean, and Marie Pierre Rols. "What is (Still not) known of the mechanism by which electroporation mediates gene transfer and expression in cells and tissues". In: *Molecular Biotechnology* 41.3 (Mar. 2009), pp. 286–295. ISSN: 10736085. DOI: 10.1007/s12033-008-9121-0.

[63] Bio Rad. "Gene Pulser II Electroporation System Instruction Manual Catalog". In: (2000).

[64] J. C. Weaver. "Electroporation theory. Concepts and mechanisms." In: *Methods in molecular biology (Clifton, N.J.)* 48 (1995), pp. 3–28. ISSN: 10643745. DOI: 10.1385/0-89603-304-x:3.

[65] James C. Weaver. "Electroporation: A general phenomenon for manipulating cells and tissues". In: *Journal of Cellular Biochemistry* 51.4 (1993), pp. 426–435. ISSN: 10974644. DOI: 10.1002/jcb.2400510407.

[66] H. Liang, W. J. Purucker, D. A. Stenger, R. T. Kubiniec, and S. W. Hui. "Uptake of fluorescence-labeled dextrans by 10T 1/2 fibroblasts following permeation by rectangular and exponential-decay electric field pulses". In: *BioTechniques* 6.6 (June 1988), pp. 550–558. ISSN: 07366205.

[67] Jonas Nørskov Søndergaard, Keyi Geng, Christian Sommerauer, Ionut Atanasoai, Xiushan Yin, and Claudia Kutter. "Successful delivery of large-size CRISPR/Cas9 vectors in hard-to-transfect human cells using small plasmids". In: *Communications Biology* 3.1 (Dec. 2020), pp. 1–6. ISSN: 23993642. DOI: 10.1038/s42003-020-1045-7.

[68] Levi Nelemans. "Characterization of 12 kDa PVP-OD nanocarriers and the influence of their size on the uptake in mammalian cells". PhD thesis. Aalborg University, 2019.

[69] Paola Franco and Iolanda De Marco. "The use of poly(N-vinyl pyrrolidone) in the delivery of drugs: A review". In: *Polymers* 12.5 (May 2020). ISSN: 20734360. DOI: 10.3390/POLYM12051114.

[70] Raymond Behrendt, Peter White, and John Offer. "Advances in Fmoc solid-phase peptide synthesis". In: *Journal of Peptide Science* 22.1 (Jan. 2016), pp. 4–27. ISSN: 10991387. DOI: 10.1002/psc.2836.

[71] Qiurong Ding, Stephanie N. Regan, Yulei Xia, Leoníe A. Oostrom, Chad A. Cowan, and Kiran Musunuru. "Enhanced efficiency of human pluripotent stem cell genome editing through replacing TALENs with CRISPRs". In: *Cell Stem Cell* 12.4 (Apr. 2013), pp. 393–394. ISSN: 19345909. DOI: 10.1016/j.stem.2013.03.006.

[72] aapptec. *Overview of Solid Phase Peptide Synthesis (SPPS)*. 2016.

[73] *Fmoc solid-phase synthesis - CRB Discovery*.

[74] Malithi P. Wickramathilaka and Bernard Y. Tao. "Characterization of covalent crosslinking strategies for synthesizing DNA-based bioconjugates". In: *Journal of Biological Engineering* 13.1 (July 2019), pp. 1–10. ISSN: 17541611. DOI: 10.1186/s13036-019-0191-2.

[75] ThermoFisher Scientific. *Carbodiimide Crosslinker Chemistry | Thermo Fisher Scientific Carbodiimide Crosslinker Chemistry Carbodiimide Crosslinker Chemistry | Thermo Fisher Scientific*. 2018.

[76] Kirk L. Sorgi. "Diisopropylethylamine". In: *Encyclopedia of Reagents for Organic Synthesis*. John Wiley & Sons, Ltd, Apr. 2001. DOI: 10.1002/047084289x.rd254.

[77] *Counting cells using a hemocytometer - Cell Culture Protocol 6 | Sigma-Aldrich*.

[78] Christine C. Conwell, Igor D. Vilfan, and Nicholas V. Hud. "Controlling the size of nanoscale toroidal DNA condensates with static curvature and ionic strength". In: *Proceedings of the National Academy of Sciences of the United States of America* 100.16 (Aug. 2003), pp. 9296–9301. ISSN: 00278424. DOI: 10.1073/pnas.1533135100.

[79] Karmani Murugan, Yahya E. Choonara, Pradeep Kumar, Divya Bijukumar, Lisa C. du Toit, and Viness Pillay. "Parameters and characteristics governing cellular internalization and trans-barrier trafficking of nanostructures". In: *International Journal of Nanomedicine* 10 (Mar. 2015), pp. 2191–2206. ISSN: 11782013. DOI: 10.2147/IJN.S75615.

[80] *Different Form of Perception ;*

[81] James Vesenka, J Vesenka, T Marsh, E Henderson, and C Vellandi. *The diameter of duplex and quadruplex DNA measured by SPM THE DIAMETER OF DUPLEX AND QUADRUPLEX DNA MEASURED BY SCANNING PROBE MICROSCOPY*. Tech. rep. 2. 1998, pp. 329–342.

[82] *PPP-FM AFM Probe - NanoAndMore*.

[83] Irina Doroshenko, Valeriy Pogorelov, and Valdas Sablinskas. "Infrared Absorption Spectra of Monohydric Alcohols". In: *Dataset Papers in Chemistry* 2013 (Oct. 2013), pp. 1–6. ISSN: 2314-5315. DOI: 10.7167/2013/329406.

[84] Anvarsadat Kianmehr, Rahman Mahdizadeh, Morteza Oladnabi, and Javad Ansari. "Recombinant expression, characterization and application of a dihydrolipoamide dehydrogenase with diaphorase activity from Bacillus sphaericus". In: *3 Biotech* 7.2 (June 2017). ISSN: 21905738. DOI: 10.1007/s13205-017-0763-0.

[85] A. Christy Hunter and S. Moein Moghimi. "Cationic carriers of genetic material and cell death: A mitochondrial tale". In: *Biochimica et Biophysica Acta - Bioenergetics* 1797.6-7 (June 2010), pp. 1203–1209. ISSN: 00052728. DOI: 10.1016/j.bbabio.2010.03.026.

[86] "Transfection of mammalian cells by electroporation". In: *Nature Methods* 3.1 (Jan. 2006), pp. 67–68. ISSN: 15487091. DOI: 10.1038/nmeth0106-67.

[87] Laura Llobet, Julio Montoya, Ester López-Gallardo, and Eduardo Ruiz-Pesini. "Side Effects of Culture Media Antibiotics on Cell Differentiation". In: *Tissue Engineering - Part C: Methods* 21.11 (Nov. 2015), pp. 1143–1147. ISSN: 19373392. DOI: 10.1089/ten.tec.2015.0062.

[88] Uffe H. Nygaard, Hanna Niehues, Gijs Rikken, Diana Rodijk-Olthuis, Joost Schalkwijk, and Ellen H. van den Bogaard. "Antibiotics in cell culture: Friend or foe? Suppression of keratinocyte growth and differentiation in monolayer cultures and 3D skin models". In: *Experimental Dermatology* 24.12 (2015), pp. 964–965. ISSN: 16000625. DOI: 10.1111/exd.12834.

[89] COMSOL. “The Particle Tracing Module User’s Guide”. In: (2013), p. 105.

Appendix A

Supporting figures

The images that have been added in this appendix are complementary to the ones that have been shown in the Results chapter. It is not necessary to see these figures to understand the results obtained in this thesis, but rather they are provided to reinforce their validity.

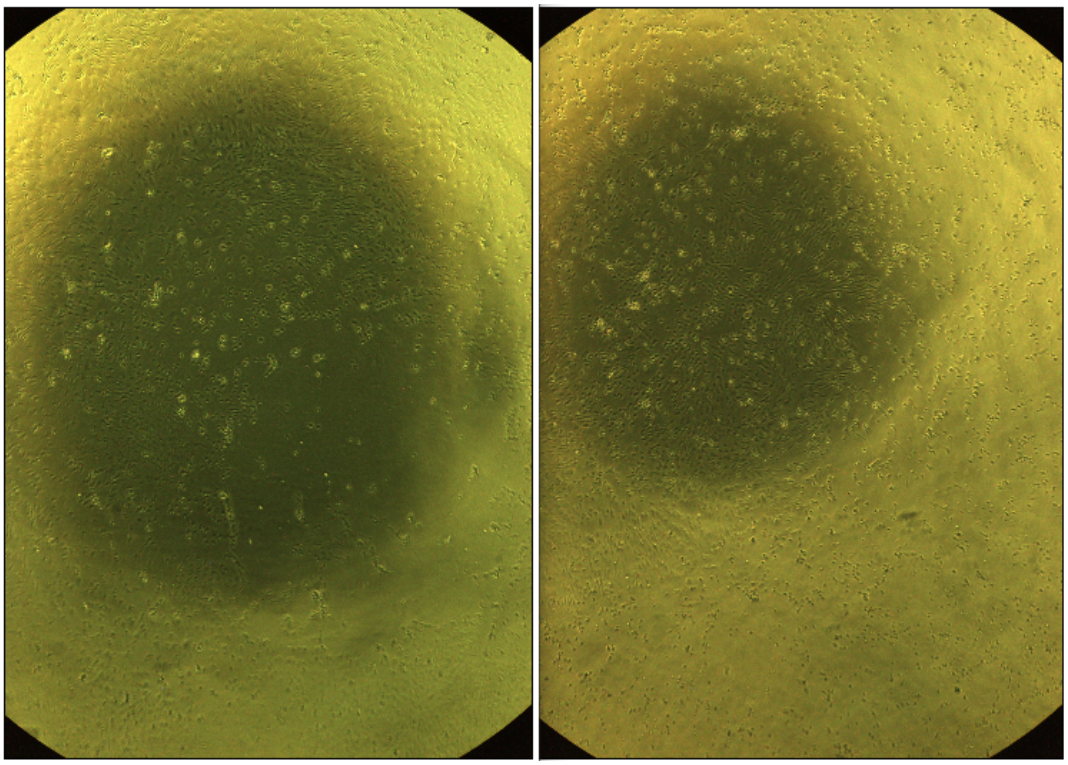

Figure A.1: Light microscopy images of two wells after addition of PVP-OD and 24 hour incubation. To the left, a ell here a concentration of 4 mg/ml was added, but fluorescent signal was low. To the right, a well with concentration of 0.66 mg/ml, where fluorescent signal was the highest.

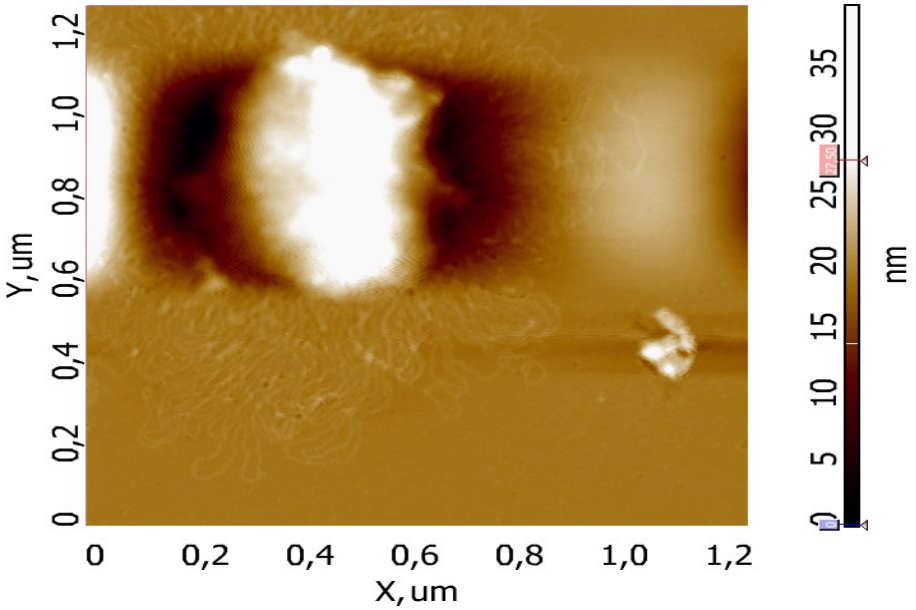

Figure A.2: AFM images of an aggregate observed when mixing 15 μl of DNA solution (concentration 5 μg/ml) and 15 μl of cationic peptide solution. Near the aggregate, some DNA chains can be observed indicating that condensation is not complete.

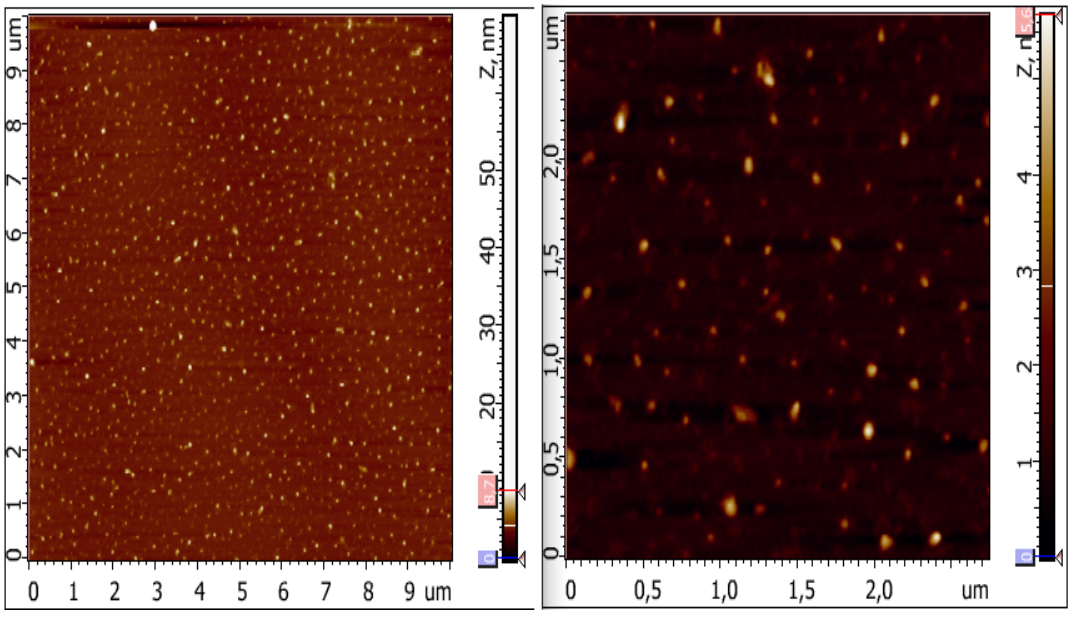

Figure A.3: AFM images of the aggregates observed when mixing 15 μl of DNA solution and 30 μl of polymer solution.

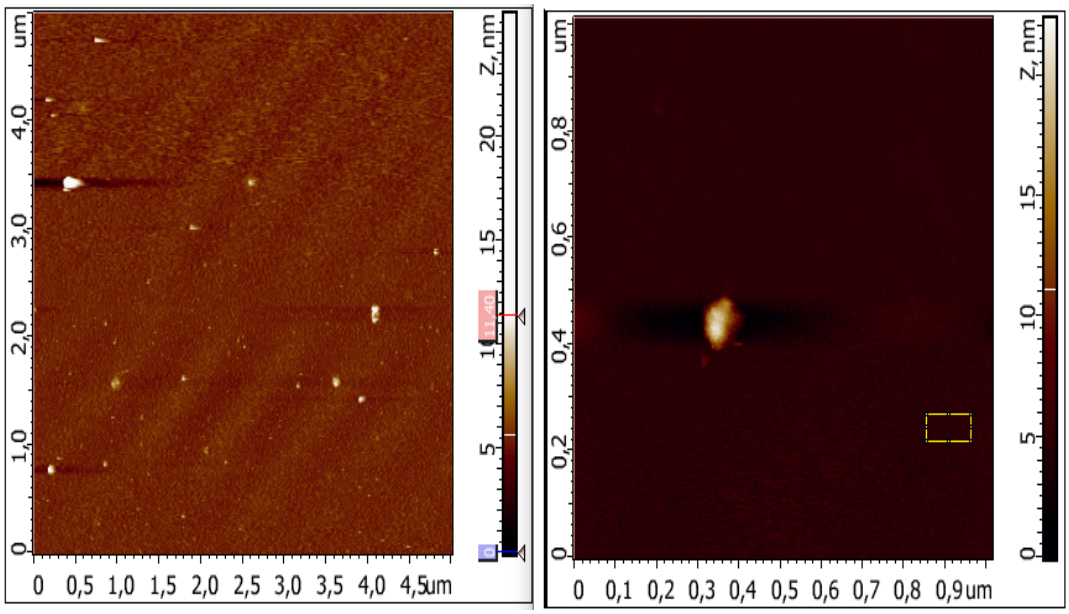

Figure A.4: AFM images of the aggregates observed when mixing 15 μl of DNA solution and 15 μl of polymer solution and incubating at 41 ºC.

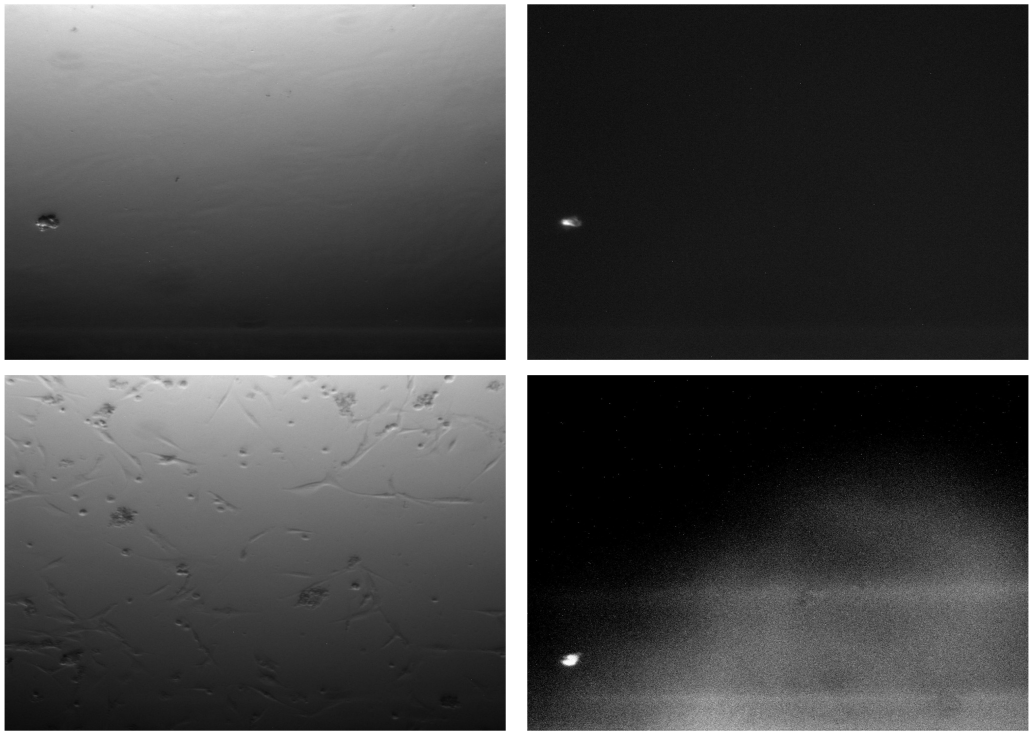

Figure A.5: Results of the last electroporation experiment (capacitance 50000 uF and voltage 500 V. To the left, there are light microscopy images, and to the right there are the corresponding areas when imaging green fluorescence.)

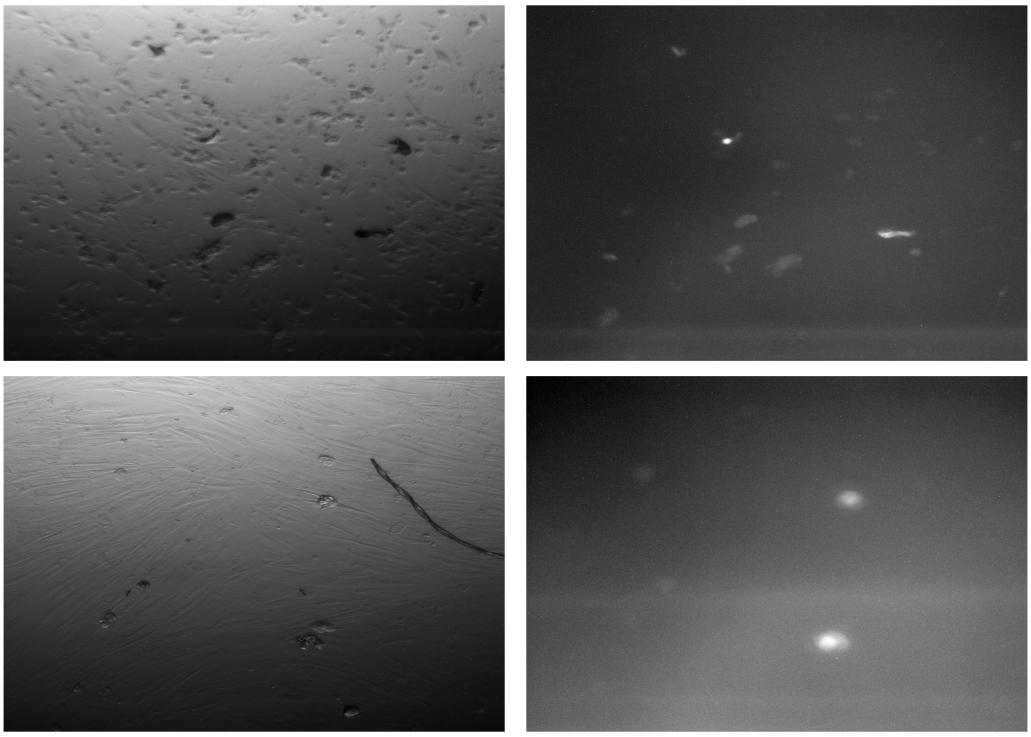

Figure A.6: Above, images corresponding to the nanocarrier trasnfection experiment with 1,33 μg of DNA per well. Below, images corresponding to the experiment with 0,45 μg/ml and free cationic peptide. To the left, there are light microscopy images, and to the right there are the corresponding areas when imaging green fluorescence.

Appendix B

Original codes for COMSOL simulation

Random porous wall generator (COMSOL Method):

```
with(app.mainWindow());
set("title", "");
endwith();
model.component("comp1").geom("geom1").lengthUnit("mm");
model.component("comp1").geom("geom1").create("rectangle1", "Rectangle");
model.component("comp1").geom("geom1").feature("rectangle1").set("size", new
double[]100.0, 20.0);
model.component("comp1").geom("geom1").create("rectangle2", "Rectangle");
model.component("comp1").geom("geom1").feature("rectangle2").set("size", new
double[]50, 15.0);
model.component("comp1").geom("geom1").feature("rectangle2").set("pos", new
double[]25, -15.25);
model.component("comp1").geom("geom1").create("rect", "Rectangle");
model.component("comp1").geom("geom1").feature("rect").set("size", new dou-
ble[]50, 0.25);
model.component("comp1").geom("geom1").feature("rect").set("pos", new dou-
ble[]25, -0.25);
double coverage = 0.5;
double current = 0.0;
double pos = 0.0;
double w = 0.0;
int ind = 1;
model.component("comp1").geom("geom1").selection().create("csel1", "Cumula-
tiveSelection");
```

```
model.component("comp1").geom("geom1").selection().create("csel2", "Cumula-
tiveSelection");
while (current < 0.5)
pos = 49*Math.random()+26;
w = 0.7+0.3*Math.random();
model.component("comp1").geom("geom1").create("rect"+ind, "Rectangle");
model.component("comp1").geom("geom1").feature("rect"+ind).set("size", new
double[]w, 0.25);
model.component("comp1").geom("geom1").feature("rect"+ind).set("pos", new
double[]pos, -0.25);
model.component("comp1").geom("geom1").create("rectA"+ind, "Rectangle");
model.component("comp1").geom("geom1").feature("rectA"+ind).set("size", new
double[]w, 0.25);
model.component("comp1").geom("geom1").feature("rectA"+ind).set("pos", new
double[]pos, -0.25);
model.component("comp1").geom("geom1").feature("rect"+ind).set("contributeto",
"csel1");
model.component("comp1").geom("geom1").feature("rectA"+ind).set("contributeto",
"csel2");
current = current+(w/50);
ind++;

model.component("comp1").geom("geom1").create("dif1", "Difference");
model.component("comp1").geom("geom1").feature("dif1").selection("input").set("rect");
model.component("comp1").geom("geom1").feature("dif1").selection("input2").named("csel1");

    model.component("comp1").geom("geom1").run();
```

Probability calculator based on particle and pore size:

```
function prob=WallProbability(C,mupar,sigmapar,muhole,sigmahole)
gauss=@(n)exp(-0.5 * ((n - muhole)./sigmahole).^2)./(sqrt(2*pi).*sigmahole);
x = randn(1)/3;
y = mupar + 5*sigmapar*x;
prob = C*integral(gauss,y,muhole+5*sigmahole);
if(prob < 0)
prob = 0;
end
end
```

Appendix C

Licenses for non-original images

Figure 1.1:
Source: Hervé Hillaireau and Patrick Couvreur.Nanocarriers' entry into the cell: Rel-evance to drug delivery. June 2009.doi:10.1007/s00018-009-0053-z.url:https://link.springer.com/article/10.1007/s00018-009-0053-z
RightsLink License Number: 5080120893079

Figure 1.2:
Source: Satoshi Uchida and Kazunori Kataoka.Design concepts of polyplex micelles forin vivo therapeutic delivery of plasmid DNA and messenger RNA. May 2019.doi:10.1002/jbm.a.36614.url:https://pubmed.ncbi.nlm.nih.gov/30665262/
RightsLink License Number: 5080131027765

Figure 1.3:
Source: D. Peak. "Fourier Transform Infrared Spectroscopy". In:Encyclopedia of Soilsin the Environment. Vol. 4. Boston, MA: Springer US, 2004, pp. 80–85.isbn:9780080547954.doi:10.1016/B0-12-348530-4/00174-0.url:http://link.springer.com/10.1007/0-387-37590-2-9.
RightsLink License Number: 5080700909302

Figure 1.5:
Source:Jean Michel Escoffre, Thomas Portet, Luc Wasungu, Justin Teissié, DavidDean, and Marie Pierre Rols.What is (Still not) known of the mechanism bywhich electroporation mediates gene transfer and expression in cells and tissues.Mar. 2009.doi:10.1007/s12033-008-9121-0.url:https://link.springer.com/article/10.1007/s12033-008-9121-0
RightsLink License Number:5080700655367